

Original paper

# Supergene mineralization of the Medvědín uranium deposit, Krkonoše Mountains, Czech Republic<sup>†</sup>

Jakub PLÁŠIL<sup>1,2\*</sup>, Jiří SEJKORA<sup>1</sup>, Jiří ČEJKA<sup>1</sup>, Radek ŠKODA<sup>3</sup>, Viktor GOLIÁŠ<sup>2</sup>

<sup>1</sup> Department of Mineralogy and Petrology, National Museum, Václavské nám. 68, 115 79 Prague 1, Czech Republic; [jakub\\_plasil@nm.cz](mailto:jakub_plasil@nm.cz)

<sup>2</sup> Institute of Geochemistry, Mineralogy and Mineral Resources, Charles University in Prague, Faculty of Science, Albertov 6, 128 43 Prague 2, Czech Republic

<sup>3</sup> Institute of Earth Sciences, Faculty of Science, Masaryk University, Kotlářská 2, 611 37 Brno, Czech Republic

\* Corresponding author

† Dedicated to everlasting memory of outstanding mineralogist Ing. Zdeněk Mrázek, CSc. (1952–1984)



Supergene mineralization of the hydrothermal vein uranium deposit Medvědín (Krkonoše Mts., northern Bohemia) is rather varied both in number of the mineral phases and their chemical variation. The supergene minerals agardite-(Y), autunite/metaautunite, dewindtite, churchite-(Y), kasolite, new unnamed phase  $Pb(Ce,REE)_3(PO_4)_3(OH)_2 \cdot nH_2O$ , parsonsrite, phosphuranylite, plumbogummite, pseudomalachite, pyromorphite, saléeite, torbernite/metatorbernite and uranophane were studied using powder XRD, EPMA, IR-spectroscopic and thermal analysis, contributing significantly to the clarification of their crystal chemistry. The alteration mineral assemblage consisting mostly of uranyl phosphates and silicates exhibits relatively high contents of REE and Pb. Minerals with a composition corresponding to pure mineral end-members have not been observed; instead most of the studied phases represent members of isomorphic series. Studied mineral assemblage is a stable association in surface conditions resulting apparently from a long-term alteration of the primary uranium mineralization.

**Keywords:** supergene minerals, uranium, XRD, EPMA, infrared spectroscopy, thermal analysis, mineral succession

Received: 15 February 2008; accepted 1 October 2008; handling editor: R. Skála

## 1. Introduction

Uranium is the key element for nuclear energy production. However, the increasing usage of uranium as a nuclear fuel brings about environmental problems, such as remediation and long-term storage of the spent nuclear fuel. Understanding behaviour of uranium in natural conditions, especially in shallow crustal levels and the mechanism of alteration processes in particular has a crucial importance for the spent nuclear fuel management and solving other environmental problems (Finch and Ewing 1992; Wronkiewicz et al. 1992). The Medvědín deposit in the northern Bohemia exhibits a well-developed alteration zone with prevalence of uranyl supergene minerals, representing a perfect natural laboratory for study of the alteration processes. This paper brings the results of our new mineralogical study concerned with this interesting mineral deposit.

The Medvědín uranium deposit (sometimes cited as Horní Mísečky deposit) occurs near a small village of Horní Mísečky. The locality is located 2.5 km northwest of the Špindlerův Mlýn in the Krkonoše Mts., northern Bohemia, Czech Republic. The Medvědín deposit occurs at an altitude of 1,000 to 1,200 m, in proximity of the Medvědín hill (1,235 m) (Figs 1–2).

The deposit was discovered by Krkonoše uranium prospection group (K-III, based in Vrchlabí) in 1952 by a detailed ground-based gamma prospecting. The radiometric anomalies coincided with outcrop structures trending NW–SE (Veselý 1982) nearby the summit of Medvědín, 1,235 m a.s.l. Trenches positioned on these structures revealed local accumulations of further unspecified secondary uranium minerals („uranium micas“) and uranium phosphates in tectonic zones up to several dm wide. Adit No. 1 (1,152 m a.s.l.) was driven in 1953 and a cluster of mineralized veins was intersected 40 to 80 m below surface. In 1954, adit No. 2 was opened from Horní Mísečky (later the third level, 1,064 m), which was driven 85 m deeper than the previous one. The adits were directed NE–SW, perpendicular to the supposed mineralized structure. When exploration works finished, the deposit was handed over to the local Trutnov branch of the Jáchymovské doly (JD) mining enterprise. After exploitation started at the levels of the adits, the JD enterprise opened the adit No. 11 and a shaft No. 6. These works revealed the deposit at the second, fourth and fifth levels, but as the situation at the fourth level indicated an increasing abundance of granite and aplite dykes, an idea of opening the fifth level was abandoned (Veselý 1982).

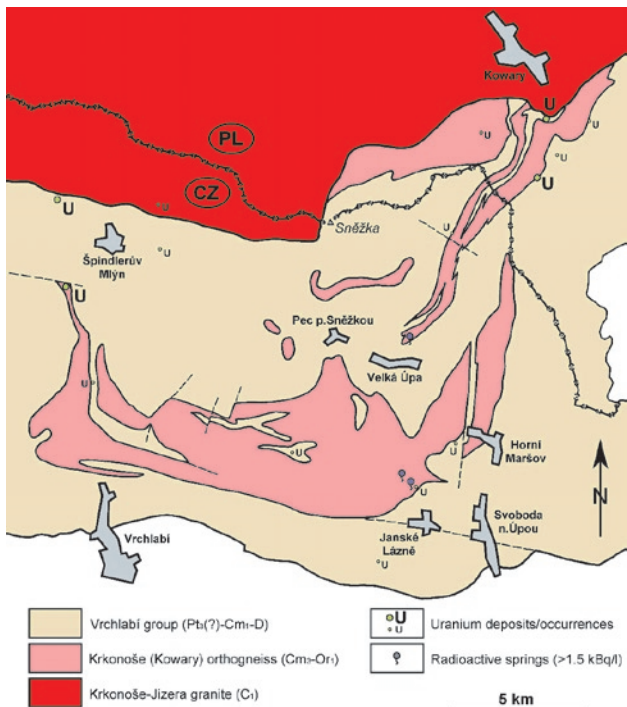


**Fig. 1** Schematic geological map of the Krkonoše Mts. area with uranium occurrences and deposits; Medvědín deposit is marked by 'U' north-west of Špindlerův Mlýn, drawing by V. Goliáš.

Altogether, 20 veins were examined, of which six contained economical uranium accumulations. During exploration until the middle of the year 1955, 72 000 m<sup>2</sup> of veins surface with a low productivity (only 0.08–0.57 kg U/m<sup>2</sup>) were discovered with ore estimate of 170.5 t of U in category C<sub>1</sub> + C<sub>2</sub>, 72.3 t of U in C<sub>1</sub>. In that time economic factors already became important. Mining was closed by JD enterprise in 1959 after production of ore equivalent to mere 24.5 t of U (Veselý 1982). This makes Medvědín the largest uranium deposit in the Krkonoše–Jizera granite pluton (Pluskal 1993) and, at the same time, the largest mining venture in the Czech part of the Krkonoše Mts.

At present, the dumps after mining are largely removed. The most extensive remains are parts of dumps (Fig. 3) along the brook Medvědinský potok in the Labský důl valley. Collapsed portals of adits Nos 1 and 2 occur there, which were driven from the Labský důl valley, but did not reach surface at places of the adits Nos 1 and 3 at Horní Mísečky. The shaft No. 6 collar was sealed. At the Horní Mísečky site, some buildings from the mining stage are preserved and used in part as recreation facilities. The portal of the adit No. 1 is sealed, the dump is removed and entry into the adit No. 3 is secured, as it was used temporarily for water supply.

## 2. Geological setting

The deposit is located in metamorphic rocks at the southern exocontact of the Krkonoše–Jizera Pluton (Fig. 1). Country-rock metapelites, metamorphosed to cordierite and andalusite hornfelses, belong to the newly defined Vrchlabí Group (Winchester et al. 2003).

The total width of the contact aureole is nearly 1.5 km. In proximity of the deposit is the Krkonoše–Jizera Pluton represented by even-grained biotite granodiorite, the so-called Harrachov granite (Klomínský 1969). The contact is trending 285–300° with a dip of 40–70° to the south (Veselý 1982). Fault structures are classified in three systems. Most important are NW–SE trending faults and they are represented by the Harrachov fault. Faults of the second system are sub-meridional to NE–SW and the last system shows E–W trend (Veselý 1982). Exploration resulted in finding three systems of veins and fractures: (1) 300–345° dipping 60–80° to the southwest, (2) 20–45° dipping to the northwest, and (3) veins trending 80–85° with a dip to the north (Veselý 1982).

Most of uranium mineralization was concentrated in the NW–SE trending veins including M3, M4, M5, M11, M12, and M18. Width of the veins varied from 2 to 20 cm, exceptionally to 80 cm. Vein filling consisted of tectonic clay, mylonite, quartz of three generations (white, grey hornstein-like quartz genetically linked with accumulations of uraninite and younger comb-structured quartz). Among the ore minerals chalcopyrite, hematite, pyrite, arsenopyrite, and supergene minerals of Cu, Fe and Mn were rarely found. Uranium mineralization was represented throughout the deposit by supergene uranium minerals: torbernite, autunite and „gummite“ (earlier described accumulations of massive uranyl oxides and hydroxides accompanied by uranyl silicates) with relics of a primary uraninite concentrated locally into separate ore lenses (Veselý 1982). The veins trending NE–SW were of a similar character but contained more tectonic clay and less quartz. The veins M16 and M17 were 2 to 50 cm thick. The vein M7 was examined as an example of the third

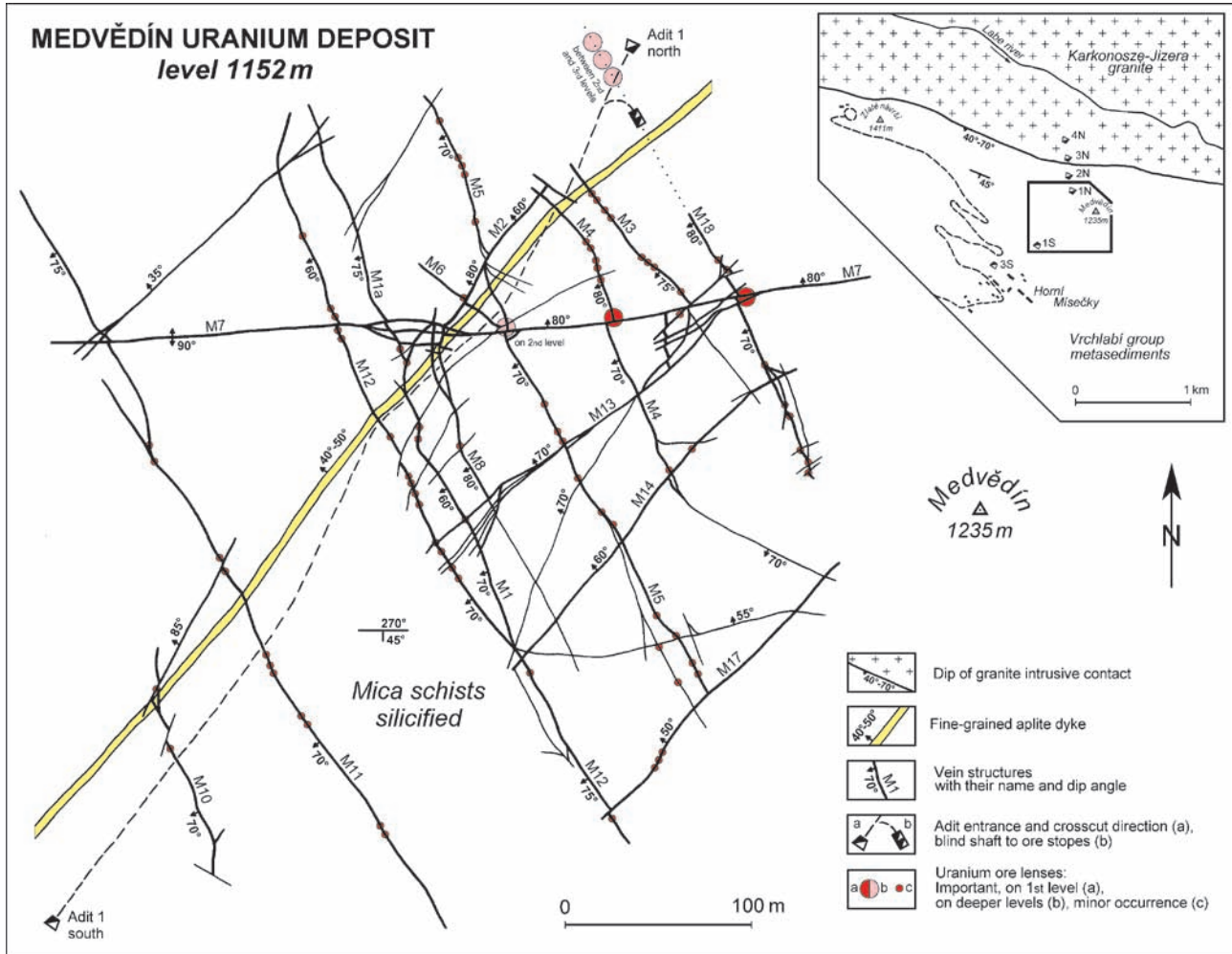


Fig. 2 Map of the Medvědín deposit showing topography, structural situation and mining objects (projection onto level of the gallery No.1), drawing by V. Goliáš.



Fig. 3 Remnants of the gallery No. 1 dump, located in the Labský důl valley; situation in June 2006, photo by B. Bureš.

set of veins. This set is relatively younger than the first two sets and offsets the NW-trending veins by two metres (Veselý 1982). The vein M18 trending 330–335° with a dip of 60–75° was most important as it yielded more than 50 % of total uranium exploited in this deposit. It was opened by mining works from the surface down to the fourth level. In the mineralized parts it was up to 1 m wide. Strukov (1958) suggested that a strong silicification and possibly the presence of aplite dykes were favourable factors in mineralization. Another favourable site was crossing of the NW–SE veins (M4, M12, M18) with NE–SW veins (M7) as at these places mineralization from the first set of veins penetrated into veins of the second set. In the youngest M7 vein mineralization is dislocated to a distance of 6 m from intersection with M18 vein (Veselý 1982).

Veselý (1982) compiled all available information on the deposit and its mineralization, using mainly data from the report by Strukov (1958). Recent studies on mineralogy of the deposit include a paper by Pauliš et al. (2005)

reporting uranophane from dumps at Medvědín and Plášil et al. (2006b) who studied supergene REE minerals and presented a list of identified supergene phases. In another contribution, Plášil et al. (2008) described bismuth mineralization from the gallery No. 3 at the Medvědín deposit. The present study is mainly based on the unpublished BSci. thesis by Plášil (2007).

### 3. Methodology

Binocular microscope was used for inspecting selected samples and to pick up minerals for identification. The surface morphology of samples was studied with the optical microscope Nikon SMZ1500 in combination with the digital camera Nikon DXM1200F, employed for photography in incandescent light.

The X-ray powder diffraction analysis was utilized for identification of unknown mineral phases. To minimize complicated shape of background due to classical glass sample holder, the samples studied were placed on the surface of flat silicon wafer from alcoholic or acetone suspension. Step-scanned powder diffraction data were collected using PANalytical X'Pert Pro diffractometer operating at 40 kV and 30 mA with a secondary monochromator producing  $\text{CuK}\alpha_{1,2}$  radiation with X'Celerator detector (X-ray diffraction Laboratory, Institute of Geochemistry, Mineralogy and Mineral Resources, Faculty of Science, Charles University, Prague). For identification of phases the search-match algorithm High-Score with PDF-2 database was used (ICDD 2003). Position of diffraction maxima and integral intensity of diffractions were refined with Xfit program using the profile function Pearson VII (Coelho and Cheary 1997). The integral intensities of individual maxima were normalized to the strongest diffraction maximum or, alternatively, relative intensities obtained with the program High-Score were used. Diffractions were indexed using theoretical data calculated with the program Powder Cell (Krause and Nolze 2000), using known crystal structure of individual phases. Unit-cell parameters were refined by the least-squares method (Burnham 1962). Specific conditions of diffraction data acquisition are presented in data tables for each studied mineral.

The electron microscope CamScan4 with an energy dispersive analyser Link ISIS 300 was used for study of qualitative chemical composition (Laboratory of Electron Microanalysis, Institute of Petrology and Structural Geology, Faculty of Science, Charles University in Prague). Natural surface of samples was used for analysis. Details of surface morphology of gold-coated samples were studied with the scanning electron microscope (SEM) Jeol JSM-6380 (Institute of Geology and Palaeontology, Charles University in Prague). Quantitative chemical

composition of minerals was analysed in polished thin sections with the electron microprobe Cameca SX100 (Joint Laboratory of the Masaryk University, Brno and the Czech Geological Survey). The analyses were acquired at 15 kV of accelerating voltage, 8–15 nA current and 2–20  $\mu\text{m}$  beam diameter. Analyses of highly hydrated uranyl minerals („uranium micas“) were carried out at beam current only 2 nA and a minimum beam diameter of 20  $\mu\text{m}$ . A smaller beam size results in unreliable values for copper and alkalis. The following lines and standards were used: K $\alpha$ : V (vanadinite), Ca and Fe (andradite), S (barite), Mg (forsterite), K, Si, Al (sanidine), Na (albite), Zn (ZnO), P, F (fluorapatite), Cl (NaCl); La: Y (YAG), La (LaB<sub>6</sub>), Ce (CeAl<sub>2</sub>), Sm (SmF<sub>3</sub>), Cu (dioptase), As (InAs); L $\beta$ : Ba (barite), Pr (PrF<sub>3</sub>), Nd (NdF<sub>3</sub>); M $\alpha$ : Pb (vanadinite), Th (ThO<sub>2</sub>); M $\beta$ : U (U), Bi (Bi). Peak counting times (CT) were 10–20 s for major elements, 40–60 s for minor to trace elements and counting time on background was  $\frac{1}{2}$  CT. The measured intensities were converted to element concentrations using the PAP program (Pouchou and Pichoir 1985). Elevated analytical totals of minerals containing a large amount of hydroxyl groups or crystal water are generally caused by water evaporation in high vacuum or heating of the analyzed spot by the electron beam. Lower analytical totals for some samples are primarily due to their porous nature or by poorly polished surface of soft or cryptocrystalline minerals.

The infrared spectra of the mineral samples (mixture with KBr powder) were recorded by micro diffuse reflectance method (DRIFTS) on a Nicolet Magna 760 FTIR spectrometer (range 4,000–600  $\text{cm}^{-1}$ , resolution 4  $\text{cm}^{-1}$ , 256 scans, Happ-Genzel apodization) equipped with Spectra Tech InspectIR micro FTIR accessory (Faculty of Science, Charles University, Prague). Explanations to infrared spectra: s strong, m medium, w weak, v very, sh shoulder, b broad. Thermal analysis of the samples was realized with Stanton Redcroft Thermobalance TG 750 (Institute of Chemical Technology, Prague), heating rate 10  $^{\circ}\text{C}.\text{min}^{-1}$ , dynamic air atmosphere, flow rate of 10  $\text{ml}.\text{min}^{-1}$ ; sample weight of parsonsite was 0.836 mg, sample weights of saléeites were 0.679 mg (saléeite I) and 0.973 mg (saléeite II).

### 4. Descriptions of minerals and their structural and chemical properties

#### 4.1. (REE)-supergene minerals

##### 4.1.1. Agardite-(Y) $(\text{Y,Ca})\text{Cu}_6(\text{AsO}_4)_3(\text{OH})_6 \cdot 3\text{H}_2\text{O}$

Agardite-(Y) forms light green crystalline coatings (Fig. 4) up to 1.5×2 cm in size. Botryoidal aggregates with spheres to 1 mm are composed of radiating transparent acicular crystals 0.1 to 0.3 mm long and 3 to 5  $\mu\text{m}$



**Fig. 4** Agardite-(Y) needle crystals on dark green pseudomalachite globular aggregates; width of photo 3.8 mm, photo J. Sejkora (Nikon SMZ1500).

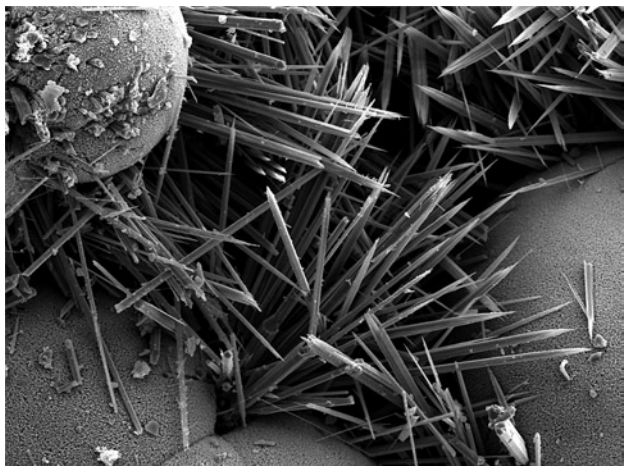


**Fig. 5** Acicular agardite-(Y) crystals on pseudomalachite globular aggregates; SEM photo J. Sejkora (Jeol JSM-6380), width of figure 197 µm.

thick (Fig. 5). Crystals of agardite-(Y) usually grow on older pseudomalachite and churchite-(Y) associated with tabular metatorbernite crystals.

Chemical composition (Tab. 1) of the studied agardite-(Y) shows extensive substitutions in cation sites. In addition to REE (up to 0.48 *apfu*), substantial contents of Ca (zálesíte, 0.23 *apfu*) or Pb components (plumboagardite, 0.23 *apfu*) may occur (Fig. 6). Anions ( $\text{PO}_4^{3-}$  up to 26 mol. %) and ( $\text{SiO}_4^{4-}$  up to 11 mol. %) may be present in addition to dominating ( $\text{AsO}_4^{3-}$ ) (64–66 mol. %) in the tetrahedral site. Empiric formula of agardite-(Y) from the Medvědín deposit is  $(\text{Ca}_{0.23}\text{Pb}_{0.20}\text{Bi}_{0.09}\text{Fe}_{0.03}(\text{REE})_{\Sigma 0.44}\text{Cu}_{6.43}[(\text{AsO}_4)_{1.95}(\text{PO}_4)_{0.75}(\text{SiO}_4)_{0.30}]_{\Sigma 3.00}(\text{OH})_{6.09} \cdot 3\text{H}_2\text{O}$ . This formula was calculated on the basis of  $(\text{As} + \text{P} + \text{Si}) = 3 \text{ apfu}$ , using average of three spot analyses (Plášil et al. 2006b).

**Tab. 1** Chemical composition of agardite-(Y)

	Mean	1	2	3
CaO	1.26	1.26	1.24	1.29
MgO	0.03	0.00	0.01	0.07
FeO	0.24	0.31	0.12	0.28
FeO	0.24	0.31	0.12	0.28
$\text{Bi}_2\text{O}_3$	2.04	2.28	1.83	2.02
PbO	4.31	4.46	5.04	3.43
$\text{Nd}_2\text{O}_3$	0.89	1.03	0.74	0.89
$\text{Sm}_2\text{O}_3$	0.32	0.28	0.12	0.55
$\text{Gd}_2\text{O}_3$	0.11	0.26	0.05	0.01
$\text{La}_2\text{O}_3$	0.92	1.18	0.78	0.82
$\text{Ce}_2\text{O}_3$	1.18	1.23	1.03	1.27
$\text{Pr}_2\text{O}_3$	0.23	0.39	0.14	0.16
$\text{Dy}_2\text{O}_3$	0.32	0.39	0.47	0.10
$\text{Y}_2\text{O}_3$	2.19	2.04	2.46	2.07
CuO	50.05	50.18	50.63	49.34
$\text{As}_2\text{O}_5$	21.96	22.12	21.38	22.39
$\text{P}_2\text{O}_5$	5.22	4.81	5.54	5.30
$\text{SiO}_2$	1.76	1.72	1.63	1.93
$\text{H}_2\text{O}^*$	10.66	10.89	10.78	10.31
Total	103.91	105.12	104.10	102.51
Ca	0.229	0.232	0.227	0.228
Mg	0.007	0.000	0.003	0.016
Fe	0.034	0.045	0.018	0.039
Bi	0.090	0.102	0.081	0.086
Pb	0.198	0.208	0.232	0.153
Nd	0.054	0.064	0.045	0.052
Sm	0.018	0.017	0.007	0.031
Gd	0.006	0.015	0.003	0.000
La	0.058	0.075	0.049	0.050
Ce	0.073	0.078	0.065	0.077
Pr	0.014	0.025	0.009	0.010
Dy	0.017	0.022	0.026	0.005
Y	0.198	0.187	0.224	0.182
$\Sigma \text{A site}$	0.996	1.068	0.989	0.931
Cu	6.425	6.552	6.555	6.169
$\Sigma \text{B site}$	6.425	6.552	6.555	6.169
As	1.951	1.999	1.916	1.937
P	0.750	0.704	0.804	0.743
Si	0.299	0.297	0.280	0.320
$\Sigma \text{T site}$	3.000	3.000	3.000	3.000
OH	6.09	6.55	6.33	5.38
$\text{H}_2\text{O}$	3.00	3.00	3.00	3.00

mean – based on 3 analyses

$\text{H}_2\text{O}^*$  – content of  $\text{H}_2\text{O}$  and OH was calculated on the basis of 3  $\text{H}_2\text{O}$  molecules in ideal agardite-(Y) formula and from charge balance

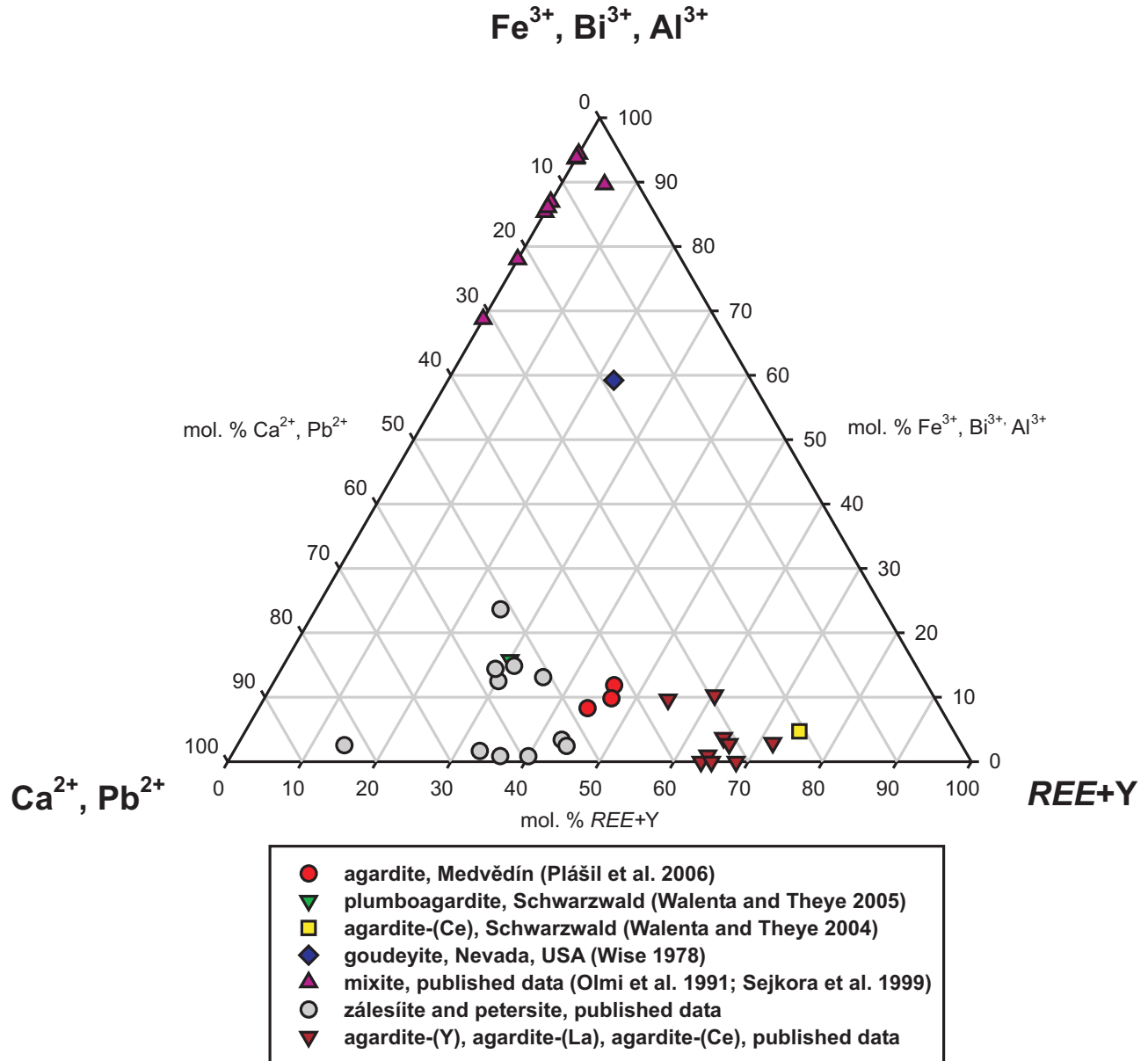


**Fig. 6** Ternary plot of A-site occupancy (atomic ratio) in mixite group minerals from Medvědín compared with other localities worldwide.

The X-ray powder diffraction pattern of the studied agardite-(Y) (Tab. 2) corresponds to published data for this mineral. Refined unit-cell parameters and the reduced volume of the unit-cell (Tab. 3) correlate with the substitution  $\text{AsP}_{\perp}$  (agardite–petersite). They are compared with published data for other members of the mixite group in Tab. 3. As seen in Fig. 7, the values of unit-cell parameter  $c$  and the unit-cell volume  $V$  permit to identify individual members of the group, perhaps except the Al-As dominated member goudeyite, for which relevant data are lacking.

Assignment of the IR absorption bands of agardite-(Y) from Medvědín is as follows (band positions in  $\text{cm}^{-1}$  units):  $\nu_1(\text{AsO}_4)^3-$  symmetric stretching vibrations 812 vs,

838 s sh;  $\nu_3(\text{AsO}_4)^3-$  antisymmetric stretching vibrations 918 m-s;  $\delta \text{M-OH}$  bending vibrations 1001 s, 1081 w sh;  $\delta(\text{AsO}_3\text{OH})^{2-}$  bending vibration, 1411 w b;  $\delta \text{H}_2\text{O}$  bending vibration 1634 w b;  $\nu \text{OH}$  stretching vibrations 3374 m-s b, 3490 m-s, sharp, 3624 w sh. A set of hydrogen bonds in the structure is assumed.

#### 4.1.2. Churchite-(Y) $\text{YPO}_4 \cdot 2\text{H}_2\text{O}$

Churchite-(Y) is of a common occurrence in the studied material. It forms rich aggregates covering surfaces of several or tens of  $\text{cm}^2$  and penetrates altered gangue as nearly monomineralic filling. The surface of whitish or

**Tab. 2** X-ray powder diffraction pattern of agardite-(Y)

$I_{rel}$	$d_{obs}$	$d_{calc}$	$h$	$k$	$l$
100	11.703	11.737	1	0	0
13	4.433	4.436	1	2	0
5	3.908	3.912	3	0	0
3	3.385	3.388	2	2	0
7	3.254	3.255	3	1	0
12	2.933	2.934	4	0	0
6	2.692	2.693	2	3	0
9	2.561	2.561	4	1	0
1	2.450	2.450	1	2	2
			3	2	1
1	2.218	2.218	2	4	0
2	2.108	2.108	1	5	0
1	1.9570	1.9561	6	0	0
1	1.9308	1.9295	4	3	0

range 5–50° 2θ, integrated step 0.02°/200 s, profile shape function Pearson VII

light grey churchite-(Y) aggregates has botryoidal shapes with semi-spherical aggregates nearly 0.2 mm across (Fig. 8). Acicular churchite-(Y) crystals are rare, they may reach length up to 0.5 mm (Fig. 9). Mineral is usually associated with metatorbernite (locally overgrowths), metaautunite, lemon yellow or grey saléeite, locally with orange acicular crystals of dewindtite and orange radiating aggregates of kasolite. The crystalline crusts of churchite-(Y) are often covered by orange-brown parsonsite crystals.

The chemical composition of churchite-(Y) from Medvědín is given in the Tab. 4. The empiric formula calculated on the basis of 2 *apfu* from average of eleven spot analyses is:



**Fig. 8** Spheroidal surface of white churchite-(Y) coatings on brown limonite; width of photo 2.2 mm, photo J. Sejkora (Nikon SMZ1500).

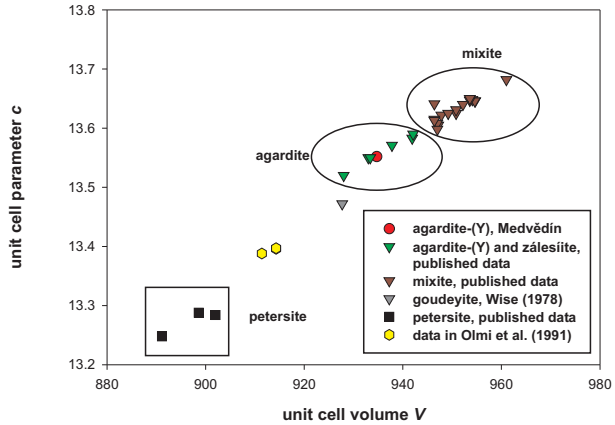


**Fig. 7** Binary plot of unit cell volume  $V$  vs. unit cell parameter  $c$  relation of the mixite group minerals.

$((\Sigma REE + Y)_{0.94} Ca_{0.06} Pb_{0.02})_{\Sigma 1.02} [(PO_4)_{0.96} (AsO_4)_{0.01}]_{\Sigma 0.97} \cdot 2H_2O$  (Plášil et al. 2006b). The distribution pattern of REE and Y contents (Fig. 10), normalized by chondrite values (Taylor and McLennan 1985), indicates an relative enrichment in *MREE* (Plášil et al. 2006b).

The X-ray powder diffraction pattern (Tab. 5) and refined unit-cell parameters of churchite-(Y) from Medvědín correspond very well to the literature data (Tab. 6).

Assignment of IR absorption bands of churchite-(Y) from the Medvědín deposit is as follows. Infrared spectrum of churchite-(Y) was published by Moenke (1966) and Sejkora et al. (1994). The studied spectrum is close to

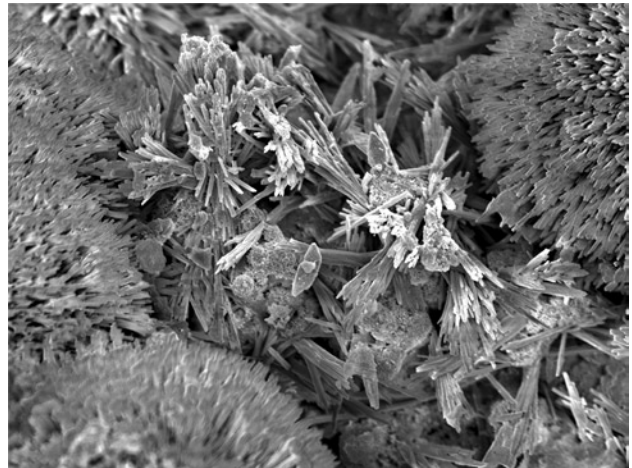


**Fig. 9** Globular aggregates of churchite-(Y) consisting of long needle crystals; SEM photo J. Plášil (Jeol JSM-6380), width of figure 140 µm.

**Tab. 3** Unit-cell parameters of agardite-(Y) from Medvědín compared with members of the mixite group from other localities (hexagonal space group  $P6_3/m$ )

Mineral	Chemical composition	Locality	Reference	a [Å]	c [Å]	V [Å <sup>3</sup> ]
agardite-(Y)	T: As>P	Medvědín	this paper	13.552(1)	5.877(3)	934.7(4)
agardite-(Y)	A: Y,Ca,H T: As	–	Dietrich et al. (1969)	13.55(5)	5.87(2)	933(10)
Ca-agardite	A: Ca <sub>0.4</sub> Y <sub>0.3</sub> ...	Synt.	Aruga and Nakai (1985)	13.583	5.895	941.9
agardite-(Y)	–	Jáchymov	Ondruš et al. (1997)	13.52(1)	5.86(1)	928
agardite-(Y)	–	–	PDF 025-0183	13.55	5.87	933.4
agardite-(Ce)	A: Ce T: As	–	Walenta and Theye (2004)	13.59(2)	5.89(1)	942.1
zálesíte	A: Ca T: (AsO <sub>4</sub> ) <sub>2</sub> (AsO <sub>3</sub> OH)	Zálesí	Sejkora et al. (1999)	13.571(1)	5.880(1)	937.8(2)
mixite	A: Bi,Ca,H T: As	–	Meraiter and Preisinger (1986)	13.646(2)	5.920(1)	954.7
mixite	–	H. Slavkov	Sejkora et al. (2006)	13.605(2)	5.909(1)	947.2
mixite	–	Jáchymov	Sejkora (1992)	13.608(5)	5.904(6)	947(1)
mixite	–	Smrkovec	Sejkora et al. (1997b)	13.6482(9)	5.9148(8)	954.1(1)
mixite	–	Cínochov	Sejkora and Šrein (1996)	13.598(6)	5.916(6)	947(1)
mixite	–	–	PDF 085-1729	13.646	5.920	954.6
goudeyite	A: Al; T: As	–	Wise (1978)	13.472(1)	5.902(4)	927.7
petersite-(Y)	A: Y T: P	Laurel Hill (USA)	Peacor and Dunn (1982)	13.288(5)	5.877(5)	898.6(8)
petersite-(Y)	–	–	PDF 044-1433	13.248	5.863	891.15
calcio-petersite	A: Ca, Y T: (PO <sub>3</sub> OH)	Domašov nad Bystřicí	Sejkora et al. (2005)	13.284(4)	5.902(4)	902.0(6)
agardite-(Y)	A: Y, Ca T: As	S. Lucia (Italy)	Olmi et al. (1991)	13.625	5.906	950.8
agardite-(Ce)	A: Ce, Ca T: As	S. Lucia (Italy)	Olmi et al. (1991)	13.622	5.901	947.8
zálesíte	A: Ca, Ce T: As	S. Lucia (Italy)	Olmi et al. (1991)	13.631	5.906	950.8
zálesíte-	A: Ca, Ce T: As>>P	S. Lucia (Italy)	Olmi et al. (1991)	13.615	5.900	946.4
zálesíte	A: Ca, Ce T: As>>P	S. Lucia (Italy)	Olmi et al. (1991)	13.641	5.898	946.4
zálesíte	A: Ca, Ce T: As	S. Lucia (Italy)	Olmi et al. (1991)	13.625	5.903	949.2
zálesíte	A: Ca, Ce, Bi, Pb T: As>>P	M. Cidro (Italy)	Olmi et al. (1991)	13.650	5.915	953.6
agardite-(Y)	A: Y, Al, Ca T: As>>P	M. Cidro (Italy)	Olmi et al. (1991)	13.647	5.912	953.6
agardite-(Ce)	A: Ce, Bi, Al, Pb, Ca T: As	M. Cidro (Italy)	Olmi et al. (1991)	13.682	5.930	961.0
agardite-(Y)	A: Y, Ca, Bi, Pb T: As>>P	M. Cidro (Italy)	Olmi et al. (1991)	13.650	5.915	953.6
zálesíte	A: Ca, Y, Bi T: As	M. Cidro (Italy)	Olmi et al. (1991)	13.613	5.899	946.4
Ca-rich petersite	A: Y, Ca T: P>As	S. Duchesa (Italy)	Olmi et al. (1991)	13.396	5.876	914.3
agardite-(La)	A: La, Pb, Ca T: As>>P	S. Duchesa (Italy)	Olmi et al. (1991)	13.640	5.913	952.2
agardite-(Y)	A: Y, Pb, Ca T: As>>P	S. Duchesa (Italy)	Olmi et al. (1991)	13.618	5.900	947.8
agardite-(Y)	A: Y, Pb T: As>P	S. Duchesa (Italy)	Olmi et al. (1991)	13.481	5.905	930.0
zálesíte	A: Ca, Y T: As>>P	S. Duchesa (Italy)	Olmi et al. (1991)	13.633	5.906	950.8
agardite-(Y)	A: Y, Ca T: As>P	S. Duchesa (Italy)	Olmi et al. (1991)	13.623	5.902	947.8
Ca-rich petersite	A: Y, Ca T: P>As	S. Duchesa (Italy)	Olmi et al. (1991)	13.397	5.878	914.3
agardite-(Y)	A: Y, Ca T: As>P	S. Duchesa (Italy)	Olmi et al. (1991)	13.39	5.87	911.40

ideal chemical formula for the mixite group members:  $\text{AB}_6\text{T}_3\text{OH}_6 \cdot 3\text{H}_2\text{O}$ ; in the column "Chemical composition" are mentioned elements present in the mineral in specific crystallochemical positions

**Tab. 4** Chemical composition of churchite-(Y)

	Mean	1	2	3	4	5	6	7	8	9	10	11
CaO	1.48	1.46	1.59	1.58	1.51	1.42	1.09	0.97	1.11	1.84	1.95	1.70
FeO	0.05	0.17	0.11	0.19	0.04	0.00	0.00	0.00	0.00	0.00	0.00	0.00
UO <sub>2</sub>	0.58	0.72	0.73	0.84	0.85	0.77	0.61	0.63	0.62	0.17	0.19	0.26
La <sub>2</sub> O <sub>3</sub>	0.34	0.40	0.35	0.35	0.36	0.36	0.30	0.26	0.28	0.38	0.33	0.38
Ce <sub>2</sub> O <sub>3</sub>	2.64	2.69	2.74	3.38	3.10	3.08	2.48	2.45	2.89	2.13	1.74	2.35
Pr <sub>2</sub> O <sub>3</sub>	0.56	0.55	0.57	0.74	0.57	0.59	0.57	0.57	0.62	0.47	0.40	0.51
Nd <sub>2</sub> O <sub>3</sub>	3.88	3.71	3.79	4.86	4.00	4.04	3.79	3.97	4.40	3.49	2.97	3.68
Sm <sub>2</sub> O <sub>3</sub>	2.61	2.22	2.27	2.95	2.52	2.69	3.17	3.25	3.63	1.93	1.82	2.21
Eu <sub>2</sub> O <sub>3</sub>	2.00	1.98	1.96	2.45	1.81	2.11	2.59	2.48	2.70	1.25	1.26	1.37
Gd <sub>2</sub> O <sub>3</sub>	4.85	4.33	4.38	5.52	4.80	4.78	4.95	5.15	5.76	4.55	4.05	5.11
Tb <sub>2</sub> O <sub>3</sub>	0.77	0.74	0.73	0.87	0.65	0.80	0.94	0.91	0.86	0.64	0.63	0.73
Dy <sub>2</sub> O <sub>3</sub>	3.71	3.26	3.22	4.11	3.43	3.65	4.15	4.40	4.57	3.43	3.05	3.55
Ho <sub>2</sub> O <sub>3</sub>	0.57	0.57	0.57	0.73	0.50	0.58	0.60	0.51	0.50	0.61	0.57	0.52
Er <sub>2</sub> O <sub>3</sub>	1.63	1.50	1.47	1.82	1.49	1.65	1.65	1.64	1.74	1.72	1.43	1.78
Yb <sub>2</sub> O <sub>3</sub>	0.90	0.82	0.78	0.91	0.96	0.95	1.14	1.00	1.18	0.74	0.70	0.78
Y <sub>2</sub> O <sub>3</sub>	28.30	28.14	29.13	27.45	27.16	27.54	26.76	26.07	26.39	30.53	31.57	30.57
SO <sub>3</sub>	0.16	0.13	0.17	0.12	0.13	0.18	0.20	0.14	0.22	0.18	0.13	0.15
P <sub>2</sub> O <sub>5</sub>	28.43	29.65	29.32	23.86	28.39	28.55	28.45	28.43	26.35	30.19	29.39	30.09
As <sub>2</sub> O <sub>5</sub>	0.58	0.67	0.69	0.80	0.89	0.80	0.70	0.74	0.83	0.11	0.10	0.08
H <sub>2</sub> O*	15.01	15.20	15.32	14.31	14.92	15.06	14.84	14.69	14.58	15.44	15.18	15.53
total	99.04	98.91	99.87	97.84	98.10	99.59	98.99	98.25	99.23	99.81	97.46	101.34
Ca	0.063	0.062	0.067	0.071	0.065	0.061	0.047	0.043	0.049	0.077	0.083	0.070
Fe	0.002	0.005	0.004	0.007	0.001	0.000	0.000	0.000	0.000	0.000	0.000	0.000
Pb	0.015	0.018	0.019	0.021	0.023	0.018	0.013	0.012	0.015	0.007	0.008	0.007
U	0.005	0.006	0.006	0.008	0.008	0.007	0.005	0.006	0.006	0.002	0.002	0.002
La	0.005	0.006	0.005	0.005	0.005	0.005	0.004	0.004	0.004	0.005	0.005	0.005
Ce	0.039	0.039	0.039	0.052	0.046	0.045	0.037	0.037	0.044	0.030	0.025	0.033
Pr	0.008	0.008	0.008	0.011	0.008	0.009	0.008	0.008	0.009	0.007	0.006	0.007
Nd	0.056	0.052	0.053	0.073	0.057	0.057	0.055	0.058	0.065	0.048	0.042	0.051
Sm	0.036	0.030	0.031	0.043	0.035	0.037	0.044	0.046	0.051	0.026	0.025	0.029
Eu	0.028	0.027	0.026	0.035	0.025	0.029	0.036	0.035	0.038	0.017	0.017	0.018
Gd	0.064	0.057	0.057	0.077	0.064	0.063	0.066	0.070	0.078	0.059	0.053	0.065
Tb	0.010	0.010	0.009	0.012	0.009	0.011	0.012	0.012	0.012	0.008	0.008	0.009
Dy	0.048	0.041	0.041	0.055	0.044	0.047	0.054	0.058	0.061	0.043	0.039	0.044
Ho	0.007	0.007	0.007	0.010	0.006	0.007	0.008	0.007	0.007	0.007	0.007	0.006
Er	0.021	0.019	0.018	0.024	0.019	0.021	0.021	0.021	0.023	0.021	0.018	0.022
Yb	0.011	0.010	0.009	0.012	0.012	0.012	0.014	0.012	0.015	0.009	0.008	0.009
Y	0.602	0.591	0.607	0.612	0.581	0.584	0.576	0.566	0.578	0.631	0.664	0.628
ΣA site	1.019	0.988	1.006	1.128	1.008	1.013	1.000	0.995	1.055	0.997	1.010	1.005
P	0.961	0.990	0.972	0.847	0.966	0.963	0.973	0.982	0.918	0.993	0.983	0.984
As	0.012	0.014	0.014	0.018	0.019	0.017	0.015	0.016	0.018	0.002	0.002	0.002
ΣT site	0.973	1.004	0.986	0.865	0.985	0.980	0.988	0.998	0.936	0.995	0.985	0.986
H <sub>2</sub> O	2.00	2.00	2.00	2.00	2.00	2.00	2.00	2.00	2.00	2.00	2.00	2.00

mean – based on 11 analyses of churchite-(Y); H<sub>2</sub>O\* – H<sub>2</sub>O content calculated on the basis of 2 H<sub>2</sub>O molecules in ideal churchite-(Y) formula

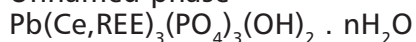
**Tab. 5** Powder diffraction pattern of churchite-(Y)

$I_{rel}$	$d_{obs}$	$d_{calc}$	$h$	$k$	$l$
61	7.531	7.541		0	2
3	5.244	5.240		1	1
9	4.707	4.710		-1	1
100	4.205	4.206		0	2
12	3.772	3.770		0	4
5	3.744	3.738		1	3
6	3.074	3.077		1	1
64	3.024	3.025		0	4
11	2.834	2.839		-2	2
4	2.620	2.620		2	2
6	2.538	2.534		0	0
5	2.510	2.514		0	6
4	2.479	2.479		-2	0
8	2.448	2.449		-1	3
7	2.403	2.402		0	2
1	2.377	2.378		-2	4
8	2.175	2.176		1	5
3	2.102	2.103		0	4
3	2.072	2.072		-2	4
7	2.054	2.054		-1	5
6	1.9753	1.9760		-1	7
6	1.8707	1.8688		2	6
14	1.7835	1.7845		0	6
	1.7835			-2	2
8	1.7673	1.7651		-2	6
6	1.6500	1.6504		-2	4
3	1.6066	1.6058		-2	8

range 9–60° 2Θ, integrated step 0.02°/300 s, profile shape function Pearson VII

both cited spectra in the range of 1000–3400 cm<sup>-1</sup>. Some differences are in the band position of the v1 (PO<sub>4</sub>)<sup>3-</sup>. The spectrum was not recorded in the region lower than 900 cm<sup>-1</sup>.

#### 4.1.3. Unnamed phase



A preliminary description of this new phase from Medvědín was presented by Plášil et al. (2006b). The unnamed phase forms botryoidal aggregates with irregular, imperfectly

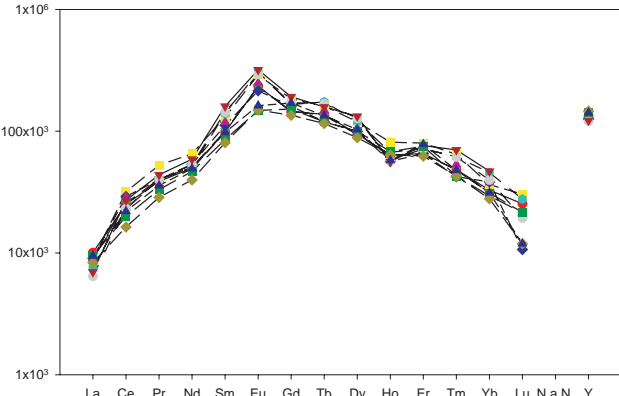


**Fig. 10** Contents of REE and Y in churchite-(Y), normalised by chondrite (according to Taylor and McLennan 1985); different colours distinguish each series of point analyses (in Plášil et al. 2006).

crystallized surface, with the size of semi-spherical units up to 0.1 mm. The aggregates form coatings several cm<sup>2</sup> in size, which are usually overgrown by younger churchite-(Y), covered in turn by crystalline aggregates of parsonsite (Fig. 11). The unnamed phase has a red-brown colour and is weakly transparent with dark red colour in thin fragments. It has a waxy to vitreous lustre.

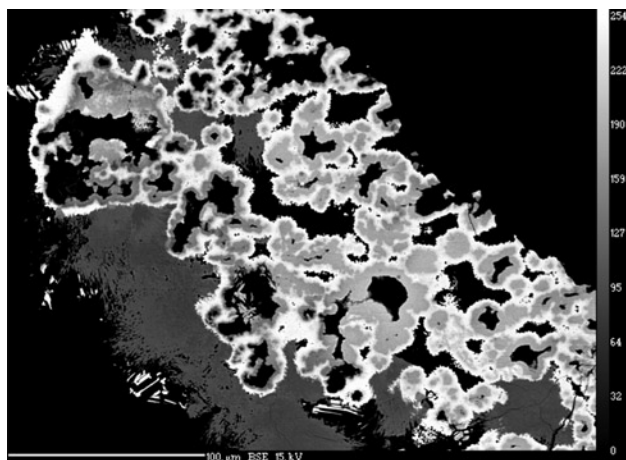


**Fig. 11** New unnamed phase Pb(Ce,REE)(PO<sub>4</sub>)<sub>3</sub>(OH)<sub>2</sub> · nH<sub>2</sub>O coatings consisting of central, darker parts (light grey) and brighter rims (white). The new phase is overgrown by churchite-(Y) aggregates (grey). BSE photo R. Škoda (Cameca SX100).

**Tab. 6** Refined unit-cell parameters of churchite-(Y) (transformed for monoclinic space group C2/c)

Locality	Reference	$a$ [Å]	$b$ [Å]	$c$ [Å]	$\beta$ [°]	$V$ [Å <sup>3</sup> ]
Medvědín	this paper	6.186(5)	15.082(6)	5.610(4)	115.39(4)	472.8(7)
synt.	Kohlmann et al. (1994)	6.149	15.006	5.578	115.51	464.52
Rýžovíště	Sejkora et al. (1994)*	5.600(5)	15.076(8)	6.180(8)	115.47(6)	470.9
Jáchymov	Ondruš et al. (1997)	6.36	15.18	5.61	117.77	479

\*only indexed pattern

**Tab. 7** Chemical composition of the new unnamed phase  $\text{Pb}(\text{Ce},\text{REE})_3(\text{PO}_4)_3(\text{OH})_2 \cdot n\text{H}_2\text{O}$ 

	rims				centres of aggregates					
	Mean <sup>1)</sup>	1	2	3	4	Mean <sup>2)</sup>	5	6	7	8
PbO	28.51	27.96	27.00	30.19	30.63	26.17	25.67	27.13	24.85	27.19
CaO	0.60	0.61	0.69	0.58	0.57	0.82	0.80	0.96	0.88	0.55
FeO	0.98	0.44	1.39	0.23	0.92	8.39	7.16	8.46	10.59	5.93
Al <sub>2</sub> O <sub>3</sub>	0.24	0.11	0.43	0.17	0.27	2.36	2.61	2.73	2.80	0.75
UO <sub>2</sub>	3.61	3.38	4.31	3.15	2.63	2.53	2.03	3.44	2.40	2.98
La <sub>2</sub> O <sub>3</sub>	1.60	1.80	1.65	1.86	1.54	1.16	0.98	1.27	1.17	1.29
Ce <sub>2</sub> O <sub>3</sub>	11.27	13.03	10.50	11.36	11.24	10.09	10.78	10.19	7.61	10.62
Pr <sub>2</sub> O <sub>3</sub>	1.58	1.64	1.56	1.71	1.46	1.33	1.58	1.25	1.25	1.50
Nd <sub>2</sub> O <sub>3</sub>	8.10	8.20	7.89	8.87	7.59	6.66	7.46	6.64	6.33	7.46
Sm <sub>2</sub> O <sub>3</sub>	2.36	2.18	2.50	2.44	2.39	2.05	2.49	1.77	2.01	2.30
Eu <sub>2</sub> O <sub>3</sub>	0.78	0.64	0.74	0.83	0.86	0.47	0.58	0.27	0.55	0.66
Gd <sub>2</sub> O <sub>3</sub>	3.05	2.73	3.07	3.37	3.19	2.59	2.59	2.45	2.68	2.85
Tb <sub>2</sub> O <sub>3</sub>	0.25	0.22	0.20	0.31	0.23	0.01	0.00	0.00	0.00	0.06
Dy <sub>2</sub> O <sub>3</sub>	0.94	0.79	0.96	1.10	1.02	0.71	0.55	0.66	0.82	1.01
Ho <sub>2</sub> O <sub>3</sub>	0.22	0.14	0.22	0.17	0.30	0.21	0.26	0.18	0.20	0.19
Er <sub>2</sub> O <sub>3</sub>	0.43	0.45	0.44	0.41	0.55	0.33	0.27	0.32	0.44	0.42
Yb <sub>2</sub> O <sub>3</sub>	0.25	0.26	0.32	0.32	0.21	0.22	0.19	0.16	0.31	0.26
Y <sub>2</sub> O <sub>3</sub>	4.28	2.90	2.99	6.63	4.67	5.53	4.96	5.80	5.09	5.42
P <sub>2</sub> O <sub>5</sub>	22.75	23.64	22.61	23.66	23.45	19.49	19.44	18.85	18.83	21.06
As <sub>2</sub> O <sub>5</sub>	1.70	2.04	1.63	1.45	1.50	1.42	1.53	1.32	1.20	1.90
SiO <sub>2</sub>	0.19	0.11	0.58	0.04	0.13	4.45	5.31	5.11	5.29	0.87
SO <sub>3</sub>	0.02	0.01	0.08	0.00	0.00	0.01	0.05	0.00	0.00	0.00
V <sub>2</sub> O <sub>5</sub>	0.00	0.02	0.00	0.00	0.00	0.04	0.04	0.06	0.04	0.05
Total	93.72	93.30	91.76	98.85	95.35	97.05	97.33	99.02	95.34	95.32
Pb	0.377	0.355	0.352	0.390	0.397	0.325	0.305	0.335	0.306	0.371
Ca	0.032	0.031	0.036	0.030	0.029	0.040	0.038	0.047	0.043	0.030
ΣA site	0.408	0.386	0.388	0.420	0.426	0.366	0.343	0.382	0.349	0.401
Fe	0.041	0.017	0.056	0.009	0.037	0.322	0.265	0.325	0.405	0.251
Al	0.014	0.006	0.025	0.010	0.015	0.127	0.136	0.148	0.151	0.045
U	0.039	0.035	0.046	0.034	0.028	0.026	0.020	0.035	0.024	0.034
La	0.029	0.031	0.029	0.033	0.027	0.020	0.016	0.021	0.020	0.024
Ce	0.202	0.225	0.186	0.200	0.198	0.170	0.174	0.171	0.127	0.197
Pr	0.029	0.028	0.028	0.030	0.026	0.022	0.025	0.021	0.021	0.028
Nd	0.142	0.138	0.137	0.152	0.131	0.110	0.118	0.109	0.103	0.135
Sm	0.040	0.035	0.042	0.040	0.040	0.033	0.038	0.028	0.032	0.040
Eu	0.013	0.010	0.012	0.014	0.014	0.007	0.009	0.004	0.009	0.011
Gd	0.050	0.043	0.049	0.054	0.051	0.040	0.038	0.037	0.041	0.048
Tb	0.004	0.003	0.003	0.005	0.004	0.000	0.000	0.000	0.000	0.001
Dy	0.015	0.012	0.015	0.017	0.016	0.011	0.008	0.010	0.012	0.016
Ho	0.003	0.002	0.003	0.003	0.005	0.003	0.004	0.003	0.003	0.003
Er	0.007	0.007	0.007	0.006	0.008	0.005	0.004	0.005	0.006	0.007
Yb	0.004	0.004	0.005	0.005	0.003	0.003	0.003	0.002	0.004	0.004
Y	0.112	0.073	0.077	0.169	0.120	0.136	0.117	0.142	0.124	0.146
ΣB site	0.743	0.669	0.720	0.781	0.723	1.035	0.975	1.061	1.082	0.990
P	0.946	0.944	0.928	0.962	0.956	0.762	0.727	0.732	0.728	0.904
As	0.044	0.050	0.041	0.036	0.038	0.035	0.035	0.032	0.029	0.050
Si	0.009	0.005	0.028	0.002	0.006	0.202	0.235	0.234	0.242	0.044
S	0.001	0.000	0.003	0.000	0.000	0.000	0.002	0.000	0.000	0.000
V	0.000	0.001	0.000	0.000	0.000	0.001	0.001	0.002	0.001	0.002
Σ T site	1.000	1.000	1.000	1.000	1.000	1.000	1.000	1.000	1.000	1.000

Mean<sup>1)</sup> – based on 9 analyses; 1–4 – representative analyses of rims of the aggregatesMean<sup>2)</sup> – based on 6 analyses; 5–8 – representative analyses of central parts of aggregates

The chemical analyses presented by Plášil et al. (2006b) can be re-calculated to an idealized formula  $A^{2+}B^{3+}_3(PO_4)_3(OH)_2 \cdot nH_2O$ , with A-position = Pb and Ca, B-position = REE accompanied by Y, Al (and U, Fe). Cerium is dominating. The BSE imaging and spot chemical analyses resulted in recognition of two chemically distinct varieties of this mineral phase with differences in chemical composition. Main differences concern Fe and Si abundances. Based on P + As + Si = 3, the older central parts of aggregates, which appear darker in BSE image can be characterized by the following formula:

$(Pb_{0.98}Ca_{0.12})_{\Sigma 1.10}((\Sigma REE+Y)_{1.69}Fe_{0.97}Al_{0.38}U_{0.08})_{\Sigma 3.12}[(PO_4)_{2.29}(SiO_4)_{0.61}(AsO_4)_{0.10}]_{\Sigma 3.00}(OH)_{2.03} \cdot nH_2O$  (average of 7 spot analyses) (Tab. 7). The younger marginal parts of aggregates, based on P + As + Si = 3, yield empiric formula:  $(Pb_{1.13}Ca_{0.10})_{\Sigma 1.23}((\Sigma REE+Y)_{2.00}U_{0.12}Fe_{0.12}Al_{0.04})_{\Sigma 2.28}[(PO_4)_{2.84}(AsO_4)_{0.13}(SiO_4)_{0.03}]_{\Sigma 3.00}(OH)_{0.39} \cdot nH_2O$  (average of 9 spot analyses) (Tab. 7).

## 4.2. Supergene uranyl minerals

### 4.2.1. Autunite/metaautunite $Ca(UO_2)_2(PO_4)_2 \cdot 10-12H_2O/(Ca(UO_2)_2(PO_4)_2 \cdot 6-7H_2O$

In relatively dry environment autunite readily dehydrates to metaautunite. This proceeds as a partly reversible reaction, depending on local temperature and humidity. Dehydration results in escape of water molecules from layered structure of autunite and in interaction of Ca ions with oxygen in uranyl groups (Locock 2004). The same author gave for synthetic autunite the content of 11 H<sub>2</sub>O; dehydration of synthetic autunite according to Sowder et al. (2000) results in a metaphase containing 7 H<sub>2</sub>O. Makarov and Ivanov (1960) gave for natural autunite the water content of 6 H<sub>2</sub>O. It is uncertain whether the dehydration of autunite yields a phase with a single type of meta-structure. Natural metaautunites probably include material corresponding to several dehydration steps. This may be the reason why the structure of natural metaautunite has not been solved yet.

Autunite, which in the course of time spontaneously alters to metaautunite, is relatively abundant in the material studied. It forms light green tabular crystals up to 3 mm across. Dehydration of the crystals kept under decreased humidity conditions proceeds relatively quickly, which is seen as dim surface of crystals. Metaautunite crystals, in contrast to autunite, are notably dull and opaque. Both minerals show very intense green luminescence in short-wave UV radiation (254 nm). Autunite and metaautunite occur most frequently in association with metatorbernite and uranophane in quartz gangue (M 12 vein). They occur in crystals up to 3 mm in size deposited on light

**Tab. 8** Chemical composition of metaautunite

	mean	1	2	3
CaO	5.54	4.91	6.33	5.37
FeO	0.06	0.13	0.04	0.00
BaO	0.18	0.23	0.08	0.22
CuO	0.75	1.60	0.03	0.63
SiO <sub>2</sub>	0.08	0.09	0.13	0.01
As <sub>2</sub> O <sub>5</sub>	0.65	1.17	0.12	0.64
P <sub>2</sub> O <sub>5</sub>	17.19	16.76	18.37	16.43
UO <sub>3</sub>	70.82	70.15	71.44	70.86
H <sub>2</sub> O*	13.16	13.18	13.68	12.8
Total	108.41	108.23	110.23	106.96
Ca	0.792	0.707	0.862	0.808
Fe	0.006	0.014	0.004	0.000
Ba	0.009	0.012	0.004	0.012
Cu	0.077	0.162	0.003	0.066
ΣA site	0.885	0.895	0.873	0.886
Si	0.010	0.012	0.017	0.002
As	0.046	0.082	0.008	0.047
P	1.944	1.905	1.975	1.951
ΣT site	2.000	2.000	2.000	2.000
U	1.991	1.978	1.906	2.089
H <sub>2</sub> O	6.00	6.00	6.00	6.00

mean based on 3 spot analyses

H<sub>2</sub>O\* – H<sub>2</sub>O content was calculated on the basis of 6 H<sub>2</sub>O molecules in ideal metaautunite formula (Makarov and Ivanov 1960)

**Tab. 9** Powder diffraction pattern of metaautunite

<i>I<sub>rel</sub></i>	<i>d<sub>obs</sub></i>	<i>d<sub>calc</sub></i>	<i>h</i>	<i>k</i>	<i>l</i>
100	8.456	8.460	0	0	2
3	5.376	5.381	1	0	2
1	4.934	4.931	1	1	0
<1	4.262	4.260	1	1	2
11	4.228	4.230	0	0	4
10	3.616	3.617	1	0	4
2	3.493	3.487	2	0	0
2	3.229	3.224	2	0	2
1	2.931	2.926	1	2	2
1	2.818	2.820	0	0	6
4	2.617	2.614	1	0	6
<1	2.510	2.510	2	1	4
1	2.202	2.205	1	3	0
14	2.115	2.115	0	0	8
1	2.025	2.024	1	0	8
1	1.9435	1.9438	1	1	8

range 7–50° 2θ, integrated step 0.02°/250s, profile shape function Pearson VII

**Tab. 10** Refined unit-cell parameters of metaautunite (tetragonal space group  $P4/n$ )

Medvědín (this paper)	Makarov and Ivanov (1960)	Rýžoviště, Sejkora et al. (1994)	Slavkovice, Sejkora et al. (1997a)
$a$ [Å]	6.974(3)	6.96	6.982(5)
$c$ [Å]	16.920(6)	16.80	16.93(1)
$V$ [Å <sup>3</sup> ]	822.9(7)	813.8	—
			841.1(1)

grey crystals of quartz grading to light-coloured smoky quartz or on crystalline aggregates of churchite-(Y). In contrast to torbernite, autunite from Medvědín shows simple tabular crystal morphology.

(Meta-) autunite from Medvědín contains nearly always an isomorphous admixture of Cu and a small proportion of  $(PO_4)^{3-}$  anions is substituted by  $(AsO_4)^{3-}$  (autunite–uranospinite series). Recalculation of an average for three spot analyses (Tab. 8) on the basis of P + As + Si = 2 *apfu* and 6 H<sub>2</sub>O *pfu*, following Makarov and Ivanov (1960), results in the following empiric formula:  $(Ca_{0.79}Cu_{0.08}Ba_{0.01}Fe_{0.01})_{\Sigma 0.89}(UO_2)_{1.99}[(PO_4)_{1.94}(AsO_4)_{0.05}(SiO_4)_{0.01}]_{\Sigma 2.00} \cdot 6H_2O$ .

The X-ray powder diffraction pattern of metaautunite from Medvědín (Tab. 9) corresponds well to data in the ICDD PDF-2 database. It was indexed using the data from metatorbernite crystal structure (Locock and Burns 2003), with substitution of Ca for Cu, and using unit-cell parameters by Makarov and Ivanov (1960). The refined unit-cell parameters of metaautunite from Medvědín correspond to published data (Tab. 10); however, Sejkora et al. (1997a) gave notably higher value of  $c$  parameter for metaautunite from the Slavkovice deposit.

#### 4.2.2. Kasolite Pb(UO<sub>2</sub>)SiO<sub>4</sub> · H<sub>2</sub>O

Radiating aggregates of kasolite up to 3 mm across at the Medvědín deposit are of orange colour and waxy lustre (Fig. 12). They occur in association with parsonsite, metatorbernite, saléeite, dewindtite, churchite-(Y) and uranophane. Kasolite also forms massive coatings of body orange colour, which support sheets of acicular uranophane. Massive kasolite overgrown by light yellow acicular uranophane in spheroidal aggregates is less common.

Locally, kasolite forms crystalline aggregates protruding into cavities a few mm across. Kasolite is also identified as a component of „gumite“ or its yellow parts, whereas orange to red-brown parts correspond to uranophane.

The quantitative chemical analyses of kasolite from Medvědín (Tab. 11) indicate a significant Pb deficiency: only 0.84–0.89 *apfu* in comparison with the ideal formula. This deficiency is partly balanced by entry of K (0.04–0.05 *apfu*) and Ca (0.01 *apfu*) into this structural position. A similar Pb deficiency was observed by Sej-



**Fig. 12** Radiating aggregates of kasolite, width of photo 2.5 mm, photo J. Sejkora (Nikon SMZ1500).

**Tab. 11** Chemical composition of kasolite

	Mean	1	2	3	4
K <sub>2</sub> O	0.37	0.34	0.32	0.40	0.41
CaO	0.09	0.09	0.10	0.08	0.09
PbO	32.71	33.40	33.04	32.79	31.59
SiO <sub>2</sub>	10.08	10.20	10.02	10.09	10.01
P <sub>2</sub> O <sub>5</sub>	0.07	0.02	0.04	0.04	0.18
UO <sub>3</sub>	52.94	53.36	53.03	52.60	52.76
H <sub>2</sub> O*	3.08	3.12	3.12	3.06	3.02
Total	99.33	100.53	99.66	99.06	98.06
K	0.046	0.043	0.041	0.050	0.052
Ca	0.009	0.009	0.010	0.008	0.010
Pb	0.869	0.880	0.885	0.872	0.837
ΣA site	0.924	0.932	0.936	0.930	0.899
Si	0.994	0.999	0.997	0.997	0.985
P	0.006	0.001	0.003	0.003	0.015
ΣT site	1.000	1.000	1.000	1.000	1.000
U	1.097	1.097	1.109	1.091	1.091
H <sub>2</sub> O	1.00	1.00	1.00	1.00	1.00

mean based on 4 spot analyses

H<sub>2</sub>O\*—H<sub>2</sub>O contents calculated assuming one H<sub>2</sub>O molecule in ideal kasolite formula (Rosenzweig and Ryan 1977)

**Tab. 12** Powder diffraction pattern of kasolite

$I_{rel}$	$d_{obs}$	$d_{calc}$	$h$	$k$	$l$	$I_{rel}$	$d_{obs}$	$d_{calc}$	$h$	$k$	$l$
31	6.507	6.505	1	0	0	5	2.123	2.121	-3	1	1
2	6.426	6.424	0	0	2	6	2.108	2.107	1	1	5
<1	6.115	6.071	0	1	1	1	2.072	2.068	3	1	0
1	5.256	5.253	-1	0	2	<1	2.063	2.059	-3	1	3
<1	4.735	4.729	1	1	0	1	2.048	2.050	2	0	4
2	4.220	4.204	1	1	1	<1	2.033	2.029	-2	0	6
1	4.196	4.177	-1	1	2	1	1.9753	1.9715	3	1	1
3	4.099	4.100	1	0	2	<1	1.9493	1.9465	-2	1	6
1	3.531	3.523	1	1	2	4	1.9180	1.9169	-2	2	5
1	3.509	3.497	-1	1	3	<1	1.9006	1.9012	1	0	6
100	3.255	3.252	2	0	0	1	1.8767	1.8688	-3	2	2
5	3.214	3.212	0	0	4	<1	1.8584	1.8533	-1	2	6
1	3.067	3.044	1	2	0	3	1.8500	1.8477	3	1	2
4	2.916	2.911	0	1	4	<1	1.8232	1.8184	0	2	6
<1	2.899	2.880	-1	2	2	4	1.7392	1.7315	1	3	4
1	2.741	2.739	2	1	1	<1	1.6975	1.6977	-3	1	6
1	2.725	2.719	-2	1	3	10	1.6782	1.6764	-4	0	2
1	2.654	2.653	2	0	2	2	1.6559	1.6555	-1	0	8
1	2.480	2.476	2	1	2	3	1.6283	1.6289	-4	1	2
<1	2.465	2.462	1	1	4	<1	1.6243	1.6262	4	0	0
<1	2.411	2.402	-2	2	1	<1	1.6167	1.6180	-4	1	1
<1	2.376	2.365	2	2	0	<1	1.5809	1.5827	4	1	0
<1	2.363	2.358	-2	2	2	2	1.4933	1.4925	4	0	2
<1	2.201	2.199	-1	0	6	2	1.4771	1.4777	1	0	8
2	2.181	2.162	0	3	2	3	1.4603	1.4587	4	1	2
13	2.170	2.168	3	0	0	1	1.3666	1.3665	3	0	6
2	2.140	2.141	0	0	6						

range 10–70° 2Θ, integrated step 0.02°/350 s, profile shape function Pearson VII

kora et al. (2007) in kasolite from Horní Halže, which contained Pb in the range of 0.71–0.81 apfu, and besides minor contents of Bi, Ca, Fe, Ba and Zn, potassium content corresponding to 0.09–0.14 apfu. Based on Si + P = 1, the empiric formula of kasolite from Medvědín (average of four spot analyses) may be expressed as follows:  $(\text{Pb}_{0.87}\text{K}_{0.05}\text{Ca}_{0.01})_{\Sigma 0.93}(\text{UO}_2)_{1.10}[(\text{SiO}_4)_{0.99}(\text{PO}_4)_{0.01}]_{\Sigma 1.00} \cdot \text{H}_2\text{O}$ .

The X-ray powder diffraction pattern of kasolite from Medvědín (Tab. 12) corresponds very well to the data in the literature (Tab. 13). The measured intensities of

diffraction maxima differ notably from the intensities calculated from kasolite crystal structure (Rosenzweig and Ryan 1977). This is probably caused by preferred orientation of the type  $h00$ . Such a situation was observed nearly with all studied natural kasolite samples (Škácha and Sejkora 2001; Sejkora et al. 2007). Refined unit-cell parameters of kasolite from Medvědín are compared in Tab. 13 with published data for this mineral. Compared to data from other localities, in particular samples from Jáchymov (Ondruš et al. 1997) and Horní Halže (Sejkora

**Tab. 13** Refined unit-cell parameters of kasolite (monoclinic space group  $P2_1/c$ )

Locality	Reference	$a$ [Å]	$b$ [Å]	$c$ [Å]	$\beta$ [°]	$V$ [Å <sup>3</sup> ]
Medvědín	this paper	6.707(2)	6.887(5)	13.247(4)	104.09(3)	593.5(5)
Katanga	Huynen et al. (1963)	6.660	6.960	13.230	104.0	595.0
Shinkolobwe	Rosenzweig and Ryan (1977)	6.704(2)	6.932(2)	13.252(7)	104.2	597.0
Rýžoviště	Sejkora et al. (1994)	6.709(4)	6.932(4)	13.240(7)	104.15(4)	597.1(6)
Příbram	Škácha and Sejkora (2001)	6.707(1)	6.950(2)	13.258(4)	104.20(2)	599.1(3)
Horní Halže	Sejkora et al. (2007)	6.738(2)	6.977(2)	13.271(4)	104.28(3)	604.6(4)
Jáchymov	Ondruš et al. (1997)	6.730(6)	7.022(7)	13.307(9)	104.90(1)	607.7

et al. 2007), the sample from Medvědín shows decreased unit cell parameters.

Assignment of IR vibrational spectra of kasolite from Medvědín is as follows:  $\nu_4$  ( $\text{SiO}_4$ ) bending vibrations and/or water molecule libration modes 650 w, 695 w; water molecule libration mode 762 m;  $\nu_1$  ( $\text{SiO}_4$ ) symmetric stretching vibration and/or  $\nu_1$  ( $\text{UO}_2$ )<sup>2+</sup> symmetric stretching vibration 827 vs;  $\nu_3$  ( $\text{UO}_2$ )<sup>2+</sup> antisymmetric stretching vibrations 863 s, 912 vs;  $\nu_3$  ( $\text{SiO}_4$ ) antisymmetric stretching vibrations 954 vs sh, 1077 w sh;  $\delta$   $\text{H}_2\text{O}$  bending vibration 1602 w;  $\nu$  OH stretching vibrations 3462 m, 3548 m sh; weak hydrogen bonds are present in the crystal structure. Observed spectrum is comparable with that for kasolite published by Čejka (1999) and Čejka et al. (1986).



**Fig. 13** Irregular semi-spheroidal orange parsonsite aggregates on white churchite-(Y) coatings; width of photo 6.8 mm, photo J. Sejkora (Nikon SMZ1500).

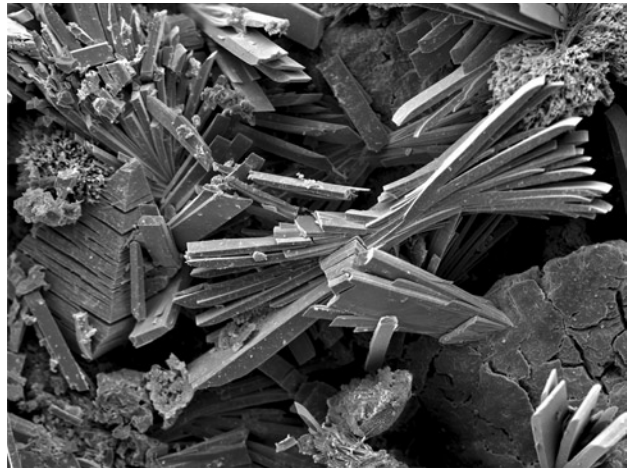


**Fig. 14** Sheaf-like parsonsite crystals cluster with globular churchite-(Y) aggregates and dipyramidal-shaped crystal of metatorbernite; SEM photo J. Plášil (Jeol JSM-6380), width of figure 330 µm.

#### 4.2.3. Metaautunite

(see autunite)

#### 4.2.4. Metatorbernite

(see torbernite)

#### 4.2.5. Parsonsite $\text{Pb}_2(\text{UO}_2)(\text{PO}_4)_2 \cdot 2\text{H}_2\text{O}$

This generally rare uranyl phosphate of lead was observed at the Medvědín deposit as fairly common crystalline coatings covering surfaces up to tens of  $\text{cm}^2$ . Parsonsite is often deposited on whitish grey botryoidal or spheroidal aggregates of churchite-(Y) (Fig. 13). The aggregates of parsonsite consist of sheaf-like crystal clusters up to 1 mm across (Fig. 14). The aggregates are composed of lath-shaped crystals of a deep orange colour (Fig. 15). Parsonsite is locally covered by younger crystalline aggregates of pyromorphite. Parsonsite was also observed as intergrowth with dipyramidal metatorbernite crystals and in close association with acicular to tabular dewindtite crystals. Samples with parsonsite often carry lemon yellow tabular crystals of saléeite and radiating aggregates of kasolite.

The chemical analyses of parsonsite from Medvědín (Tab. 14) show increased content of  $(\text{AsO}_4)^{3-}$  (up to 0.46 apfu), which shows isomorphic substitution with  $(\text{PO}_4)^{3-}$  (Fig. 16). The increasing content of arsenic corresponds to the hallimondite component (Walenta 1965b).

Problematic remains the water content in parsonsite. A synthetic analogue of parsonsite is anhydrous or contains only 0.5  $\text{H}_2\text{O}$  (Vochten et al. 1991; Locock 2004, Locock et al. 2005). The natural material probably contains

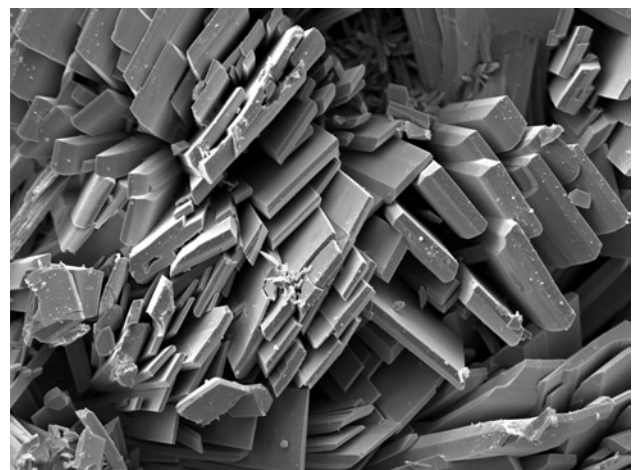


**Fig. 15** Termination of tabular parsonsite crystals; SEM photo J. Plášil (Jeol JSM-6380), width of image 200 µm.

**Tab. 14** Chemical composition of parsonsite

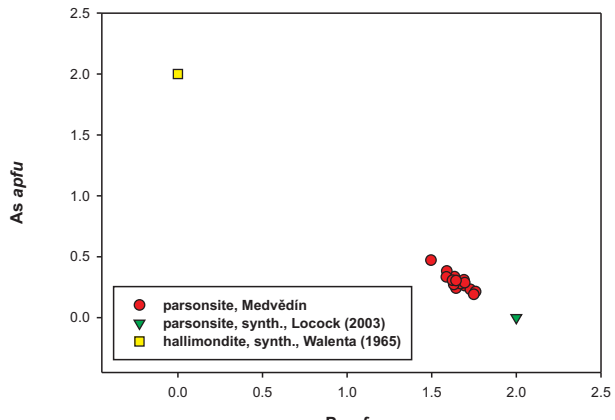
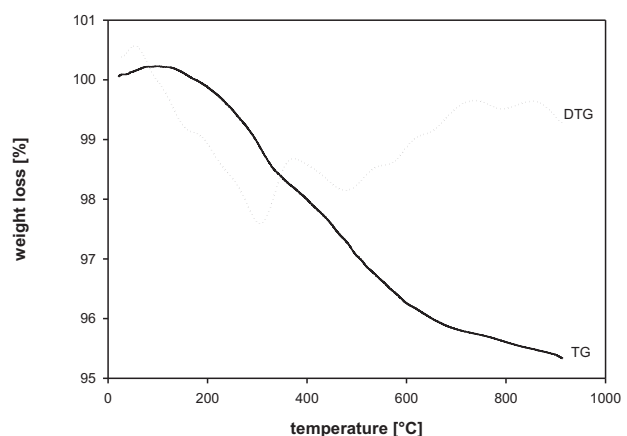
	Mean	1	2	3	4	5
CaO	0.21	0.29	0.24	0.29	0.15	0.28
FeO	0.03	0.00	0.01	0.00	0.05	0.06
BaO	0.03	0.00	0.00	0.00	0.00	0.11
MgO	0.03	0.03	0.08	0.03	0.04	0.03
PbO	45.84	46.32	46.84	50.78	47.12	44.63
CuO	0.04	0.08	0.00	0.03	0.21	0.00
ZnO	0.02	0.09	0.00	0.00	0.06	0.05
Al <sub>2</sub> O <sub>3</sub>	0.01	0.02	0.00	0.00	0.00	0.00
Bi <sub>2</sub> O <sub>3</sub>	0.41	0.65	0.00	0.12	0.00	1.04
SiO <sub>2</sub>	0.23	0.02	0.60	0.09	0.47	0.15
As <sub>2</sub> O <sub>5</sub>	3.47	5.32	3.01	3.75	4.19	2.46
P <sub>2</sub> O <sub>5</sub>	12.08	10.39	12.60	13.67	12.28	12.48
V <sub>2</sub> O <sub>5</sub>	0.07	0.25	0.10	0.00	0.05	0.00
SO <sub>3</sub>	0.03	0.00	0.11	0.05	0.03	0.01
UO <sub>3</sub>	28.42	26.39	31.72	28.53	31.58	26.57
Cl	0.03	0.02	0.03	0.01	0.04	0.05
H <sub>2</sub> O*	3.77	3.86	3.86	3.98	3.89	3.71
Total	94.73	93.72	99.21	101.32	100.16	91.62
Ca	0.036	0.052	0.039	0.045	0.025	0.049
Fe	0.003	0.000	0.002	0.000	0.007	0.009
Ba	0.002	0.000	0.000	0.000	0.000	0.007
Mg	0.008	0.007	0.019	0.007	0.008	0.007
Pb	2.002	2.120	1.942	2.002	1.936	2.000
Cu	0.005	0.010	0.000	0.004	0.024	0.000
Zn	0.003	0.011	0.000	0.000	0.006	0.006
ΣM <sup>2+</sup>	2.060	2.201	2.002	2.058	2.006	2.079
Al	0.002	0.005	0.000	0.000	0.000	0.000
Bi	0.018	0.029	0.000	0.004	0.000	0.045
ΣM <sup>3+</sup>	0.020	0.033	0.000	0.004	0.000	0.045
ΣA site	2.080	2.234	2.002	2.062	2.006	2.123
Si	0.036	0.004	0.092	0.012	0.072	0.025
As	0.295	0.473	0.242	0.287	0.335	0.214
P	1.657	1.495	1.643	1.694	1.586	1.759
V	0.008	0.029	0.010	0.000	0.005	0.000
S	0.004	0.000	0.012	0.006	0.003	0.001
ΣT site	2.000	2.000	2.000	2.000	2.000	2.000
U	0.965	0.942	1.026	0.878	1.013	0.929
Cl	0.007	0.004	0.008	0.002	0.011	0.013
H <sub>2</sub> O	2.00	2.00	2.00	2.00	2.00	2.00

mean based on 16 spot analyses

1–5 – representative analyses

H<sub>2</sub>O\* – H<sub>2</sub>O content calculated from the result of the TG analysis  
(c. 4 weight % loss)

more molecular water, after Anthony et al. (2000) even up to 2 H<sub>2</sub>O. Indeed, the thermal analysis of parsonsite from Medvědín indicates a water loss corresponding to c. 4 wt. %, which is near 2 molecules of H<sub>2</sub>O (theoretical 3.96 wt. %) (Fig. 17). The following empirical formula was calculated from the average of sixteen spot analyses

**Fig. 16** A plot of apfu P vs. As in T-site of parsonsites studied from Medvědín.**Fig. 17** Thermal gravimetric (TG) and differential thermal gravimetric (DTG) curves of parsonsite.

on the basis of (P + As + Si) = 2: (Pb<sub>2.00</sub>Ca<sub>0.04</sub>)<sub>Σ2.04</sub>(UO<sub>2</sub>)<sub>0.97</sub>[(PO<sub>4</sub>)<sub>1.66</sub>(AsO<sub>4</sub>)<sub>0.30</sub>(SiO<sub>4</sub>)<sub>0.04</sub>]<sub>Σ2.00</sub> · 2H<sub>2</sub>O.

The X-ray powder diffraction data for parsonsite from Medvědín (Tab. 15) closely correspond to those calculated from crystal structure published by Burns (2000) for a natural sample from La Feye (France). Refined unit-cell parameters (Tab. 16) are in good agreement with the published data. The unit-cell parameters are definitely affected by (AsP<sub>1</sub>)<sub>1</sub> substitution and may be, additionally, influenced by variable content of molecular water in the structure.

Assignment of the IR vibrational spectra of parsonsite from Medvědín is as follows: water molecule libration mode 769 vw; v<sub>1</sub>(UO<sub>2</sub>)<sup>2+</sup> symmetric stretching vibration 805 w; v<sub>3</sub>(UO<sub>2</sub>)<sup>2+</sup> antisymmetric stretching vibrations 888 m-s, 952 m-s; v<sub>3</sub>(PO<sub>4</sub>)<sup>3-</sup> antisymmetric stretching vibrations 966 s, 1037 vs; δ H<sub>2</sub>O bending vibration 1634 vw b, ν OH stretching vibration 3407 m b; hydrogen

**Tab. 15** Powder diffraction pattern of parsonsite

$I_{rel}$	$d_{obs}$	$d_{calc}$	$h$	$k$	$l$	$I_{rel}$	$d_{obs}$	$d_{calc}$	$h$	$k$	$l$
15	10.176	10.191	0	1	0	3	2.612	2.613	-1	3	1
3	6.808	6.779	1	0	0	3	2.612	2.610	1	-2	2
2	6.056	6.006	0	-1	1	8	2.551	2.546	-1	-3	2
5	5.758	5.742	1	1	0	8	2.551	2.545	-2	-1	2
8	5.098	5.096	0	2	0	3	2.525	2.529	0	2	2
4	5.049	5.058	0	1	1	4	2.448	2.444	2	3	0
1	4.868	4.854	-1	-1	1	2	2.418	2.414	1	4	0
3	4.426	4.405	1	0	1	3	2.359	2.357	-1	4	0
38	4.231	4.229	-1	1	1	3	2.359	2.357	-2	3	0
18	4.155	4.147	1	2	0	3	2.320	2.327	1	-3	2
1	4.009	4.003	-1	2	0	6	2.270	2.260	3	0	0
5	3.902	3.899	1	1	1	10	2.235	2.233	0	4	1
1	3.680	3.685	0	2	1	4	2.211	2.223	3	1	0
100	3.399	3.397	0	3	0	2	2.195	2.200	2	-1	2
1	3.308	3.305	-1	2	1	2	2.119	2.124	-2	-4	1
33	3.266	3.272	0	-3	1	7	2.041	2.038	0	1	3
5	3.185	3.181	-2	0	1	12	1.9755	1.9803	-3	0	2
8	3.161	3.174	1	2	1	47	1.9170	1.9139	3	3	0
6	3.089	3.088	-1	0	2	4	1.8748	1.8781	-1	-5	2
1	3.077	3.082	1	3	0	3	1.8475	1.8491	-1	2	3
3	3.012	3.003	0	-2	2	13	1.8359	1.8419	0	4	2
2	2.998	2.994	-1	3	0	7	1.7862	1.7847	-1	5	1
9	2.943	2.935	0	1	2	14	1.7276	1.7243	0	-6	1
2	2.913	2.904	-1	-2	2	5	1.7179	1.7192	-2	5	0
3	2.805	2.807	-1	1	2	1	1.7058	1.7087	-2	-4	3
14	2.782	2.786	2	-1	1	2	1.6992	1.7008	2	-5	1
2	2.716	2.712	2	1	1	8	1.6639	1.6631	2	1	3

range 7–80° 2Θ, integrated step 0.02°/350 s, profile shape function Pearson VII

**Tab. 16** Refined unit-cell parameters of parsonsite (triclinic space group P-1)

	Medvědín, this paper	La Feye (France), Burns (2000)	syn., Locock (2004)
$a$ [Å]	6.852(6)	6.842(4)	6.8432(5)
$b$ [Å]	10.395(7)	10.383(6)	10.4105(7)
$c$ [Å]	6.669(6)	6.670(4)	6.6718(4)
$\alpha$ [°]	101.20(6)	101.26(7)	101.418(1)
$\beta$ [°]	98.12(7)	98.17(7)	98.347(2)
$\gamma$ [°]	86.39(7)	86.38(7)	86.264(2)
$V$ [Å <sup>3</sup> ]	461.0(6)	459.8(7)	460.64(5)

bonds are present in the structure. Infrared spectrum of parsonsite sample studied is close to infrared and Raman spectra of parsonsite described by Frost et al. (2006a).

#### 4.2.6. Phosphuranylite group minerals

**Dewindtite**  $Pb_3(UO_2)_6H_2(PO_4)_4O_4 \cdot 12H_2O$  (Piret et al. 1990)

**Phosphuranylite**  $KCa(H_3O)_3(UO_2)_7(PO_4)_4O_4 \cdot 8H_2O$  (Demartin et al. 1991)

**“Yingjiangite”**  $(K_2, Ca)(UO_2)_7(PO_4)_4(OH)_6 \cdot 6H_2O$  (Zhangru et al. 1990)

Minerals of the phosphuranylite group are widespread at the Medvědín deposit. They usually form radiating aggregates of yellow to yellow-orange colour (Fig. 18), or yellow-green crystalline aggregates (Fig. 19); exceptional

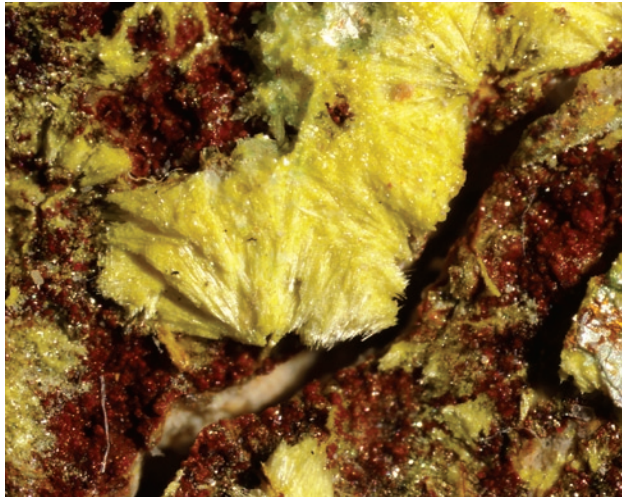


**Fig. 18** Semi-radial coatings of phosphuranylite (sample XME7ZV), width of photo 3.8 mm, photo J. Sejkora (Nikon SMZ1500).

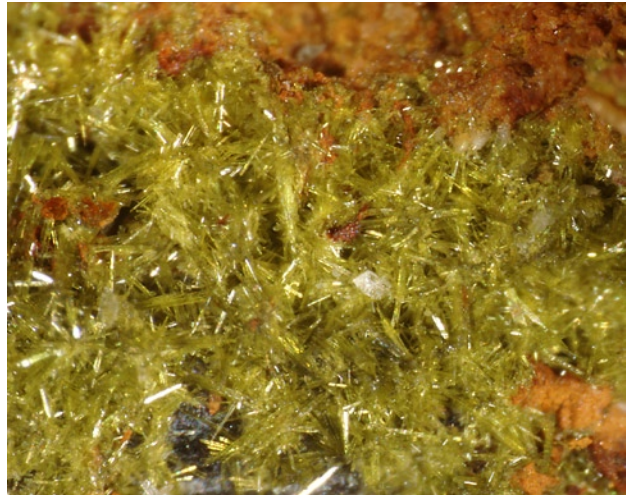


**Fig. 19** Acicular crystals of dewindtite (sample M29), width of photo 2 mm, photo J. Sejkora (Nikon SMZ1500).



**Fig. 20** Rich aggregates of tabular dewindtite crystals (sample P2) with green metatorbernite; width of image 1.3 mm, photo J. Sejkora (Nikon SMZ1500).

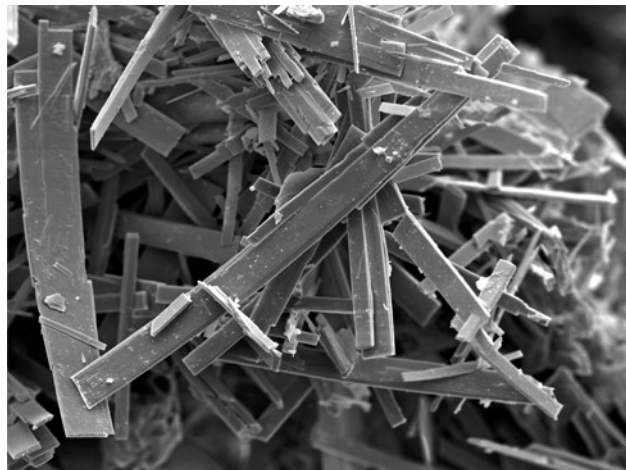


**Fig. 21** Long prismatic crystals of dewindtite (sample XME7ZZ); SEM photo J. Plášil (Jeol JSM-6380), width of figure 150 µm.

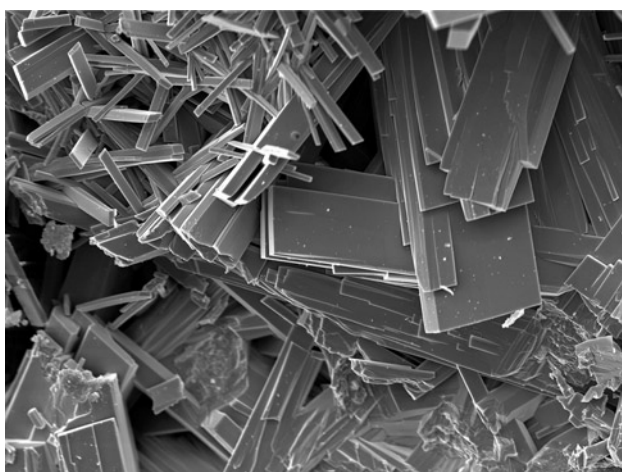


**Fig. 22** Thick tabular crystals of phosphuranylite (sample M25); SEM photo J. Plášil (Jeol JSM-6380), width of figure 140 µm.

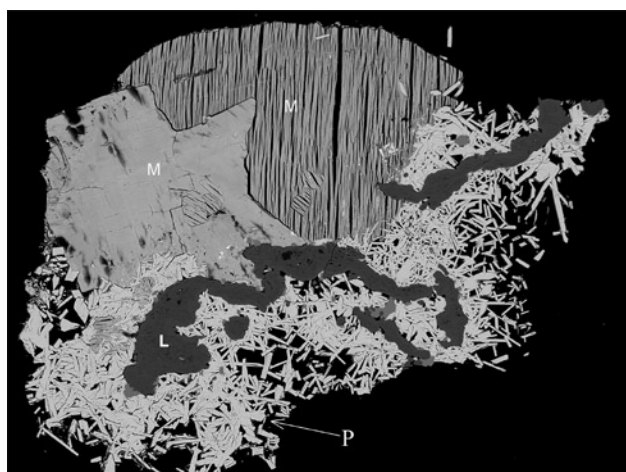


**Fig. 23** Aggregates of twinned metatorbernite (M) with tabular phosphuranylite (P) overgrow limonite (L). Sample M25, width of photo 600 µm, BSE photo by J. Sejkora a R. Škoda (Cameca SX100).

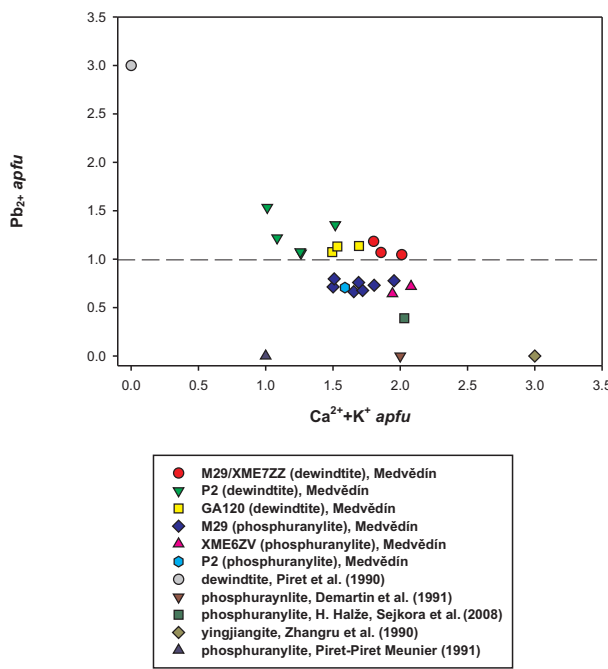


**Fig. 24** Binary plot of  $\text{apfu Ca} + \text{K}$  vs.  $\text{Pb}$  in A-site of the phosphuranylite group minerals.

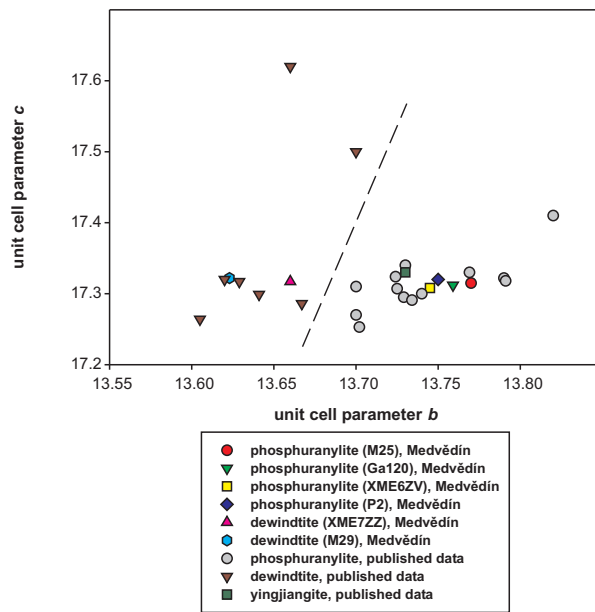


**Fig. 25** Binary plot of unit cell parameters  $b$  vs.  $c$  for phosphuranylite, dewindtite and yingjiangite.

are yellow-green well-formed tabular crystals up to 2 mm (Fig. 20). The crystals are often elongated parallel to  $c$  (Figs 21–22). Minerals of this group are associated with saléeite, dipyramidal crystals of metatorbernite (Fig. 23), tabular crystals of parsonsite and semi-spheroidal ag-

**Tab. 17** Chemical composition of dewindtite samples M29 and XME7ZZ

	Mean	M29	M29	XME7ZZ
$\text{K}_2\text{O}$	1.63	1.87	1.67	1.36
$\text{CaO}$	2.09	2.08	2.09	2.09
$\text{FeO}$	0.32	0.46	0.46	0.05
$\text{BaO}$	0.54	0.41	0.40	0.80
$\text{PbO}$	9.32	8.90	9.36	9.70
$\text{ZnO}$	0.05	0.05	0.00	0.11
$\text{SiO}_2$	0.32	0.31	0.51	0.14
$\text{As}_2\text{O}_5$	0.59	0.50	0.38	0.90
$\text{P}_2\text{O}_5$	9.92	10.15	10.04	9.59
$\text{SO}_3$	0.11	0.00	0.26	0.08
$\text{UO}_3$	68.31	68.46	67.92	68.57
$\text{H}_2\text{O}^*$	8.88	8.93	9.37	8.34
Total	102.09	102.10	102.46	101.71
K	0.912	1.039	0.907	0.790
$\Sigma \text{M}^+$	0.912	1.039	0.907	0.790
Ca	0.982	0.972	0.954	1.020
Fe	0.116	0.168	0.165	0.017
Ba	0.093	0.070	0.067	0.142
Pb	1.103	1.047	1.072	1.190
Zn	0.017	0.015	0.000	0.037
$\Sigma \text{M}^{2+}$	2.312	2.271	2.258	2.406
$\Sigma \text{A site}$	3.224	3.310	3.165	3.196
Si	0.138	0.135	0.218	0.061
As	0.138	0.114	0.084	0.215
P	3.687	3.750	3.615	3.697
S	0.037	0.000	0.084	0.027
$\Sigma \text{T site}$	4.000	4.000	4.000	4.000
U	6.303	6.280	6.070	6.560
H	1.96	1.99	2.57	1.31
$\text{H}_2\text{O}$	12.00	12.00	12.00	12.00
Ratio P/U	0.6	0.6	0.6	0.6
Ideal ratio P/U	0.5	0.5	0.5	0.5

mean of 3 spot analyses

$\text{H}_2\text{O}^*$  –  $\text{H}_2\text{O}$  and  $\text{H}^+$  contents calculated from the charge balance and assuming 12  $\text{H}_2\text{O}$  molecules in the ideal dewindtite formula

gregates of churchite-(Y) in a studied samples. In some specimens minerals of the phosphuranylite group are deposited on grey crystals of saléeite I.

Quantitative chemical analyses and X-ray powder diffraction study resulted in identification of phosphuranylite and dewindtite in these aggregates. Our new data for material from the Medvědín deposit strongly support a probable identity of phosphuranylite and yingjiangite, proposed by Coutinho and Atencio (2000). Yingjiangite has unit-cell identical with that of phosphuranylite. With regard to significant potassium contents in all recent

**Tab. 18** XRD patterns of dewindtite (samples M29 and XME7ZZ)

M29 sample <sup>1)</sup>						XME7ZZ sample <sup>2)</sup>					
<i>I<sub>rel</sub></i>	<i>d<sub>obs</sub></i>	<i>d<sub>calc</sub></i>	<i>h</i>	<i>k</i>	<i>l</i>	<i>I<sub>rel</sub></i>	<i>d<sub>obs</sub></i>	<i>d<sub>calc</sub></i>	<i>h</i>	<i>k</i>	<i>l</i>
3	10.307	10.329	1	1	0	3	10.341	10.339	1	1	0
<1	8.881	8.871	1	1	1						
1	8.646	8.661	0	0	2	6	8.674	8.659	0	0	2
100	7.905	7.920	2	0	0	100	7.879	7.859	2	0	0
1	6.326	6.339	0	2	1						
17	5.837	5.845	2	0	2	9	5.829	5.819	2	0	2
2	4.948	4.949	2	2	1	1	4.954	4.954	2	2	1
4	4.727	4.736	3	1	1	2	4.711	4.710	3	1	1
5	4.403	4.404	0	2	3	3	4.412	4.418	0	2	3
<1	4.324	4.331	0	0	4						
						15	4.254	4.261	3	1	2
								4.259	1	3	1
72	3.958	3.960	4	0	0	55	3.937	3.929	4	0	0
6	3.850	3.849	2	2	3	<1	3.846	3.851	2	2	3
5	3.800	3.800	2	0	4	2	3.797	3.792	2	0	4
1	3.487	3.482	1	3	3						
<1	3.440	3.443	3	3	0						
4	3.405	3.406	0	4	0						
						9	3.343	3.346	4	2	1
1	3.168	3.169	0	4	2						
11	3.127	3.129	2	4	0						
14	3.089	3.088	0	2	5	6	3.092	3.092	0	2	5
	3.086	3.086	5	1	0	<1	3.071	3.064	5	1	0
3	3.034	3.038	5	1	1	<1	3.013	3.017	5	1	1
6	2.943	2.943	2	4	2						
	2.945	2.945	4	2	3	3	2.936	2.936	4	2	3
<1	2.924	2.922	4	0	4	<1	2.908	2.910	4	0	4
16	2.878	2.877	2	2	5	8	2.875	2.877	2	2	5
1	2.832	2.833	3	1	5						
<1	2.640	2.640	6	0	0	1	2.617	2.620	6	0	0
2	2.521	2.520	2	2	6						
<1	2.470	2.475	4	4	2						
7	2.436	2.435	4	2	5	3	2.428	2.430	4	2	5
3	2.281	2.282	1	5	4						
3	2.256	2.254	6	0	4						
4	2.215	2.218	4	4	4						
	2.214	2.214	7	1	1						
5	2.168	2.165	0	0	8	2	2.167	2.165	0	0	8
1	2.114	2.113	0	6	3	4	2.128	2.127	0	6	3
						<1	2.123	2.120	3	5	4
5	2.088	2.089	2	0	8						
	2.087	2.087	6	4	0						
2	2.042	2.042	2	6	3						
4	2.008	2.007	6	2	5	2	1.9986	1.9987	6	2	5
8	1.9802	1.9801	8	0	0						
						3	1.9714	1.9736	1	5	6
1	1.9492	1.9490	2	6	4						
<1	1.9329	1.9313	5	3	6						
4	1.9000	1.8990	0	6	5						
	1.8921	1.8921	1	1	9						
6	1.8897	1.8900	8	2	1	2	1.8781	1.8777	8	2	1
1	1.8476	1.8466	2	6	5						

<sup>1)</sup> range 6–50° 2Θ, integrated step 0.02°/300 s; <sup>2)</sup> range 6–60° 2Θ, integrated step 0.05°/150 s; profile shape function Pearson VII

**Tab. 19** Refined unit-cell parameters of dewindtite (orthorhombic space group *Cmcm*)

Locality	Reference	<i>a</i> [Å]	<i>b</i> [Å]	<i>c</i> [Å]	<i>V</i> [Å <sup>3</sup> ]
Medvědín (XME7ZZ)	this paper	15.738(8)	13.66(1)	17.345(9)	3728(3)
Medvědín (M29)	this paper	15.841(4)	13.623(4)	17.322(5)	3738(1)
Shinkolobwe (Zaire)	Piret et al. (1990)	16.031(6)	13.605(2)	17.264(6)	3765
Rýžoviště (CZ)	Sejkora et al. (2003)	15.725(2)	13.629(3)	17.317(3)	3711(1)
Jáchymov (CZ)	Ondruš et al. (1997)	15.817(8)	13.667(5)	17.286(6)	3737
Jáchymov (CZ)	Ondruš et al. (1997)	15.79(3)	13.62(1)	17.32(1)	3725
Grury (France)	PDF 39-1350	15.826(6)	13.641(2)	17.299(7)	3735
Kasolo (Zaire)	Hogarth and Nuffield (1954)	16.00	13.66	17.62	3851
Katanga (Zaire)	PDF 8-328	16.01	13.70	17.50	3838

phosphuranylite analyses obtained with wavelength dispersion analyser (Demartin et al. 1991; Coutinho and Atencio 2000; Sejkora et al. 2007), the data given by Zhangru et al. (1990) and Jingyi et al. (1992) does not represent new mineral species but only a variety of phosphuranylite, which should be redefined.

Phosphuranylite differs from dewindtite in its crystal structure and composition. Both minerals have the same topology of the uranyl sheets (Burns et al. 1996; Burns 2005) but show differences in the interlayer space. Dewindtite in contrast to phosphuranylite does not contain U<sup>6+</sup> as (UO<sub>2</sub>)<sup>2+</sup> in the interlayer space, which results in a lower U : P ratio in dewindtite (3 : 2 in contrast to 7 : 4 in phosphuranylite). A presence of H<sub>3</sub>O<sup>+</sup>, indicated by Demartin et al. (1991) has not been proved by study of infrared absorption spectra (Čejka 1999). Demartin et al. (1991) and Piret et al. (1990) derived the chemical formulae of dewindtite and phosphuranylite from analyses of crystal structures, which were not supported by reliable data on chemical composition.

Due to similarity in crystal structure of the two minerals and also in the unit-cell parameters, it is very difficult to distinguish phosphuranylite from dewindtite by X-ray powder diffraction. To identify minerals of the phosphuranylite group from the Medvědín deposit we have used the method described by Sejkora et al. (2003), based on comparison of unit-cell parameters *b* and *c* (Fig. 25).

Chemical microanalyses of samples from Medvědín prove an extensive substitution in the phosphuranylite–dewindtite series. In addition, the data obtained indicate complexity in heterovalent substitutions (predominance of 3Pb<sup>2+</sup> – 2(K<sup>+</sup>, Ca<sup>2+</sup>) substitution) and accompanying variation in crystal structure of these phases. With regard to complicated chemical composition of the studied minerals and the fact that at the Medvědín deposit the minerals are not represented by phases close to ideal end-member compositions, in the following text are discussed analytical data for each of the samples individually.

**Tab. 20** Chemical composition of dewindtite sample P2

	Mean	1	2	3	4	5
K <sub>2</sub> O	1.38	1.29	1.46	1.18	1.55	1.43
CaO	0.98	1.18	1.00	0.95	1.34	0.42
BaO	1.38	1.50	1.39	1.65	0.93	1.42
PbO	10.63	9.12	9.33	10.55	11.34	12.79
CuO	0.21	0.08	0.00	0.30	0.43	0.25
Bi <sub>2</sub> O <sub>3</sub>	0.11	0.28	0.02	0.00	0.00	0.22
SiO <sub>2</sub>	0.25	0.20	0.38	0.19	0.33	0.15
As <sub>2</sub> O <sub>5</sub>	0.74	0.65	1.35	0.53	0.55	0.60
P <sub>2</sub> O <sub>5</sub>	10.00	10.20	9.64	10.30	9.81	10.05
SO <sub>3</sub>	0.08	0.09	0.06	0.15	0.11	0.00
UO <sub>3</sub>	67.22	67.83	68.37	64.94	68.20	66.75
H <sub>2</sub> O*	9.25	9.40	9.54	9.62	8.75	8.93
Total	102.21	101.83	102.54	100.36	103.34	103.01
K	0.771	0.713	0.800	0.648	0.880	0.813
ΣM <sup>+</sup>	0.771	0.713	0.800	0.648	0.880	0.813
Ca	0.457	0.549	0.463	0.438	0.637	0.199
Ba	0.235	0.254	0.235	0.277	0.162	0.249
Pb	1.251	1.063	1.082	1.220	1.355	1.534
Cu	0.070	0.026	0.000	0.097	0.145	0.084
ΣM <sup>2+</sup>	2.014	1.892	1.779	2.032	2.300	2.066
Bi	0.012	0.032	0.002	0.000	0.000	0.026
ΣM <sup>3+</sup>	0.012	0.032	0.002	0.000	0.000	0.026
ΣA site	2.797	2.637	2.582	2.680	3.180	2.904
Si	0.109	0.086	0.162	0.082	0.148	0.068
As	0.168	0.148	0.304	0.120	0.127	0.139
P	3.696	3.738	3.514	3.749	3.689	3.793
S	0.027	0.029	0.020	0.049	0.036	0.000
ΣT site	4.000	4.000	4.000	4.000	4.000	4.000
U	6.166	6.167	6.185	5.865	6.363	6.249
H	2.92	3.13	3.41	3.59	1.91	2.55
H <sub>2</sub> O	12.00	12.00	12.00	12.00	12.00	12.00
Ratio P/U	0.6	0.6	0.6	0.6	0.6	0.6
Ideal ratio P/U	0.5	0.5	0.5	0.5	0.5	0.5

mean of 5 spot analyses

H<sub>2</sub>O\* – H<sub>2</sub>O and H<sup>+</sup> contents calculated from the charge balance and assuming 12 H<sub>2</sub>O molecules in the ideal dewindtite formula

**Tab. 21** XRD patterns of XME6ZV and P2 phosphuranylite samples

XME6ZV sample <sup>1)</sup>						P2 sample <sup>2)</sup>					
<i>I<sub>rel</sub></i>	<i>d<sub>obs</sub></i>	<i>d<sub>calc</sub></i>	<i>h</i>	<i>k</i>	<i>l</i>	<i>I<sub>rel</sub></i>	<i>d<sub>obs</sub></i>	<i>d<sub>calc</sub></i>	<i>h</i>	<i>k</i>	<i>l</i>
3	10.359	10.349	1	1	0	1	10.333	10.370	1	1	0
27	8.670	8.654	0	0	2	13	8.645	8.660	0	0	2
100	7.904	7.872	2	0	0	100	7.888	7.896	2	0	0
4	6.627	6.639	1	1	2	6	5.833	5.835	2	0	2
1	6.378	6.382	0	2	1						
9	5.828	5.823	2	0	2						
1	4.898	4.902	3	1	0						
1	4.719	4.717	3	1	1	1	4.721	4.729	3	1	1
4	4.409	4.417	0	2	3						
						1	4.404	4.402	1	3	0
4	4.325	4.327	0	0	4	2	4.331	4.330	0	0	4
							4.266	4.266	1	3	1
1	4.269	4.265	3	1	2	<1	4.269	4.275	3	1	2
53	3.947	3.936	4	0	0	63	3.948	3.948	4	0	0
4	3.852	3.852	2	2	3	1	3.849	3.858	2	2	3
2	3.791	3.792	2	0	4	1	3.798	3.797	2	0	4
						1	3.677	3.664	0	2	4
1	3.510	3.496	1	3	3						
5	3.421	3.433	0	4	0						
1	3.392	3.383	3	3	1	3	3.402	3.390	3	3	1
5	3.352	3.350	4	2	1	1	3.354	3.359	4	2	1
1	3.282	3.283	1	1	5	1	3.285	3.286	1	1	5
2	3.207	3.191	0	4	2						
<1	3.185	3.176	4	2	2						
12	3.141	3.147	2	4	0						
						1	3.090	3.093	0	2	5
7	3.089	3.083	0	2	5	<1	3.081	3.087	1	3	4
<1	3.061	3.069	5	1	0						
2	3.028	3.022	5	1	1						
4	2.937	2.939	4	2	3	1	2.945	2.945	4	2	3
<1	2.910	2.912	4	0	4	<1	2.918	2.917	4	0	4
11	2.877	2.877	2	2	5	3	2.876	2.880	2	2	5
1	2.828	2.828	3	1	5						
2	2.699	2.697	3	3	4						
<1	2.678	2.673	1	5	1						
						1	2.632	2.632	6	0	0
2	2.580	2.587	4	4	0						
<1	2.564	2.566	5	3	1						
<1	2.525	2.520	2	2	6						
2	2.509	2.503	5	1	4						
<1	2.475	2.479	4	4	2						
4	2.429	2.431	4	2	5	1	2.431	2.435	4	2	5
							2.434	2.434	6	2	1
1	2.250	2.244	6	0	4	<1	2.246	2.249	6	0	4
<1	2.217	2.212	0	6	2						
						1	2.211	2.210	3	1	7
							2.208	2.208	7	1	1
3	2.207	2.204	4	2	6						
4	2.161	2.163	0	0	8	3	2.167	2.165	0	0	8
2	2.124	2.121	3	5	4						
4	2.084	2.086	6	4	0						
3	2.051	2.054	2	6	3						
						1	2.006	2.005	4	2	7
							2.005	2.005	6	2	5
5	1.995	2.000	6	2	5						
3	1.9684	1.9681	8	0	0	4	1.9752	1.9754	1	5	6
2	1.9074	1.9091	0	6	5	1	1.8996	1.9741	8	0	0
						1	1.8862	1.8983	4	0	8
4	1.8769	1.8807	8	2	1						
2	1.8521	1.8553	2	6	5						
1	1.8295	1.8303	0	4	8						
1	1.7839	1.7828	2	4	8						
2	1.7310	1.7308	0	0	10						

<sup>1)</sup> XME6ZV, range 6–60° 2Θ, integrated step 0.05°/150 s, profile shape function Pearson VII<sup>2)</sup> P2, range 7–56° 2Θ, integrated step 0.02°/300 s, profile shape function Pearson VII

**Tab. 22** Unit-cell parameters of phosphuranylites and yingjiangite (orthorhombic space group *Cmcm*)

Mineral	Locality	Reference	<i>a</i> [Å]	<i>b</i> [Å]	<i>c</i> [Å]	<i>V</i> [Å <sup>3</sup> ]
phosphuranylite	Medvědín (M25)	this paper	15.793(7)	13.768(5)	17.323(7)	3766(1)
phosphuranylite	Medvědín (GA 120)	this paper	15.769(5)	13.759(7)	17.313(8)	3757(2)
phosphuranylite	Medvědín (XME6ZV)	this paper	15.770(9)	13.757(9)	17.319(9)	3757(3)
phosphuranylite	Medvědín (P2)	this paper	15.793(6)	13.75(1)	17.320(7)	3761(3)
phosphuranylite	Bois Noir (France)	Demartin et al. (1991)	15.778(3)	13.769(2)	17.330(3)	3765
phosphuranylite	Sardinia (Italy)	Demartin et al. (1991)	15.899(2)	13.740(2)	17.300(3)	3779
phosphuranylite	Peveragno (Italy)	Demartin et al. (1991)	15.890(6)	13.790(5)	17.322(5)	3796
phosphuranylite	Zambia	Demartin et al. (1991)	15.862(6)	13.702(5)	17.253(7)	3750
phosphuranylite	Margnac (France)	Piret and Piret-Meunier (1991)	15.835(7)	13.724(4)	17.324(6)	3765
phosphuranylite	Horní Halže	Sejkora et al. (2007)	15.743(2)	13.729(4)	17.295(4)	3736(1)
phosphuranylite	Rýžoviště	Sejkora et al. (1994)	15.780(7)	13.725(8)	17.307(8)	3748(2)
phosphuranylite	Kladská	Pauliš et al. (1999)	15.82	13.73	17.34	3766
phosphuranylite	Horní Slavkov	Plášil et al. (2006)	15.774(4)	13.791(3)	17.318(4)	3767.5
phosphuranylite	Jáchymov	Ondruš et al. (1997)	15.48(2)	13.82(2)	17.41(4)	3725
phosphuranylite	Předbořice	Sejkora (1993)	15.85(1)	13.70(1)	17.31(1)	3759
phosphuranylite	Kladská	Sejkora (1993)	15.83(2)	13.70(1)	17.27(2)	3745
phosphuranylite	Chotěboř	Sejkora (1993)	15.772(4)	13.734(4)	17.291(5)	3745
yingjiangite	Tongbiguan (China)	Zhangru et al. (1990)	15.99(1)	13.73(2)	17.33(1)	3804(5)

Elongated crystals up to 1 mm long, green or green to light yellow along *c* (samples M29 and XME7ZZ) (Fig. 19), have been identified by electron microprobe as dewindtite (Fig. 24). Using average of three spot analyses (Tab. 17) the following empiric formula has been calculated ( $P + As + Si + S = 4$  apfu):  $(Pb_{1.10}Ca_{0.98}K_{0.91}Fe_{0.12}Ba_{0.09}Zn_{0.02})_{\Sigma 3.22}H_{1.96}(UO_2)_{6.30}O_4[(PO_4)_{3.69}(SiO_4)_{0.14}(AsO_4)_{0.14}(SO_4)_{0.04}]_{\Sigma 4.00} \cdot 12H_2O$ . Unit-cell parameters of this phase refined from powder X-ray diffraction patterns (Tab. 18) correspond to dewindtite (Tab. 19, Fig. 25). Infrared vibrational spectra of the sample M29 show water molecule libration mode 798 w;  $\nu_3$  ( $UO_2$ )<sup>2+</sup> antisymmetric stretching vibration 909 s;  $\nu_3$  ( $PO_3$ )<sup>3-</sup> antisymmetric stretching vibrations 1011 vs sh, 1044 vs, 1086 vs;  $\delta H_2O$  bending vibration 1642 w;  $\nu$  OH stretching vibrations 3241 m sh, 3473 s b; some hydrogen bonds are present in the structure.

The rich crystalline aggregates of yellow-green colour (Fig. 20) in the sample P2 contain both dewindtite and phosphuranylite as indicated by quantitative chemical analyses (Fig. 24). Empiric formula for dewindtite was calculated from an average of five spot analyses ( $P + As + Si + S = 4$ ) (Tab. 20):  $(Pb_{1.25}K_{0.77}Ca_{0.46}Ba_{0.24}Cu_{0.07}Bi_{0.01})_{\Sigma 2.80}H_{2.92}(UO_2)_{6.17}O_4[(PO_4)_{3.69}(AsO_4)_{0.17}(SiO_4)_{0.11}(SO_4)_{0.02}]_{\Sigma 4.00} \cdot 12H_2O$ . The empiric formula of phosphuranylite in the same sample (one spot analysis) is  $K_{0.78}(Ca_{0.81}Pb_{0.71}Ba_{0.22}Mg_{0.07}Fe_{0.02}Bi_{0.01})_{\Sigma 1.84}(H_3O)_{3.12}(UO_2)_{6.29}O_4[(PO_4)_{3.44}(AsO_4)_{0.33}(SiO_4)_{0.19}(SO_4)_{0.04}]_{\Sigma 4.00} \cdot 8H_2O$ . The powder X-ray analysis (Tab. 21) has not indicated a phase corresponding to dewindtite and the refined unit-cell parameters of the analysed mineral (Tab. 22) correspond to phosphuranylite. A tentative assignment of the vibrational bands of the yellow parts of P2 sample is following: water molecule libration mode 675 w;  $\nu_3$  ( $UO_2$ )<sup>2+</sup> antisymmetric stretch-

**Tab. 23** Chemical composition of dewindtite sample Ga120

	Mean	1	2	3
Na <sub>2</sub> O	0.05	0.03	0.03	0.08
K <sub>2</sub> O	1.04	0.99	1.12	1.02
CaO	1.95	1.89	1.98	1.99
FeO	0.07	0.12	0.00	0.10
BaO	0.40	0.39	0.37	0.44
MgO	0.09	0.06	0.14	0.08
PbO	9.01	8.78	8.84	9.41
CuO	0.36	0.35	0.33	0.39
SiO <sub>2</sub>	0.61	0.29	0.68	0.86
As <sub>2</sub> O <sub>5</sub>	0.49	0.54	0.43	0.51
P <sub>2</sub> O <sub>5</sub>	9.26	9.73	8.81	9.25
UO <sub>3</sub>	63.00	65.74	60.41	62.85
H <sub>2</sub> O	8.73	8.74	8.34	9.13
Total	95.07	97.64	91.47	96.09
Na	0.040	0.024	0.031	0.065
K	0.613	0.576	0.680	0.583
$\Sigma M^+$	0.653	0.600	0.711	0.648
Ca	0.962	0.919	1.016	0.950
Fe	0.027	0.044	0.000	0.036
Ba	0.072	0.069	0.070	0.076
Mg	0.065	0.041	0.099	0.055
Pb	1.114	1.073	1.138	1.131
Cu	0.123	0.121	0.118	0.131
$\Sigma M^{2+}$	2.362	2.266	2.441	2.379
$\Sigma A$ site	3.015	2.866	3.152	3.027
Si	0.281	0.133	0.325	0.385
As	0.118	0.128	0.107	0.119
P	3.601	3.740	3.569	3.496
$\Sigma T$ site	4.000	4.000	4.000	4.000
U	6.079	6.272	6.071	5.894
H	2.75	2.46	2.59	3.19
H <sub>2</sub> O	12.00	12.00	12.00	12.00
Ratio P/U	0.6	0.6	0.6	0.6
Ideal ratio P/U	0.5	0.5	0.5	0.5

mean of 3 spot analyses

 $H_2O^*$  –  $H_2O$  and  $H^+$  contents calculated from the charge balance and assuming 12  $H_2O$  molecules in the ideal dewindtite formula

**Tab. 24** XRD patterns of phosphuranylite samples M25 and Ga120

M25 <sup>1)</sup>						Ga120 <sup>2)</sup>					
<i>I<sub>rel</sub></i>	<i>d<sub>obs</sub></i>	<i>d<sub>calc</sub></i>	<i>h</i>	<i>k</i>	<i>l</i>	<i>I<sub>rel</sub></i>	<i>d<sub>obs</sub></i>	<i>d<sub>calc</sub></i>	<i>h</i>	<i>k</i>	<i>l</i>
2	10.328	10.383	1	1	0	2	10.285	10.368	1	1	0
7	8.677	8.657	0	0	2	1	8.654	8.656	0	0	2
100	7.904	7.903	2	0	0	100	7.880	7.885	2	0	0
7	5.838	5.837	2	0	2	7	5.828	5.829	2	0	2
1	4.957	4.973	2	2	1	1	4.936	4.966	2	2	1
						1		4.911	3	1	0
2	4.731	4.733	3	1	1	2	4.717	4.724	3	1	1
2	4.408	4.423	0	2	3						
2		4.408	1	3	0	2	4.406	4.404	1	3	0
1	4.341	4.329	0	0	4						
		4.278	3	1	2						
1	4.278	4.272	1	3	1						
48	3.954	3.951	4	0	0	35	3.943	3.943	4	0	0
2	3.854	3.860	2	2	3	2	3.848	3.856	2	2	3
3	3.797	3.796	2	0	4	2	3.798	3.794	2	0	4
1	3.440	3.443	0	4	0	<1	3.438	3.440	0	4	0
						<1		3.421	4	2	0
2	3.355	3.362	4	2	1	3	3.346	3.356	4	2	1
						<1	3.251	3.247	3	1	4
4	3.087	3.094	0	2	5	2	3.091	3.093	0	2	5
	3.087	3.089	1	3	4			3.087	1	3	4
						2	3.067	3.074	5	1	0
1	3.032	3.033	5	1	1	1	3.029	3.027	5	1	1
1	2.945	2.947	4	2	3	1	2.939	2.943	4	2	3
						<1	2.913	2.915	4	0	4
4	2.877	2.881	2	2	5	3	2.876	2.879	2	2	5
1	2.827	2.832	3	1	5	<1	2.831	2.830	3	1	5
		2.634				<1	2.682	2.684	4	2	4
1	2.635		6	0	0	<1	2.632	2.628	6	0	0
1	2.581	2.574	5	3	1	<1	2.577	2.570	5	3	1
<1	2.521	2.522	2	2	6						
						<1	2.517	2.515	6	0	2
						<1	2.487	2.483	4	4	2
2	2.434	2.436	4	2	5	2	2.429	2.433	4	2	5
	2.434	2.436	6	2	1			2.431	6	2	1
<1	2.261	2.263	6	2	3						
1	2.252	2.250	6	0	4	1	2.247	2.247	6	0	4
						1		2.246	3	5	3
						1	2.215	2.217	0	6	2
						1		2.215	3	3	6
1	2.211	2.210	3	1	7	1	2.204	2.206	4	2	6
	2.210		7	1	1	1		2.205	7	1	1
1	2.168	2.164	0	0	8	1	2.168	2.164	0	0	8
						<1	2.152	2.153	7	1	2
<1	2.117	2.119	1	1	8	<1	2.116	2.118	1	1	8
1	2.086	2.087	2	0	8	1	2.082	2.087	2	0	8
1	2.007	2.006	6	2	5	1	2.003	2.003	6	2	5
2	1.9768	1.9767	1	5	6						
	1.9768	1.9757	8	0	0	1	1.9712	1.9713	8	0	0
							1.9694		4	6	1
						<1	1.9417	1.9431	6	0	6
						<1	1.9235	1.9221	8	0	2
1	1.9006	1.8982	4	0	8	1	1.9006	1.8970	4	0	8
1	1.8872	1.8877	8	2	1	1	1.8814	1.8838	8	2	1
<1	1.8495	1.8492	1	7	3	<1	1.8476	1.8478	6	4	4
<1	1.8034	1.8040	4	6	4	<1	1.8002	1.8005	8	2	3
1	1.7984	1.7963	0	6	6						
<1	1.7984	1.7973	8	0	4	<1	1.7948	1.7940	8	0	4
<1	1.7357	1.7373	7	5	1	<1	1.7330	1.7345	7	5	1
1	1.7138	1.7128	0	8	1	<1	1.7113	1.7115	0	8	1
						<1	1.6920	1.6909	2	0	10

<sup>1)</sup> M25, range 7–58° 2Θ, integrated step 0.02°/250 s<sup>2)</sup> Ga120, range 6–55° 2Θ, integrated step 0.02°/400 s  
profile shape function Pearson VII

ing vibration 908 s;  $\nu_3$  ( $\text{PO}_4$ )<sup>3-</sup> antisymmetric stretching vibrations 1002 vs, 1048 vs, 1089 vs;  $\delta$   $\text{H}_2\text{O}$  bending vibration 1649 w;  $\nu$  OH stretching vibrations 3289 m b, 3502 m; hydrogen bonds are present in the structure.

Aggregates of yellow crystals associated with a yellow saléeite II and dipyramidal crystals of metatorbernite in the sample Ga120 have been identified chemically as dewindtite (Tab. 23, Fig. 24), but unit-cell parameters refined from X-ray powder diffraction pattern (Tab. 24) are closer to those of phosphuranylite (Tab. 22, Fig. 25). It is possible that the sample contains both minerals, which cannot be identified macroscopically and the microanalysis did not confirm a presence of phosphuranylite, either. Based on  $(\text{P} + \text{As} + \text{Si} + \text{S}) = 4$  the empirical formula of dewindtite (Ga 120) was calculated from average of three spot analyses (Tab. 23):  $(\text{Pb}_{1.11}\text{Ca}_{0.96}\text{K}_{0.61}\text{Cu}_{0.12}\text{Ba}_{0.07}\text{Mg}_{0.07}\text{Na}_{0.04}\text{Fe}_{0.03})_{\Sigma 3.01}\text{H}_{2.75}(\text{UO}_2)_{6.08}\text{O}_4[(\text{PO}_4)_{3.60}(\text{SiO}_4)_{0.28}(\text{AsO}_4)_{0.12}]_{\Sigma 4.00} \cdot 12\text{H}_2\text{O}$ . Infrared vibrational spectra of Ga120 sample represent:  $\nu_1$  ( $\text{UO}_2$ )<sup>2+</sup> symmetric stretching vibration 817 w;  $\nu_3$  ( $\text{UO}_2$ )<sup>2+</sup> antisymmetric stretching vibration 912 s;  $\nu_3$  ( $\text{PO}_4$ )<sup>3-</sup> antisymmetric stretching vibrations 996 vs, 1047 vs, 1085 vs;  $\delta$  U-OH bending vibration 1290 vw;  $\delta$   $\text{H}_2\text{O}$  bending vibration 1630 w;  $\nu$  OH stretching vibrations 3239 m, 3484 s; hydrogen bonds are present in the structure.

Chemical composition of yellow radiating aggregates (sample XME6ZV) (Fig. 18), associated with saléeite and parsonsite, corresponds to phosphuranylite (Fig. 24). The following empiric formula based on  $(\text{P} + \text{As} + \text{Si} + \text{S}) = 4$  was calculated from average of three spot analyses (Tab. 25):  $\text{K}_{1.02}(\text{Ca}_{0.99}\text{Pb}_{0.68}\text{Al}_{0.10}\text{Zn}_{0.09}\text{Mg}_{0.08}\text{Ba}_{0.07}\text{Fe}_{0.02})_{\Sigma 2.03}(\text{H}_3\text{O})_{2.60}(\text{UO}_2)_{6.25}\text{O}_4[(\text{PO}_4)_{3.53}(\text{SiO}_4)_{0.31}(\text{AsO}_4)_{0.16}]_{\Sigma 4.00} \cdot 8\text{H}_2\text{O}$ . The refined unit cell parameters of the sample XME6ZV (for X-ray diffraction pattern see Tab. 21) correspond to the unit-cell parameters of phosphuranylite (Tab. 22, Fig. 25). Infrared vibrational spectra of the sample XME6ZV show water molecule libration mode 728 w;  $\nu_1$  ( $\text{UO}_2$ )<sup>2+</sup> symmetric stretching vibration 813 w;  $\nu_3$  ( $\text{UO}_2$ )<sup>2+</sup> antisymmetric stretching vibration 908 s;  $\nu_3$  ( $\text{PO}_4$ )<sup>3-</sup> antisymmetric stretching vibrations 997 vs, 1051 vs, 1085 vs;  $\delta$  U-OH bending vibration 1469 w;  $\delta$   $\text{H}_2\text{O}$  bending vibration 1635 m; combination band or overtone 1742 w;  $\nu$  OH stretching vibrations 3242 s sh, 3399 s sh, 3479 s; some hydrogen bonds are present in the structure.

Orange to orange-yellow crystalline aggregates associated with metatorbernite, uranophane, kasolite and parsonsite (sample M25) correspond to phosphuranylite, as indicated by quantitative chemical analyses (Fig. 24). Their chemical composition (Tab. 26) can be expressed by the following empiric formula (average of seven analyses;  $\text{P} + \text{As} + \text{Si} = 4$ ):  $\text{K}_{0.84}(\text{Ca}_{0.85}\text{Pb}_{0.73}\text{Ba}_{0.16}\text{Zn}_{0.02}\text{Fe}_{0.02})_{\Sigma 1.78}(\text{H}_3\text{O})_{2.86}(\text{UO}_2)_{6.45}\text{O}_4[(\text{PO}_4)_{3.63}(\text{SiO}_4)_{0.20}$

**Tab. 25** Chemical composition of phosphuranylite sample XME6ZV

	Mean	1	2
$\text{K}_2\text{O}$	1.85	1.88	1.82
$\text{CaO}$	2.13	2.12	2.14
$\text{FeO}$	0.07	0.14	0.00
$\text{BaO}$	0.41	0.48	0.35
$\text{MgO}$	0.12	0.12	0.12
$\text{PbO}$	5.83	5.73	5.92
$\text{ZnO}$	0.28	0.32	0.23
$\text{Al}_2\text{O}_3$	0.21	0.43	0.00
$\text{SiO}_2$	0.72	1.17	0.28
$\text{As}_2\text{O}_5$	0.71	0.68	0.74
$\text{P}_2\text{O}_5$	9.62	9.54	9.69
$\text{UO}_3$	68.54	66.04	71.03
$\text{H}_2\text{O}^*$	6.45	7.03	5.88
Total	96.94	95.66	98.21
K	1.022	0.998	1.046
Ca	0.990	0.945	1.035
$\Sigma \text{A site}$	2.012	1.943	2.081
Fe	0.024	0.049	0.000
Ba	0.070	0.078	0.062
Mg	0.077	0.071	0.082
Pb	0.681	0.643	0.719
Zn	0.088	0.099	0.077
Al	0.105	0.211	0.000
$\Sigma \text{B site}$	1.045	1.150	0.940
Si	0.306	0.485	0.127
As	0.162	0.149	0.175
P	3.532	3.366	3.698
$\Sigma \text{T site}$	4.000	4.000	4.000
U	6.254	5.781	6.727
$\text{H}_3\text{O}^+$	2.60	3.52	1.68
$\text{H}_2\text{O}$	8.00	8.00	8.00
Ratio P/U	0.56	0.58	0.55
Ideal ratio P/U	0.75	0.75	0.75

mean of 2 spot analyses

$\text{H}_2\text{O}^*$  –  $\text{H}_2\text{O}$  and  $\text{H}_3\text{O}^+$  contents calculated from the charge balance and assuming 8  $\text{H}_2\text{O}$  molecules in the ideal phosphuranylite formula (Demartin et al. 1991)

$(\text{AsO}_4)_{0.17}]_{\Sigma 4.00} \cdot 8\text{H}_2\text{O}$ . Unit-cell parameters refined from the powder X-ray diffraction data (Tab. 24) correspond to phosphuranylite (Tab. 22, Fig. 25). Assignment of IR vibrational bands is:  $\nu_1$  ( $\text{UO}_2$ )<sup>2+</sup> symmetric stretching vibration 812 w;  $\nu_3$  ( $\text{UO}_2$ )<sup>2+</sup> antisymmetric stretching vibration 912 s;  $\nu_3$  ( $\text{PO}_4$ )<sup>3-</sup> antisymmetric stretching vibrations 997 vs, 1050 vs, 1089 vs;  $\delta$   $\text{H}_2\text{O}$  bending vibration 1636 w;  $\nu$  OH stretching vibrations 3237 m, 3364 m sh, 3476 m; some hydrogen bonds are present in the structure.

There are only small differences between infrared spectra of studied phosphuranylite–dewindtite samples. Observed infrared spectra of all three minerals are comparable with published infrared spectra of phosphuranylite (Sejkora et al. 1994; Čejka 1999; Frost et al. 2008), yingjiangite (Zhangru et al. 1990; Jingyi et al. 1992; Frost et al. 2008) and dewindtite (Frost et al. 2006b).

**Tab. 26** Chemical composition of phosphuranylite sample M25

	Mean	1	2	3	4	5	6	7
K <sub>2</sub> O	1.52	1.56	1.54	1.75	1.85	1.35	1.69	0.93
CaO	1.85	1.74	1.92	1.61	1.79	1.81	1.87	2.24
FeO	0.06	0.03	0.16	0.03	0.00	0.01	0.05	0.11
BaO	0.95	0.97	0.96	1.23	0.96	1.11	0.87	0.51
PbO	6.33	5.75	5.88	5.94	6.33	6.47	6.93	7.04
ZnO	0.06	0.07	0.03	0.23	0.00	0.00	0.00	0.10
SiO <sub>2</sub>	0.47	0.66	0.44	0.48	0.50	0.51	0.61	0.09
As <sub>2</sub> O <sub>5</sub>	0.77	0.53	0.67	0.64	0.75	0.66	1.15	1.00
P <sub>2</sub> O <sub>5</sub>	9.96	9.86	10.10	9.36	9.27	10.53	10.17	10.45
UO <sub>3</sub>	71.34	72.17	71.95	70.17	70.71	71.60	69.98	72.80
H <sub>2</sub> O	6.59	6.62	6.59	5.91	5.86	7.25	7.33	6.61
Total	99.91	100.00	100.26	97.50	98.10	101.36	100.74	102.05
K	0.841	0.857	0.840	1.021	1.081	0.707	0.879	0.502
Ca	0.854	0.804	0.881	0.789	0.879	0.794	0.815	1.016
ΣA site	1.695	1.661	1.722	1.810	1.960	1.501	1.694	1.518
Fe	0.020	0.011	0.058	0.012	0.000	0.005	0.018	0.038
Ba	0.160	0.164	0.161	0.221	0.173	0.178	0.139	0.085
Pb	0.733	0.667	0.678	0.732	0.780	0.713	0.760	0.801
Zn	0.020	0.023	0.010	0.077	0.000	0.000	0.000	0.032
ΣB site	0.934	0.865	0.906	1.043	0.952	0.896	0.917	0.955
Si	0.202	0.285	0.187	0.220	0.228	0.209	0.249	0.038
As	0.172	0.119	0.149	0.153	0.178	0.141	0.244	0.222
P	3.625	3.596	3.663	3.627	3.593	3.650	3.507	3.740
ΣT site	4.000	4.000	4.000	4.000	4.000	4.000	4.000	4.000
U	6.452	6.530	6.474	6.748	6.799	6.160	5.989	6.467
H <sub>3</sub> O <sup>+</sup>	2.86	3.02	2.82	2.03	1.86	3.78	3.89	2.62
H <sub>2</sub> O	8.00	8.00	8.00	8.00	8.00	8.00	8.00	8.00
Ratio P/U	0.56	0.55	0.57	0.54	0.53	0.59	0.59	0.58
Ideal ratio P/U	0.75	0.75	0.75	0.75	0.75	0.75	0.75	0.75

mean of 7 spot analyses

H<sub>2</sub>O\* – H<sub>2</sub>O and H<sub>3</sub>O<sup>+</sup> content calculated from the charge balance and assuming 8 H<sub>2</sub>O molecules in the ideal phosphuranylite formula (Demartin et al. 1991)

#### 4.2.7. Saléeite Mg(UO<sub>2</sub>)<sub>2</sub>(PO<sub>4</sub>)<sub>2</sub> · 10H<sub>2</sub>O

Crystallized saléeite is a common mineral among the recently studied samples from Medvědín. It occurs in two morphologically different generations. Older saléeite I forms thin tabular crystals of light brown and grey colour, up to several mm across (Fig. 26), which are transparent to translucent. Saléeite I coats druses of thin tabular crystals of (meta)torbernite (Fig. 27). It is often intergrown with younger saléeite II of lemon yellow colour, in crystals up to 3 mm (Fig. 28). The crystals of saléeite II are thinner than those of saléeite I and are characterized by a vitreous lustre with pearl flashes. Saléeite II shows intense yellow fluorescence in short-wave UV radiation (254 nm), whereas saléeite I either has none or weak. Both generations occur with minerals of the dewindtite–phosphuranylite series, kasolite, churchite-(Y) and parsonsite.

The compositional study of saléeite I from Medvědín (Tab. 27) proved rather extensive substitution in the

cation site (Fig. 29). Besides the dominant Mg (0.71–0.98 apfu), Ca, Cu, Pb and K occur in quantities of 0.02 to 0.29 apfu. The dominating anion in the tetrahedral site of saléeite I (Fig. 29) is (PO<sub>4</sub>)<sup>3-</sup> (1.65–1.91 apfu), subordinate is (AsO<sub>4</sub>)<sup>3-</sup> (0.05–0.34 apfu) accompanied by minor (SiO<sub>4</sub>)<sup>4-</sup> and (SO<sub>4</sub>)<sup>2-</sup> anions (less than 0.05 apfu). The empiric formula of saléeite I calculated from average of 20 spot analyses on the basis of (P + As + Si + S) = 2 apfu is: (Mg<sub>0.90</sub>Ca<sub>0.06</sub>Cu<sub>0.04</sub>Pb<sub>0.04</sub>K<sub>0.02</sub>)<sub>Σ1.06</sub>(UO<sub>2</sub>)<sub>2.05</sub> [(PO<sub>4</sub>)<sub>1.82</sub>(AsO<sub>4</sub>)<sub>0.15</sub>(SiO<sub>4</sub>)<sub>0.02</sub>(SO<sub>4</sub>)<sub>0.01</sub>]<sub>Σ2.00</sub> · 10H<sub>2</sub>O.

In saléeite II magnesium strongly predominates in the cation site (Mg = 0.86–0.99 apfu). The K, Ca and Pb contents reach only 0.12 apfu and, in contrast to saléeite I, no copper is present (Tab. 28). The tetrahedral site besides the predominant (PO<sub>4</sub>)<sup>3-</sup> ion (1.66–1.75 apfu) contains increased amount of the (AsO<sub>4</sub>)<sup>3-</sup> component (up to 0.32 apfu) indicating substitution towards nováčekite (Fig. 29). The empiric formula of saléeite II from Medvědín (average of six spot analyses, Tab. 28), based on (P + As + Si + S) = 2, is: (Mg<sub>0.94</sub>K<sub>0.02</sub>Ca<sub>0.02</sub>Pb<sub>0.01</sub>)<sub>Σ0.99</sub>(UO<sub>2</sub>)<sub>2.05</sub> [(PO<sub>4</sub>)<sub>1.69</sub>(AsO<sub>4</sub>)<sub>0.26</sub>(SiO<sub>4</sub>)<sub>0.03</sub>(SO<sub>4</sub>)<sub>0.02</sub>]<sub>Σ2.00</sub> · 10H<sub>2</sub>O.

The X-ray diffraction study of saléeite from Medvědín indicates an admix-



**Fig. 26** Brown tabular crystals of saléeite I with green metatorbernite on grey churchite-(Y) aggregates; width of image 2.4 mm, photo J. Sejkora (Nikon SMZ1500).



**Fig. 27** Zoned dipyrasoidal crystal of brown saléeite I and green meta-torbernite, width of photo 1 mm, photo J. Sejkora (Nikon SMZ1500).



**Fig. 28** Yellow tabular saléeite II crystals; width of photo 2.3 mm, photo J. Sejkora (Nikon SMZ1500).

**Tab. 27** Chemical composition of saléeite I

	Mean	1	2	3	4	5	6	7	8	9
K <sub>2</sub> O	0.09	0.12	0.01	0.17	0.14	0.06	0.10	0.04	0.03	0.06
CaO	0.37	0.19	0.09	1.26	0.93	0.75	0.55	0.29	0.38	0.14
MgO	4.22	4.04	5.02	2.90	3.59	3.88	4.22	4.21	4.03	4.20
PbO	0.91	0.32	0.08	0.76	0.52	0.22	0.63	0.62	0.41	0.00
CuO	0.39	0.00	0.66	0.00	0.00	0.95	0.47	0.88	0.52	0.05
SiO <sub>2</sub>	0.09	0.00	0.03	0.28	0.23	0.00	0.11	0.00	0.13	0.02
As <sub>2</sub> O <sub>5</sub>	2.09	2.61	5.04	1.21	0.64	1.04	1.70	3.38	1.86	1.69
P <sub>2</sub> O <sub>5</sub>	15.03	16.65	15.05	13.35	14.75	15.39	16.08	14.99	13.10	15.59
SO <sub>3</sub>	0.10	0.03	0.00	0.00	0.06	0.10	0.08	0.00	0.13	0.00
UO <sub>3</sub>	68.23	68.58	71.61	64.11	65.26	65.39	66.73	71.25	61.26	71.09
H <sub>2</sub> O*	21.19	22.52	23.19	18.68	19.91	20.70	21.86	21.90	18.87	21.22
Total	112.70	115.15	121.12	103.16	106.70	108.64	112.80	117.75	101.09	114.06
K	0.016	0.019	0.002	0.035	0.027	0.011	0.017	0.008	0.007	0.011
Ca	0.059	0.026	0.013	0.222	0.152	0.117	0.081	0.043	0.066	0.021
Mg	0.898	0.778	0.972	0.709	0.817	0.848	0.857	0.868	0.978	0.887
Pb	0.035	0.011	0.003	0.034	0.021	0.009	0.023	0.023	0.018	0.000
Cu	0.042	0.000	0.065	0.000	0.000	0.106	0.048	0.092	0.063	0.005
Zn	0.007	0.000	0.031	0.000	0.038	0.009	0.000	0.000	0.003	0.000
ΣA site	1.058	0.834	1.085	1.000	1.057	1.100	1.026	1.034	1.136	0.924
Si	0.014	0.000	0.004	0.046	0.035	0.000	0.015	0.000	0.021	0.003
As	0.154	0.176	0.342	0.103	0.051	0.079	0.121	0.245	0.158	0.125
P	1.822	1.821	1.654	1.851	1.907	1.909	1.856	1.755	1.804	1.872
S	0.011	0.003	0.000	0.000	0.006	0.011	0.008	0.000	0.016	0.000
ΣT site	2.000	2.000	2.000	2.000	2.000	2.000	2.000	2.000	2.000	2.000
U	2.054	1.861	1.953	2.206	2.094	2.013	1.911	2.070	2.093	2.118
H <sub>2</sub> O	10.00	10.00	10.00	10.00	10.00	10.00	10.00	10.00	10.00	10.00

mean based on 20 analyses

H<sub>2</sub>O\* – H<sub>2</sub>O content calculated on the basis of 10 H<sub>2</sub>O molecules in the ideal saléeite formula

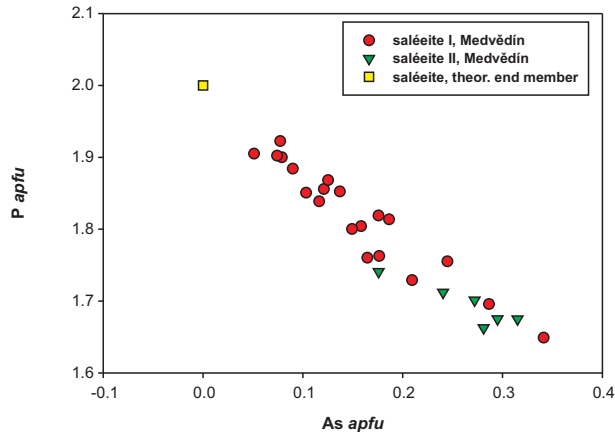


**Fig. 29** Binary plot of *apfu* As vs. P in T-site of saléeites from Medvědín.

ture of metatorbernite ( $d_{002}$  8.652 Å) and, in the case of saléeite I, also metaautunite ( $d_{002}$  8.453 Å). For both generations of saléeite is characteristic a strong preferred orientation, probably of the type *0k0*, caused by perfect cleavage of the mineral (Tab. 29). Thoreau and Vaes (1932) first described saléeite as being of a tetragonal

symmetry. The monoclinic symmetry was recognised by Piret and Deliens (1980) using the Weissenberg method. The crystal structure with the monoclinic space group  $P2_1/n$  was identified by Miller and Taylor (1986), who pointed out the pseudo-tetragonal character of the mineral. The refined unit-cell parameters for both types of saléeite from Medvědín are in agreement with data published for this mineral (Tab. 30).

Infrared vibrational spectra of saléeite I show water molecule libration 669,  $\nu_1$  ( $\text{UO}_2$ )<sup>2+</sup> symmetric stretching vibrations 807 m, 851 s;  $\nu_3$  ( $\text{UO}_2$ )<sup>2+</sup> antisymmetric stretching vibration 921 vs;  $\nu_3$  ( $\text{PO}_4$ )<sup>3-</sup> antisymmetric stretching vibrations 1010 vs, 1113 s, 1226 m;  $\delta \text{H}_2\text{O}$  bending vibrations 1637 m, 1698 m; combination band or overtone 1742 w;  $\nu \text{OH}$  stretching vibrations 3356 m, 3511 m; symmetrically different water molecules are present in the structure together with some hydrogen bonds. Vibrational bands of saléeite II could be assigned to the water molecule libration 712 m;  $\nu_1$  ( $\text{UO}_2$ )<sup>2+</sup> symmetric stretching vibrations 807 m, 851 m;  $\nu_3$  ( $\text{UO}_2$ )<sup>2+</sup> antisymmetric stretching vibration 922 s;  $\nu_3$  ( $\text{PO}_4$ )<sup>3-</sup> antisymmetric stretching vibrations 1010 vs, 1116 s;  $\delta \text{H}_2\text{O}$  bending vibration 1652 m; combination band or overtone 1739 m;  $\nu \text{OH}$  stretching bands 3262 s sh, 3364 s b, 3500 s; sym-

**Tab. 28** Chemical composition of saléeite II

	Mean	1	2	3	4	5	6
K <sub>2</sub> O	0.10	0.05	0.08	0.02	0.13	0.06	0.28
CaO	0.12	0.19	0.29	0.05	0.04	0.15	0.00
MgO	4.47	4.13	4.51	4.45	4.76	4.69	4.31
PbO	0.31	0.63	0.22	0.16	0.00	0.68	0.16
SiO <sub>2</sub>	0.18	0.15	0.28	0.07	0.14	0.36	0.07
As <sub>2</sub> O <sub>5</sub>	3.60	3.73	3.39	4.16	4.22	3.81	2.29
P <sub>2</sub> O <sub>5</sub>	14.29	14.42	14.92	13.66	14.81	13.92	14.02
SO <sub>3</sub>	0.13	0.01	0.07	0.00	0.11	0.05	0.57
UO <sub>3</sub>	69.47	69.40	71.65	70.57	71.39	70.12	63.70
H <sub>2</sub> O	21.44	21.38	22.09	21.00	22.40	21.46	20.33
Total	114.12	114.22	117.52	114.32	118.20	115.36	105.99
K	0.019	0.009	0.013	0.004	0.022	0.011	0.053
Ca	0.018	0.028	0.042	0.008	0.006	0.022	0.000
Mg	0.935	0.859	0.913	0.959	0.947	0.987	0.947
Pb	0.012	0.024	0.008	0.006	0.000	0.026	0.006
ΣA site	0.984	0.921	0.976	0.978	0.976	1.045	1.007
Si	0.025	0.021	0.038	0.010	0.019	0.051	0.010
As	0.264	0.273	0.241	0.315	0.295	0.281	0.177
P	1.697	1.706	1.715	1.675	1.675	1.663	1.750
S	0.015	0.001	0.007	0.000	0.011	0.006	0.064
ΣT site	2.000	2.000	2.000	2.000	2.000	2.000	2.000
U	2.047	2.037	2.043	2.146	2.004	2.079	1.973
H <sub>2</sub> O	10.00	10.00	10.00	10.00	10.00	10.00	10.00

mean based on 6 analyses

H<sub>2</sub>O\* – H<sub>2</sub>O content calculated on the basis of 10 H<sub>2</sub>O molecules in ideal saléeite formula

**Tab. 29** XRD patterns of saléeite

saleéite I <sup>1)</sup>						saleéite II <sup>2)</sup>					
<sup>1)</sup> $I_{rel}$	<sup>1)</sup> $d_{obs}$	<sup>1)</sup> $d_{calc}$	$h$	$k$	$l$	<sup>2)</sup> $I_{rel}$	<sup>2)</sup> $d_{obs}$	<sup>2)</sup> $d_{calc}$	$h$	$k$	$l$
100	9.947	9.973	0	2	0	100	9.956	9.972	0	2	0
22	4.983	4.987	0	4	0	21	4.986	4.986	0	4	0
2	4.947	4.943	1	0	-2	<1	4.947	4.950	1	0	-2
						<1	4.905	4.903	1	0	0
						<1	4.819	4.815	0	3	1
						<1	3.955	3.946	1	3	0
						<1	3.495	3.492	0	0	2
2	3.478	3.476	2	0	-2	<1	3.480	3.475	2	0	-2
2	3.460	3.461	0	5	1	<1	3.465	3.464	0	5	1
2	3.323	3.324	0	6	0	1	3.325	3.324	0	6	0
<1	3.099	3.087	1	1	-3						
1	2.634	2.637	0	7	1	<1	2.641	2.638	0	7	1
3	2.493	2.493	0	8	0	2	2.494	2.493	0	8	0
<1	2.205	2.205	3	0	-4	<1	2.205	2.205	3	0	-4
						<1	2.159	2.161	1	2	-4
2	2.141	2.141	3	2	-2						
1	2.113	2.112	0	9	1	<1	2.109	2.108	1	7	-3
						<1	2.101	2.101	3	4	-3
<1	2.002	2.004	3	5	-3	<1	2.004	2.003	3	5	-3
1	1.9945	1.9947	0	10	0	4	1.9954	1.9947	0	10	0
<1	1.8495	1.8472	1	10	0						
<1	1.8067	1.8077	1	9	-3						
<1	1.7325	1.7313	4	1	-4						
1	1.6657	1.6663	4	2	-5						
1	1.6623	1.6627	3	6	-1	<1	1.6627	1.6640	3	6	-1
<1	1.6588	1.6588	4	2	-3						
<1	1.5746	1.5740	1	12	0						

<sup>1)</sup> range 7–60° 2θ, integrated step 0.02°/150 s<sup>2)</sup> range 5–60° 2θ, integrated step 0.02°/150 s

profile shape function Pearson VII

**Tab. 30** Unit-cell parameters of saléeite (monoclinic space group  $P2_1/c$ )

saleéite I		saleéite II		Ranger I mine, Miller and Taylor (1986)	Rýžoviště, Sejkora et al. (1998)
Medvědín (this paper)	Medvědín (this paper)	Medvědín (this paper)	Ranger I mine, Miller and Taylor (1986)	Rýžoviště, Sejkora et al. (1998)	
$a$ [Å]	6.952(8)	6.951(9)	6.951	7.016(7)	
$b$ [Å]	19.947(4)	19.945(8)	19.947	19.99(1)	
$c$ [Å]	9.89(1)	9.90(1)	9.896	10.045(9)	
$\beta$ [°]	135.24(4)	135.14(4)	135.17	135.67(3)	
$V$ [Å <sup>3</sup> ]	965(3)	968(3)	967.34	985(2)	

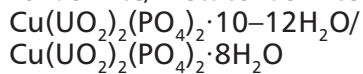
metrically distinct water molecules and some hydrogen bonds are present in the structure.

Unclear is the vibrational band near 1700 cm<sup>-1</sup>, which is not derived from H<sub>2</sub>O vibration but may be a combination vibration ( $v_1 + v_3$ ) (UO<sub>2</sub>)<sup>2+</sup>. No substantial differences were observed between infrared spectra of both studied saléeite samples. The newly obtained spectra are also

close to those published in literature (Čejka Jr. et al. 1984; Sejkora et al. 1998; Frost and Weier 2004).

Thermal analysis confirmed that both types of saléeites contain c. 10 H<sub>2</sub>O molecules, which is equal to the theoretical composition. The presence of non-equivalent H<sub>2</sub>O groups in the saléeite crystal structure could be inferred from the analysis.

#### 4.2.8. Torbernite/Metatorbernite



Torbernite and metatorbernite, the latter resulting from the spontaneous dehydration of the former, are relatively abundant in the studied material and can be observed in association with majority of other identified minerals. Compared to autunite they have a darker green colour. Found were both tetragonal tabular crystals (combination of prismatic and basal faces; Fig. 30) and well-formed dipyramidal crystals (combination of dipyramidal and basal faces) up to 2 mm across. Some crystals show zoning with alternation of green (metatorbernite) and brown (saléeite) zones (Fig. 27).

The cation site of metatorbernite from Medvědín (Tab. 31) is dominated by Cu (0.49–1.12 *apfu*; Fig. 31)

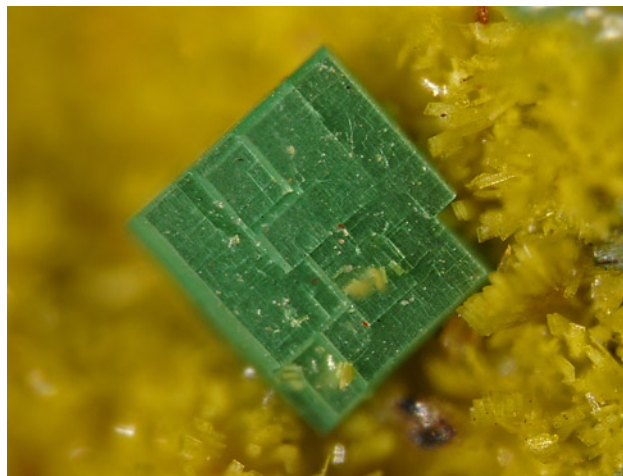


**Fig. 30** Tabular metatorbernite crystal on rich dewindtite aggregates (P2); width of photo 1.0 mm, photo J. Sejkora (Nikon SMZ1500).

**Tab. 31** Representative analyses of metatorbernite

	Mean	1	2	3	4	5	6	7	8
K <sub>2</sub> O	0.07	0.12	0.00	0.01	0.04	0.05	0.01	0.14	0.31
CaO	0.81	0.13	0.17	0.51	0.54	0.56	0.94	1.62	1.83
MgO	0.08	0.00	0.08	0.09	0.15	0.06	0.00	0.00	0.16
PbO	0.32	0.43	0.35	0.40	0.07	0.43	0.09	0.71	0.43
CuO	7.39	8.47	11.19	8.34	8.36	4.52	6.83	4.56	4.34
SiO <sub>2</sub>	0.06	0.06	0.05	0.09	0.11	0.00	0.03	0.14	0.00
As <sub>2</sub> O <sub>5</sub>	3.57	6.40	2.11	1.01	4.97	3.51	2.84	2.76	3.29
P <sub>2</sub> O <sub>5</sub>	13.93	12.12	15.90	16.46	12.82	13.86	14.83	14.77	13.17
SO <sub>3</sub>	0.05	0.03	0.07	0.25	0.00	0.00	0.00	0.00	0.12
UO <sub>3</sub>	66.72	68.39	68.76	68.20	66.31	69.13	64.77	67.61	61.27
H <sub>2</sub> O*	16.53	16.59	18.00	17.48	16.50	15.80	16.49	16.43	15.33
Total	109.53	112.74	116.69	112.83	109.87	107.90	106.81	108.72	100.26
K	0.013	0.023	0.000	0.001	0.008	0.009	0.001	0.025	0.062
Ca	0.128	0.021	0.025	0.074	0.085	0.088	0.143	0.247	0.303
Ba	0.003	0.003	0.011	0.000	0.009	0.000	0.004	0.000	0.001
Mg	0.017	0.000	0.017	0.018	0.033	0.013	0.000	0.000	0.037
Pb	0.012	0.017	0.013	0.015	0.003	0.017	0.003	0.027	0.018
Cu	0.809	0.935	1.152	0.855	0.931	0.503	0.734	0.489	0.506
ΣA site	0.982	0.999	1.218	0.964	1.069	0.630	0.884	0.788	0.927
Si	0.009	0.008	0.007	0.012	0.017	0.000	0.004	0.019	0.000
As	0.273	0.489	0.151	0.072	0.383	0.271	0.211	0.205	0.266
P	1.713	1.500	1.836	1.891	1.600	1.729	1.785	1.776	1.720
S	0.006	0.003	0.007	0.025	0.000	0.000	0.000	0.000	0.014
ΣT site	2.000	2.000	2.000	2.000	2.000	2.000	2.000	2.000	2.000
U	2.039	2.100	1.969	1.945	2.054	2.140	1.934	2.017	1.986
H <sub>2</sub> O	8.00	8.00	8.00	8.00	8.00	8.00	8.00	8.00	8.00

mean based on 13 analyses

H<sub>2</sub>O\* – H<sub>2</sub>O content calculated assuming 8 H<sub>2</sub>O molecules in ideal metatorbernite formula

**Tab. 32** XRD patterns of metatorbernite and „UV-active metatorbernite“

Metatorbernite <sup>1)</sup>						UV-active metatorbernite <sup>2)</sup>					
$I_{rel}$	$d_{obs}$	$d_{calc}$	$h$	$k$	$l$	$I_{rel}$	$d_{obs}$	$d_{calc}$	$h$	$k$	$l$
100	8.651	8.662	0	0	2	100	8.657	8.667	0	0	2
1	5.432	5.433	1	0	2						
<1	4.987	4.933	1	1	0						
15	4.329	4.331	0	0	4	7	4.331	4.333	0	0	4
7	3.678	3.680	1	0	4	1	3.678	3.675	1	0	4
1	3.488	3.488	2	0	0						
1	3.235	3.236	2	0	2						
<1	2.9317	2.9353	1	2	2						
<1	2.8877	2.8873	0	0	6						
1	2.7182	2.7166	2	0	4						
2	2.6679	2.6679	1	0	6	<1	2.6685	2.6666	1	0	6
<1	2.5335	2.5315	1	2	4						
<1	2.4935	2.4919	1	1	6						
<1	2.2073	2.2061	3	1	0						
22	2.1658	2.1655	0	0	8	4	2.1661	2.1667	0	0	8
						<1	2.1486	2.1456	3	0	3
<1	2.1166	2.1191	2	1	6	<1	2.1160	2.1135	2	1	6
						<1		2.1135	1	2	6
1	2.0686	2.0681	1	0	8	<1	2.0689	2.068	1	0	8
<1	2.0498	2.0488	3	0	4						
1	1.9834	1.9829	1	1	8	<1	1.9845	1.9817	1	1	8
<1	1.8399	1.8398	2	0	8	<1	1.8394	1.8373	2	0	8
<1	1.8104	1.8111	3	0	6	<1	1.8068	1.8045	3	0	6
2	1.7328	1.7324	0	0	10	1	1.7330	1.7333	0	0	10
						1	1.7331	4	0	0	
						<1	1.6350	1.6342	1	1	10
						<1	1.4440	1.4444	0	0	12
						<1	1.4140	1.4152	2	2	10
						<1	1.4151	4	2	5	
						<1	1.4151	2	4	5	
						<1	1.3860	1.3866	3	0	10
						<1	1.2190	1.2188	1	0	14
						<1	1.0830	1.0833	0	0	16
						<1	1.0700	1.0703	1	0	16

<sup>1)</sup> range 5–60° 2Θ, integrated step 0.02°/150 s; <sup>2)</sup> range 8–100° 2Θ, integrated step 0.05°/350 s; profile shape function Pearson VII

accompanied by Ca (metaautunite) component ranging between 0.02 and 0.30 apfu. The  $(\text{PO}_4)^{3-}$  anion predominating in the tetrahedral site (1.50–1.89 apfu) shows substitution by  $(\text{AsO}_4)^{3-}$  anion (up to 0.49 apfu), corresponding to PAs<sub>-1</sub> isomorphism in the metatorbernite–metazeunerite series. Based on  $(\text{P} + \text{As} + \text{Si} + \text{S}) = 2$  the empiric formula of metatorbernite (average of 13 spot analyses) can be expressed as follows:  $(\text{Cu}_{0.81}\text{Ca}_{0.13}\text{Mg}_{0.02}\text{K}_{0.01}\text{Pb}_{0.01})_{\Sigma 0.98}(\text{UO}_2)_{2.04}[(\text{PO}_4)_{1.71}(\text{AsO}_4)_{0.27}(\text{SiO}_4)_{0.01}(\text{SO}_4)_{0.01}]_{\Sigma 2.00} \cdot 8\text{H}_2\text{O}$ .

The X-ray powder diffraction pattern of metatorbernite from Medvědín (Tab. 32) is perfectly consistent with the published data (Tab. 33). Its refined unit-cell parameters correspond to those of metatorbernite (Tab. 33), regardless the relatively high content of the metazeunerite (As) component (Fig. 32).

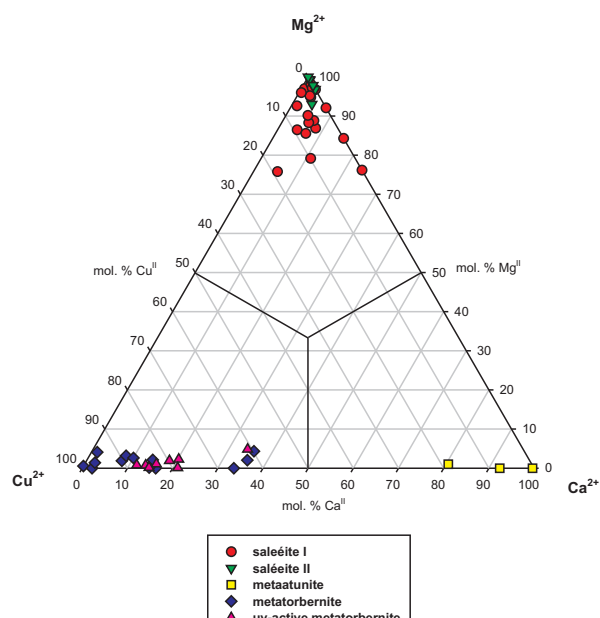
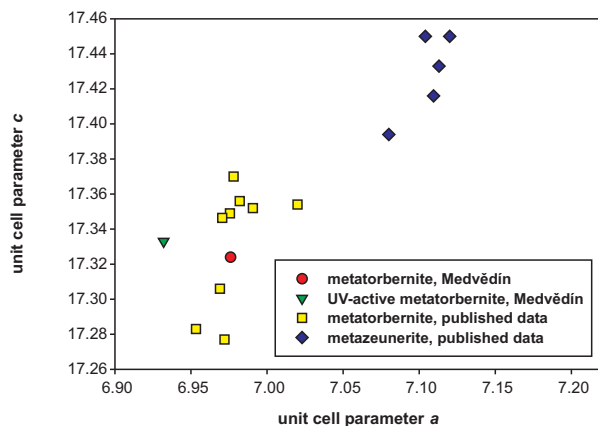


Fig. 31 Ternary plot of A-site occupancy (atomic ratio) of the autunite group minerals from Medvědín.

**Tab. 33** Refined unit-cell parameters of metatorbernite from Medvědín in comparison with metatorbernite and metazeunerite from other localities (tetragonal space group  $P4/n$ )

Mineral	Locality	Reference	$a$ [Å]	$c$ [Å]	$V$ [Å $^3$ ]
Metatorbernite, P>As	Medvědín	this paper	6.976(2)	17.324(3)	843.1(4)
UV-active metatorbernite	Medvědín	this paper	6.932(3)	17.333(3)	833.0(6)
Metatorbernite	synthetic	Locock and Burns (2003)	6.9756	17.349	844.2(1)
Metatorbernite, P	Rýžoviště	Sejkora et al. (1994)	6.9533(8)	17.283(3)	835.6
Metatorbernite, P>As	H. Halže	Sejkora et al. (2007)	6.9907(8)	17.352(2)	848.1(1)
Metatorbernite, P>>As	Příbram	Ondruš and Hyršl (1989)	7.020(1)	17.354(3)	855.2
Metatorbernite	H. Slavkov	Plášil et al. (2006)	6.9705(7)	17.3464(8)	842.8
Metatorbernite, P	Jáchymov	Ondruš et al. (1997)	6.978(3)	17.37(1)	845.8
Metatorbernite, P	Jáchymov	Ondruš et al. (1997)	6.982(1)	17.356(5)	846.1
Metatorbernite, P	Schneeberg (BRD)	Ross et al. (1964)	6.969(1)	17.306(1)	840.5
Metatorbernite, P	Vathi (Greece)	Stergiou et al. (1993)	6.972(1)	17.277(8)	839.8
Metazeunerite, As	synthetic	Locock and Burns (2003)	7.1094(1)	17.416(1)	880.3(1)
Metazeunerite, As	Majuba Hill	Ross et al. (1964)	7.12	17.45	884.6
Metazeunerite, As	Schwarzwald	Walenta (1965a)	7.104	17.45	880.6
Metazeunerite, As>P	Cínovec	Jansa et al. (1998)	7.080(2)	17.394(5)	871.9
Metazeunerite, As	Jáchymov	Ondruš et al. (1997)	7.113(1)	17.433(3)	882.0

**Fig. 32** Binary plot of the unit cell parameters  $b$  vs.  $c$  for metatorbernite–metazeunerite series.

Assignment of IR vibrations bands of metatorbernite from Medvědín are: water molecule libration 699 m;  $\nu_1$  ( $UO_2$ ) $^{2+}$  symmetric stretching vibrations 809 m, 845 s;  $\nu_3$  ( $UO_2$ ) $^{2+}$  antisymmetric stretching vibrations 879 m, 917 s;  $\nu_3$  ( $PO_4$ ) $^{3-}$  antisymmetric stretching vibrations 10001 vs, 1103 sh;  $\delta H_2O$  molecular water bending vibrations 1556 vw, 1654 w;  $\nu OH$  stretching vibrations 3352 s, 3416 s. Symmetrically distinct hydrogen bonded water molecules are present in the structure.

#### 4.2.9. Metatorbernite showing UV-fluorescence

Some of the studied samples carried crystalline coatings of metatorbernite up to several cm $^2$  across, typically associated with „limonite“ coatings. Individual tabular crys-

tals reach size up to 1 mm (Fig. 33). They show notably lighter green colour than other studied metatorbernites. Peculiar is a moderately intense light green fluorescence in short-wave UV light (254 nm). This is rather surprising, as one of characteristic and diagnostic properties of metatorbernite (as well as torbernite and (meta)autunite) is the absence of fluorescence in UV light.

The anomalous Medvědín metatorbernite shows in addition to dominating Cu (0.35–0.98 apfu) increased contents of Ca (0.13–0.20 apfu – Tab. 34; Fig. 31). However, the presence of calcium does not explain the unusual UV fluorescence, as the other metatorbernite samples – containing even higher Ca contents – are nonfluorescent. Possible presence of a fine intergrowth of phases dominated alternatively by Cu and Ca up to the EPMA resolution limit of  $c.$  0.5–1  $\mu$ m was tested with negative results. Besides predominating ( $PO_4$ ) $^{3-}$  anion (1.74–1.93 apfu) the tetrahedral sites of this metatorbernite contain ( $AsO_4$ ) $^{3-}$  anion in the range of 0.05–0.25 apfu. The PAs $_{-1}$  isomorphism has no effect on fluorescence of the studied phase, as the As analogue – (meta-) zeunerite – lacks fluorescence in the UV light. The empirical formula of UV-active metatorbernite from Medvědín (average of 8 spot analyses), based on (P + As + Si + S + V) = 2 is:  $(Cu_{0.77}Ca_{0.17}K_{0.02}Mg_{0.01}Fe_{0.01}Pb_{0.01})_{\Sigma 0.99}(UO_2)_{2.07}[(PO_4)_{1.79}(AsO_4)_{0.18}(SiO_4)_{0.02}(SO_4)_{0.01}]_{\Sigma 2.00} \cdot 8H_2O$ .

The X-ray powder diffraction pattern of the UV-active metatorbernite (Tab. 32) corresponds well to the published data (ICDD 2003). The X-ray pattern suggests a possible presence of an additional mineral, which has an asymmetric character of high intensity diffractions of the  $00l$  type. Refined unit-cell parameters of the studied



**Fig. 33** Aggregate of light green tabular UV-active metatorbernite crystals; width of photo 2.3 mm, photo J. Sejkora (Nikon SMZ1500).

**Tab. 34** Representative analyses of “UV-active metatorbernite”

	Mean	1	2	3	4	5
K <sub>2</sub> O	0.08	0.13	0.07	0.04	0.10	0.03
CaO	0.97	0.86	0.84	1.13	1.17	0.90
FeO	0.08	0.23	0.00	0.00	0.05	0.09
MgO	0.05	0.04	0.03	0.09	0.00	0.01
PbO	0.20	0.37	0.29	0.07	0.29	0.00
CuO	6.34	9.08	7.48	6.14	6.21	7.39
SiO <sub>2</sub>	0.13	0.00	0.28	0.04	0.05	0.02
As <sub>2</sub> O <sub>5</sub>	2.15	0.70	2.08	2.54	3.15	2.24
P <sub>2</sub> O <sub>5</sub>	13.17	15.91	12.90	13.92	13.39	12.46
SO <sub>3</sub>	0.07	0.15	0.00	0.00	0.04	0.25
UO <sub>3</sub>	61.18	66.72	61.70	63.18	61.86	60.56
H <sub>2</sub> O	15.00	17.14	15.08	15.64	15.53	14.77
Total	99.42	111.31	100.76	102.78	101.86	98.71
K	0.016	0.023	0.015	0.007	0.019	0.006
Ca	0.167	0.131	0.147	0.184	0.192	0.162
Fe	0.010	0.027	0.000	0.000	0.007	0.012
Mg	0.012	0.009	0.008	0.021	0.001	0.002
Pb	0.009	0.014	0.013	0.003	0.012	0.000
Cu	0.766	0.984	0.920	0.705	0.718	0.936
ΣA site	0.981	1.188	1.103	0.919	0.949	1.117
Si	0.022	0.000	0.045	0.007	0.008	0.003
As	0.182	0.053	0.177	0.202	0.252	0.196
P	1.788	1.932	1.777	1.792	1.735	1.769
S	0.008	0.016	0.000	0.000	0.005	0.032
ΣT site	2.000	2.000	2.000	2.000	2.000	2.000
U	2.066	2.010	2.110	2.018	1.989	2.133
H <sub>2</sub> O	8.00	8.00	8.00	8.00	8.00	8.00

Mean based on 8 analyses

H<sub>2</sub>O\* – H<sub>2</sub>O content calculated assuming 8 H<sub>2</sub>O molecules in ideal metatorbernite formula

phase differ from the data published for metatorbernite, particularly in the *a* parameter (Tab. 33, Fig. 32).

Infrared vibration bands of studied metatorbernite represent water molecule libration 681 w, 718 vw; v<sub>1</sub> (UO<sub>2</sub>)<sup>2+</sup> symmetric stretching vibrations 806, 847; v<sub>3</sub> (UO<sub>2</sub>)<sup>2+</sup> anti-symmetric stretching vibration 921; v<sub>3</sub> (PO<sub>4</sub>)<sup>3-</sup> anti-symmetric stretching vibrations 1001 vs, 1112 m-s; δ H<sub>2</sub>O bending vibration 1638 w; v OH stretching vibrations 3363 s, 3417 s. Hydrogen bonds are expected in this structure.

No substantial differences were found between infrared spectra of both studied torbernite/metatorbernite samples. They are close to the published infrared metatorbernite spectra (e.g. Čejka Jr. et al. 1984).

#### 4.2.10. Uranophane Ca(UO<sub>2</sub>)<sub>2</sub>[SiO<sub>3</sub>(OH)<sub>2</sub>]· 5H<sub>2</sub>O

Uranophane from dumps at the Medvědín deposit was described by Pauliš et al. (2005). Semiquantitative chemical analyses and X-ray diffraction data were also presented by the same authors.

In the course of the present project, uranophane was observed in samples from the tunnel No. 1 as a predominant component of compact brown, red and orange parts of the so-called „gumite“. In studied samples from adit No. 2 uranophane forms yellow spheroidal aggregates in proximity of kasolite and churchite-(Y) or coats orange aggregates of kasolite.

Around kasolite aggregates it forms radiating aggregates composed of acicular crystals (Fig. 34). Several samples from the same location contain well-formed uranophane needles up to 2.5 mm long, which are grouped to yellow compact crystalline aggregates macroscopically resembling phosphuranylite (Fig. 35).

Chemical composition of uranophane from Medvědín (Tab. 35), based on average of four spot analyses and



**Fig. 34** Acicular aggregates of uranophane with torbernite crystal aggregates; width of photo 2.3 mm, photo J. Sejkora (Nikon SMZ1500).

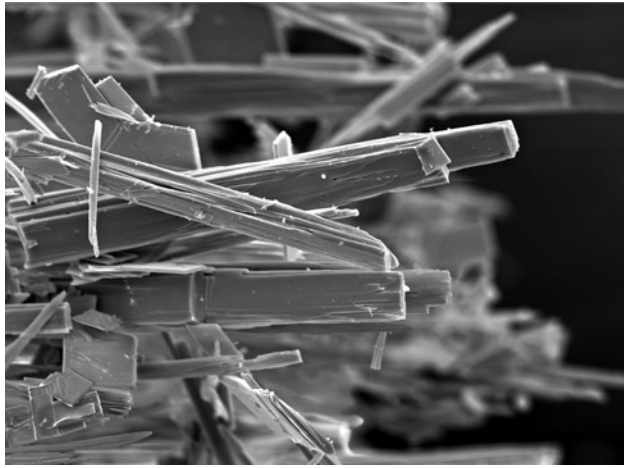
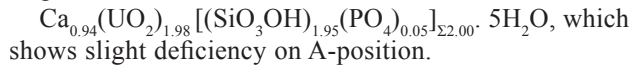


**Fig. 35** Parallel oriented uranophane crystals; SEM photo J. Plášil (Jeol JSM-6380), width of figure 112 µm.

the relation  $(\text{Si} + \text{P}) = 2$ , corresponds to the following empiric formula:



The X-ray powder diffraction pattern of uranophane from Medvědín (Tab. 36) as well as refined unit-cell parameters (Tab. 37) correspond well to published data from other localities and theoretical XRD pattern calculated from crystal structure (Ginderów 1988).

**Tab. 35** Chemical composition of uranophane

	Mean	1	2	3	4
CaO	6.76	6.59	6.69	7.20	6.57
SiO <sub>2</sub>	15.08	15.02	15.20	15.28	14.81
P <sub>2</sub> O <sub>5</sub>	0.47	0.55	0.39	0.44	0.50
UO <sub>3</sub>	73.14	72.70	74.13	72.11	73.62
H <sub>2</sub> O*	13.86	13.86	13.92	14.03	13.64
Total	109.31	108.72	110.33	109.05	109.14
Ca	0.936	0.912	0.924	0.985	0.924
ΣA site	0.936	0.912	0.924	0.985	0.924
Si	1.949	1.940	1.958	1.953	1.944
P	0.051	0.060	0.042	0.047	0.056
ΣT site	2.000	2.000	2.000	2.000	2.000
U	1.986	1.973	2.005	1.935	2.030
OH <sup>-</sup>	1.95	1.94	1.96	1.95	1.94
H <sub>2</sub> O	5.00	5.00	5.00	5.00	5.00

mean based on 4 analyses

H<sub>2</sub>O\* – H<sub>2</sub>O and OH<sup>-</sup> contents calculated from charge balance and assuming 5 H<sub>2</sub>O molecules in ideal uranophane formula (Ginderów 1988)

Tentative assignment of IR vibrational bands of uranophane from Medvědín: v<sub>4</sub> (SiO<sub>4</sub>) bending vibration 672 w; v<sub>1</sub> (UO<sub>2</sub>)<sup>2+</sup> symmetric stretching vibration 780 w; v<sub>3</sub> (UO<sub>2</sub>)<sup>2+</sup> anti-symmetric stretching vibration 865 vs; v<sub>3</sub> (SiO<sub>4</sub>) anti-symmetric stretching vibrations 944 s [v<sub>1</sub> (SiO<sub>4</sub>) symmetric stretching vibration ?],

**Tab. 36** XRD pattern of uranophane

I <sub>rel</sub>	d <sub>obs</sub>	d <sub>calc</sub>	h	k	l	I <sub>rel</sub>	d <sub>obs</sub>	d <sub>calc</sub>	h	k	l
100	7.908	7.902	2	0	0	2	2.209	2.208	0	0	3
5	6.621	6.623	0	0	1	1	2.106	2.106	6	2	0
6	5.422	5.424	2	0	-1	2	2.100	2.100	6	1	-2
5	4.785	4.788	2	0	1	1	2.070	2.068	6	2	-1
1	4.295	4.291	2	1	-1	2	2.060	2.060	2	0	3
66	3.952	3.951	4	0	0	1	2.040	2.040	4	0	-3
9	3.600	3.599	4	0	-1	15	1.9766	1.9755	8	0	0
1	3.508	3.507	0	2	0	7	1.9624	1.9620	8	0	-1
4	3.211	3.205	2	2	0	2	1.9138	1.9128	1	3	-2
2	2.994	2.995	0	1	2	1	1.8900	1.8917	4	3	1
5	2.925	2.926	4	1	1	2	1.8755	1.8746	6	1	2
<1	2.827	2.829	2	2	1	1	1.8320	1.8315	4	0	3
19	2.635	2.634	6	0	0	<1	1.8079	1.8079	6	0	-3
4	2.559	2.561	6	0	-1	1	1.7553	1.7552	3	3	2
1	2.530	2.529	4	1	-2	6	1.7422	1.7429	8	1	-2
<1	2.512	2.512	4	2	-1	2	1.7124	1.7123	8	2	-1
1	2.407	2.406	6	1	-1	1	1.6639	1.6637	3	4	0
1	2.349	2.348	5	2	0	3	1.6551	1.6567	6	3	1
1	2.267	2.265	4	1	2	3	1.5956	1.5959	6	0	3
1	2.227	2.227	6	1	1	6	1.5824	1.5829	10	0	-1

range 3–60° 2Θ, integrated step 0.05°/100 s, profile shape function Pearson VII

**Tab. 37** Refined unit-cell parameters of uranophane (monoclinic space group  $P2_1$ )

	Medvědín, this paper	Bois Noir, Ginderów (1988)	Rýžoviště, Sejkora et al. (1994)	Slavkovice, Sejkora et al. (1997a)
<i>a</i> [Å]	15.931(3)	15.909(6)	15.968(9)	15.928(6)
<i>b</i> [Å]	7.019(2)	7.002(3)	7.024(3)	7.002(3)
<i>c</i> [Å]	6.677(1)	6.665(3)	6.680(3)	6.637(2)
$\beta$ [°]	97.24(2)	97.27	97.12(5)	97.04(4)
<i>V</i> [Å <sup>3</sup> ]	740.1(2)	736.48	743.4	734.7(4)

1005 s, 1101 w, 1151 vw;  $\delta$  H<sub>2</sub>O bending vibrations 1636 vw b, 1669 vw b;  $\nu$  OH stretching vibrations 3195 m sh, 3437 m, 3502 m sh; symmetrically distinct water molecules and a set of hydrogen bonds are present in the structure. Infrared spectra of uranophane were published by many authors; the observed spectra are close to these (see e.g. Čejka et al. 1986; Čejka 1999).

#### 4.3. Other supergene minerals

##### 4.3.1. Plumbogummite PbAl<sub>3</sub>(PO<sub>4</sub>)<sub>2</sub>(OH)<sub>5</sub>·H<sub>2</sub>O

Mineral with chemical composition corresponding to plumbogummite has been found in a single sample coming from the M7 vein. It is a part of fine-grained aggregates consisting of limonite with intergrowths of metatorbernite tabular crystals. Plumbogummite is associated with parsonsite, churchite-(Y), metatorbernite and (meta-) autunite.

Chemical composition of plumbogummite (average of four spot analyses – Tab. 38), recalculated on the basis of (P + As + Si + S) = 2, yields the following formula: (Pb<sub>1.13</sub>Ca<sub>0.02</sub>Ba<sub>0.01</sub>(UO<sub>2</sub>)<sub>0.07</sub>)<sub>21.23</sub>(Al<sub>2.56</sub>Fe<sub>0.31</sub>Cu<sub>0.02</sub>Zn<sub>0.01</sub>)<sub>22.90</sub>[{(PO<sub>4</sub>)<sub>1.89</sub>(AsO<sub>4</sub>)<sub>0.07</sub>(SO<sub>4</sub>)<sub>0.02</sub>(SiO<sub>4</sub>)<sub>0.02</sub>}<sub>22.00</sub>(OH)<sub>4.85</sub>Cl<sub>0.01</sub>)<sub>24.86</sub>·H<sub>2</sub>O. Interesting are the increased uranium contents (up to 0.08 apfu). Certain deviation from stoichiometry, observed in occupancy of the cation sites, possibly correlates with poor crystallinity of the studied sample. Due to minimal dimensions of this mineral and its intergrowth with metatorbernite and other phases it was not examined by the X-ray powder diffraction.

##### 4.3.2. Pseudomalachite Cu<sub>5</sub>(PO<sub>4</sub>)<sub>2</sub>(OH)<sub>4</sub>

Pseudomalachite forms opaque, semi-spheroidal to spheroidal aggregates up to 1 mm across of grass green colour and vitreous lustre. It is often intergrown with metatorbernite and overgrown by acicular crystals of agardite-(Y) (Figs 4–5). Churchite-(Y) also occurs in this assemblage.

Chemical composition of pseudomalachite from Medvědín (Tab. 39), besides major Cu, shows also minor contents of Pb (up to 0.03 apfu) and Mg (to 0.02 apfu) in the cation site. The tetrahedral site contains some (AsO<sub>4</sub>)<sup>3-</sup>

**Tab. 38** Chemical composition of plumbogummite

	Mean	1	2	3	4
CaO	0.15	0.00	0.23	0.13	0.23
BaO	0.33	0.38	0.24	0.42	0.27
MgO	0.03	0.00	0.00	0.01	0.13
PbO	37.08	36.33	37.84	38.13	36.04
CuO	0.18	0.00	0.01	0.55	0.17
ZnO	0.08	0.00	0.04	0.27	0.00
Fe <sub>2</sub> O <sub>3</sub>	3.31	2.71	4.82	1.91	3.80
Al <sub>2</sub> O <sub>3</sub>	19.24	18.49	18.74	20.00	19.74
Bi <sub>2</sub> O <sub>3</sub>	0.07	0.00	0.00	0.28	0.00
SiO <sub>2</sub>	0.14	0.07	0.18	0.26	0.06
As <sub>2</sub> O <sub>5</sub>	1.24	1.22	1.57	0.86	1.32
P <sub>2</sub> O <sub>5</sub>	19.70	19.97	18.79	20.10	19.96
V <sub>2</sub> O <sub>5</sub>	0.05	0.13	0.03	0.07	0.00
SO <sub>3</sub>	0.26	0.11	0.40	0.22	0.30
UO <sub>3</sub>	3.02	3.07	2.51	3.44	3.06
Cl	0.04	0.06	0.01	0.05	0.05
H <sub>2</sub> O	9.08	8.32	9.32	9.28	9.40
Total	94.01	90.85	94.72	95.96	94.52
Ca	0.018	0.000	0.029	0.016	0.027
Ba	0.014	0.017	0.011	0.018	0.012
Mg	0.005	0.000	0.000	0.001	0.021
Pb	1.128	1.100	1.183	1.144	1.086
$\Sigma M^{2+}$	1.166	1.118	1.223	1.179	1.145
Cu	0.015	0.000	0.001	0.046	0.014
Zn	0.006	0.000	0.003	0.022	0.000
Fe	0.314	0.255	0.468	0.178	0.356
Al	2.562	2.452	2.566	2.628	2.603
Bi	0.002	0.000	0.000	0.008	0.000
$\Sigma M^{3+}$	2.900	2.708	3.039	2.882	2.973
Si	0.016	0.008	0.020	0.029	0.007
As	0.074	0.072	0.096	0.050	0.077
P	1.884	1.902	1.848	1.898	1.890
V	0.004	0.009	0.002	0.005	0.000
S	0.022	0.010	0.035	0.018	0.026
$\Sigma T$ site	2.000	2.000	2.000	2.000	2.000
U	0.072	0.073	0.061	0.081	0.072
Cl	0.008	0.011	0.002	0.009	0.009
OH*	4.847	4.252	5.226	4.903	5.007
H <sub>2</sub> O	1.00	1.00	1.00	1.00	1.00

mean based on 4 spot microanalyses

H<sub>2</sub>O and OH\* – H<sub>2</sub>O and OH<sup>-</sup> contents calculated from charge balance and assuming one H<sub>2</sub>O molecule in ideal plumbogummite formula

**Tab. 39** Chemical composition of pseudomalachite

	Mean	1	2	3
FeO	0.03	0.00	0.07	0.03
MgO	0.09	0.06	0.13	0.07
PbO	0.97	0.89	1.14	0.88
CuO	64.45	64.30	65.86	63.18
ZnO	0.05	0.09	0.02	0.04
Al <sub>2</sub> O <sub>3</sub>	0.02	0.00	0.05	0.02
Bi <sub>2</sub> O <sub>3</sub>	0.10	0.10	0.21	0.00
As <sub>2</sub> O <sub>5</sub>	7.86	7.87	8.12	7.61
P <sub>2</sub> O <sub>5</sub>	17.18	17.19	17.18	17.17
SO <sub>3</sub>	0.02	0.01	0.04	0.00
H <sub>2</sub> O*	6.36	6.29	6.68	6.10
Total	97.13	96.79	99.49	95.10
Fe	0.003	0.000	0.006	0.003
Mg	0.014	0.009	0.021	0.011
Pb	0.028	0.026	0.033	0.025
Cu	5.215	5.202	5.287	5.156
Zn	0.004	0.007	0.001	0.003
Al	0.003	0.000	0.007	0.002
Bi	0.003	0.003	0.006	0.000
ΣA site	5.269	5.247	5.360	5.201
As	0.440	0.440	0.451	0.430
P	1.558	1.558	1.546	1.570
S	0.001	0.001	0.003	0.000
ΣT site	2.000	2.000	2.000	2.000
OH	4.545	4.497	4.735	4.404

mean based on 3 spot analyses

H<sub>2</sub>O\* – content of OH<sup>-</sup> molecules calculated from the charge balance

(0.43–0.45 apfu), in addition to dominating (PO<sub>4</sub>)<sup>3-</sup> ions (1.55–1.57 apfu). Unlimited PAs<sub>-1</sub> isomorphism in the pseudomalachite–cornwallite series was described by Artl and Ambruster (1999). The empirical formula of studied pseudomalachite (average of three spot analyses) can be expressed on the basis of (P + As + S) = 2 as follows: (Cu<sub>5.21</sub>Pb<sub>0.03</sub>Mg<sub>0.01</sub>)<sub>Σ5.25</sub>[(PO<sub>4</sub>)<sub>1.56</sub>(AsO<sub>4</sub>)<sub>0.44</sub>]<sub>Σ2.00</sub>(OH)<sub>4.50</sub>.

The X-ray powder diffraction pattern of the studied phase corresponds well to published data for pseudomalachite (ICDD 2003). The polymorphs reichenbachite and ludjibajite have not been found as admixtures. Due to numerous coincidences of pseudomalachite with the intergrown metatorbernite and agardite-(Y) it was not possible to index the X-ray powder pattern reliably and to refine its unit-cell parameters.

#### 4.3.3. Pyromorphite Pb<sub>5</sub>(PO<sub>4</sub>)<sub>3</sub>Cl

The mineral forms transparent to translucent acicular crystals with imperfect morphology, up to 4 mm long (Fig. 36). The crystals with a strong vitreous lustre are light yellow to yellow-brown, grouped in small radiating



**Fig. 36** Prismatic crystals of pyromorphite on churchite-(Y) globular coatings with green torbernite; width of image 3 mm, photo J. Sejkora (Nikon SMZ1500).



**Fig. 37** Pyromorphite aggregate in a cavity of orange parsonsite coatings with metatorbernite; width of photo 6 mm, photo J. Sejkora (Nikon SMZ1500).

clusters (Fig. 37). Pyromorphite has been found in the M7 vein in association with Pb-rich supergene minerals – parsonsite, dewindtite, kasolite and unnamed phase Pb(Ce,REE)<sub>3</sub>(PO<sub>4</sub>)<sub>3</sub>(OH)<sub>2</sub>·nH<sub>2</sub>O. The studied samples also contained saléeite, metatorbernite and churchite-(Y).

The pyromorphite contains only minor Ca (reaching up to 0.04 apfu) besides Pb dominating the cation site (4.87–5.02 apfu; Tab. 40). The tetrahedral site contains a significant (AsO<sub>4</sub>)<sup>3-</sup> [mimetite] component (0.59–1.18 apfu) in addition to the dominating (PO<sub>4</sub>)<sup>3-</sup> anions (1.81–2.39 apfu). Empiric formula (average of six spot analyses), calculated on the basis of (P + As = 3 apfu), is (Pb<sub>4.91</sub>Ca<sub>0.02</sub>Zn<sub>0.01</sub>)<sub>Σ4.94</sub>[(PO<sub>4</sub>)<sub>2.05</sub>(AsO<sub>4</sub>)<sub>0.95</sub>]<sub>Σ3.00</sub>Cl<sub>0.97</sub>.

The X-ray powder diffraction pattern of pyromorphite from Medvědín (Tab. 41) matches well the data for P-rich

**Tab. 40** Chemical composition of pyromorphite

	Mean	1	2	3	4	5	6
CaO	0.08	0.08	0.03	0.06	0.16	0.07	0.07
PbO	79.48	79.68	78.87	80.78	80.25	79.75	77.53
ZnO	0.05	0.05	0.06	0.17	0.00	0.00	0.00
As <sub>2</sub> O <sub>5</sub>	7.85	9.79	9.48	5.16	5.17	7.87	9.64
P <sub>2</sub> O <sub>5</sub>	10.59	9.26	9.14	12.99	12.60	10.27	9.27
Cl	2.50	2.50	2.48	2.63	2.57	2.42	2.37
-O=Cl	0.56	0.56	0.56	0.59	0.58	0.55	0.54
H <sub>2</sub> O	0.04	0.03	0.01	0.04	0.03	0.05	0.08
Total	101.14	101.96	100.62	102.42	101.36	100.98	99.49
Ca	0.020	0.021	0.008	0.015	0.039	0.018	0.018
Pb	4.900	4.970	5.001	4.871	4.913	5.018	4.957
Zn	0.008	0.009	0.010	0.028	0.000	0.001	0.000
ΣA site	4.928	5.000	5.019	4.914	4.952	5.037	4.975
As	0.949	1.185	1.172	0.591	0.606	0.963	1.174
P	2.051	1.815	1.828	2.409	2.394	2.037	1.826
ΣT site	3.000	3.000	3.000	3.000	3.000	3.000	3.000
Cl	0.968	0.980	0.989	0.998	0.992	0.959	0.955
OH	0.032	0.024	0.008	0.030	0.025	0.040	0.066

mean based on 6 analyses

H<sub>2</sub>O\* – content of OH<sup>-</sup> calculated on the basis of valence balance**Tab. 41** XRD pattern of pyromorphite

<i>I<sub>rel</sub></i>	<i>d<sub>obs</sub></i>	<i>d<sub>calc</sub></i>	<i>h</i>	<i>k</i>	<i>l</i>	<i>I<sub>rel</sub></i>	<i>d<sub>obs</sub></i>	<i>d<sub>calc</sub></i>	<i>h</i>	<i>k</i>	<i>l</i>
10	8.655	8.706	1	0	0	12	2.206	2.208	1	1	3
7	5.028	5.026	1	1	0	8	2.174	2.177	4	0	0
34	4.349	4.353	2	0	0	39	2.075	2.077	2	2	2
36	4.148	4.153	1	1	1	21	2.020	2.020	3	1	2
2	3.753	3.749	2	0	1	12	1.9964	1.9973	2	3	0
12	3.683	3.687	0	0	2	12	1.9964	1.9973	3	2	0
32	3.394	3.395	1	0	2	27	1.9691	1.9692	2	1	3
14	3.305	3.291	2	1	0	27	1.9691	1.9692	1	2	3
26	3.288	3.291	1	2	0	11	1.9271	1.9279	3	2	1
78	3.016	3.005	2	1	1	11	1.9271	1.9279	2	3	1
23	3.003	3.005	1	2	1	11	1.8738	1.8743	4	0	2
100	2.971	2.973	1	1	2	7	1.8439	1.8434	0	0	4
71	2.901	2.902	3	0	0	12	1.7288	1.7307	1	1	4
3	2.813	2.813	2	0	2	15	1.6979	1.6974	2	0	4
8	2.516	2.513	2	2	0	8	1.6096	1.6082	2	1	4
7	2.458	2.455	1	2	2	21	1.5554	1.5560	3	0	4
21	2.282	2.280	3	0	2	15	1.5284	1.5297	1	5	1

range 10–80°2Θ, integrated step 0.02°/400 s, profile shape function Pearson VII

**Tab. 42** Refined unit-cell parameters of pyromorphite (hexagonal space group *P6<sub>3</sub>/m*)

Mineral	Locality	Reference	<i>a</i> [Å]	<i>c</i> [Å]	<i>V</i> [Å <sup>3</sup> ]	mol.% As
pyromorphite	Medvědín	this paper	10.051(3)	7.373(2)	645.1(3)	32 mol. % As
pyromorphite	Arizona, USA	Dai and Hughes (1989)	9.977(1)	7.351(2)	633.6	0 mol. % As
mimetite	Durango, Mexico	Dai et al. (1991)	10.212(2)	7.419(4)	669.9	100 mol. % As

members of the pyromorphite–mimetite series (Dai and Hughes 1989). The refined unit-cell parameters (Tab. 42) show characteristic increase, compared to P-rich end-member. This increase correlates well with the range of the PAs<sub>1</sub> substitution indicated by chemical analyses.

#### 4.4. Bi mineralization

Bismuth minerals have been identified in a single sample collected in the No. 18 vein in the gallery No. 3. Plášil et al. (2008) documented the presence of bismite, bismuthite and eulytite, formed probably in the course of late hydrothermal alteration of primary native bismuth. A detailed description of the Bi-mineralization is presented in the paper mentioned above.

## 5. Comments on the origin of supergene mineralization at the Medvědín deposit

The studied mineral association of supergene uranium minerals represents a typical uranyl phases assemblage in the supergene zone of uranium deposits. The supergene alteration zone at the Medvědín deposit has a large vertical extent, reaching about 350 m below the surface. The ore body is developed in a belt (*c.* 300–400 m wide) of contact metamorphic rocks more resistant to erosion than the surrounding strata. The deposit is limited geomorphologically by the Labský důl valley in the north, the Jizerka river valley in the south and by the Elbe river valley in the east. The Labský důl valley was formed due to glacial activity. The upper parts of the Medvědín deposit were probably removed by denudation already during Tertiary (Zlaté návrší peneplain).

Only rare relicts of uraninite and native bismuth (Plášil et al. 2008) with scarce pyrite and arsenopyrite were found in the deposit. Absence of sulphides indicates a strong and long-term leaching of the primary mineralization. In the presence of oxygen uranyl ions liberated from dissolved uraninite form various complexes which are highly mobile in aqueous solution (Deliens 1977; Langmuir 1978; Chernikov 1981; Belova and Doynikova 2003; Brugger et al. 2003; Grenthe et al. 2004). No products of early *in-situ* uraninite weathering, elsewhere most commonly represented by hydrated Pb-oxyhydroxides of U<sup>6+</sup> (vandendriesscheite and fourmarierite) with schoepite (Finch and Murakami 1999), were found in Medvědín. Abundance of these phases could be considered as a measure for the degree of alteration of the primary mineralization. Uranyl phosphates and silicates represent probably precipitation products from an aqueous solution rich in uranyl complexes (sulphate complexes) at a high activity of PO<sub>4</sub><sup>3-</sup> and SiO<sub>4</sub><sup>4-</sup> ions. Precipitation of uranyl phosphates is mostly induced by highly acidic environment, whereas alkaline conditions drive precipitation of uranyl silicates.

Based on previous geological survey and current research, we assume a rather intense alteration of primary uraninite + sulphides mineralization. Relicts of uraninite co-formed by massive uranophane and torbernite were found during exploration works on the deposit outcrop. Around the vein, an aureole up to 2 m thick (outcrop of the vein M11) of uranyl phosphates (described as “uranium micas”) was found, documenting the primary ores leaching. Deeply penetrating meteoritic waters could have transported uranyl-rich solutions to the lower parts of the deposit and precipitate there. Crystallization of the uranyl phosphates (as the most abundant group of supergene minerals on the deposit) at the contact of descending solutions with the ground water level could have taken place. This may have caused the observed enrichment of

the veins at the third level of the deposit (similar to the zone of supergene enrichment typical of the base metal vein deposits) coupled with a depletion of the veins near the surface (1<sup>st</sup> level). To the evolution of oxidation zone contributed geomorphologic aspects such as the developed outcrop situated on the top of the Medvědín hill (mountain humid environment, less vegetation).

Taken together, we suppose the following mineral succession. Products of the early uraninite alteration (hydrated Pb-oxyhydroxides of U<sup>6+</sup> – see above) were replaced by uranyl silicates, mainly by uranophane, whereas kasolite is less abundant due to the loss of Pb. Hydrated uranyl phosphates precipitated in the suitable environment (Eh/pH changes, changes in concentrations of dissolved P) further from the uranium source (dissolving uraninite). Sequence of uranyl phosphates begun by REE-bearing phases, which are the oldest on the deposit. Parsonsosite, saléeite I and II, dewindtite/phosphuranylite and pyromorphite followed. Here and there aggregates of probably younger uranophane and kasolite were formed. Oxidic Bi-mineralization from gallery No. 3 had probably a different genesis, being presumably of late-hydrothermal origin. No recent uranyl phases, connected with weathering of primary U-minerals in the environment of the open adit were found. This seems to be the proof for high level of their alteration and leaching.

Relatively high REE and Pb contents in supergene minerals are characteristic of the studied mineral association. Lead was probably supplied from galena, which was completely decomposed in the supergene alteration zone but its small proportion is probably of radiogenic origin (bound first in uraninite). The increased REE abundances, notable mainly in churchite-(Y), are probably derived from metasedimentary rocks of the Vrchlabí Group, which have high REE concentrations (Winchester et al. 2003). Other elements such as P and Mg could have been derived from these rocks as well.

## 6. Conclusions

Studied assemblage of supergene minerals containing uranium and other elements is a product of a long-term alteration of the primary mineralization. Uranyl phosphates and arsenates represent stable association of mineral phases under the surface conditions. Mostly intermediate members of the isomorphic mineral series were observed and studied. Most of them exhibit pronounced substitution trends both in cation and anion positions. Occurrences of agardite-(Y), parsonsosite and dewindtite are exceptional within the Czech Republic. The presence of molecular water up to 2 molecules per formula unit was confirmed in parsonsosite. Description of two interesting and not known species is proposed,

“new unnamed phase  $\text{Pb}(\text{Ce},\text{REE})_3(\text{PO}_4)_3(\text{OH})_2 \cdot n\text{H}_2\text{O}$ ” and metatorbernite showing UV fluorescence (interesting variety of metatorbernite exhibiting such an unique property). Problematic crystal chemistry of the phosphuranylite group minerals is uncovered, new quantitative chemical data are given. Increased concentrations of REE were observed in some minerals, in particular agardite-(Y), churchite-(Y) and the above-mentioned “new unnamed phase”. The REE came probably from host rocks, uranyl minerals formed from primary uraninite, which has been totally dissolved and is present only in small relicts. Other elements have probably originated from base-metal sulphides, which were dissolved during the presumed long-term alteration.

**Acknowledgements.** The authors would like to thank the Ministry of Culture of the Czech Republic, which has financially supported this work as a part of the project MK00002327201 and Grant Agency of the Academy of Science of the Czech Republic (project A3407401). We are thankful to J. Ederová (Institute of Chemical Technology, Prague), I. Němec and M. Mazuch (both Faculty of Science, Charles University in Prague) for extensive help with the instrumental methods used in this work. The authors thank reviewers R. Frost (QUT, Brisbane, Australia) and F. Veselovský (Czech Geological Survey, Prague) as well as editor V. Janoušek (Czech Geological Survey, Prague) for their valuable comments on the manuscript.

## References

- ANTHONY JW, BIDEAUX RA, BLADH KW, NICHOLS MC (2000) Handbook of Mineralogy IV, Arsenates, Phosphates, Vanadates. Mineral Data Publishing, Tucson, Arizona, pp 1–680
- ARTL T, AMBRUSTER T (1999) Single X-ray structure refinement of cornwallite,  $\text{Cu}_5(\text{AsO}_4)_2(\text{OH})_4$ : a comparison with its polymorph cornubite and the  $\text{PO}_4$ -analogue pseudomalachite. *Neu J Mineral, Mh* 10: 468–480
- ARUGA A, NAKAI I (1985) Structure of Ca-rich agardite. *Acta Cryst C41*: 161–163
- BEOLOVA LN, DOYNIKOVA OA (2003) Conditions of formation of uranium minerals in the oxidation zone of uranium deposits. *Geolog Rud Mestor* 45: 148–151 (in Russian)
- BRUGGER J, BURNS C P, MEISSER N (2003) Contribution to the acid drainage of uranium minerals: marecottite and the zippeite group. *Amer Miner* 88: 676–685
- BURNHAM CW (1962) Lattice constant refinement. *Carn Inst Wash Year Book* 61: 132–135
- BURNS PC (2000) A new uranyl phosphate chain in the structure of parsonsite. *Amer Miner* 85: 801–805
- BURNS PC (2005)  $\text{U}^{6+}$  minerals and inorganic compounds: insights into an expanded structural hierarchy of crystal structures. *Canad Mineral* 43: 1839–1894
- BURNS PC, MILLER ML, EWING RC (1996)  $\text{U}^{6+}$  minerals and inorganic phases: a comparison and hierarchy of crystal structures. *Canad Mineral* 34: 845–880
- CHERNIKOV AA (1981) Behaviour of uranium in the supergene zone. Nedra, Moscow, pp 1–207 (in Russian)
- COELHO AA, CHEARY RW (1997) X-ray Line Profile Fitting Program, XFIT. Program.
- COUTINHO JMV, ATENCIO D (2000) Phosphuranylite from Minas Gerais, Brazil and its identity with yingjiangite. In: 4<sup>th</sup> International Mineralogy in Museums Conference, Melbourne: 35
- ČEJKA J (1999) Infrared spectroscopy and thermal analysis of the uranyl minerals. In: BURNS PC, EWING RC (eds) Uranium: Mineralogy, Geochemistry and the Environment. Mineralogical Society of America and Geochemical Society Reviews in Mineralogy and Geochemistry 38, Washington, pp 521–622
- ČEJKA J, URBANEC Z, MRÁZEK Z (1986) Secondary uranium minerals in the collection of the National Museum in Prague XII. Uranyl silicates. *Čas Nár muz, ř přírod* 45: 30–44 (in Czech)
- ČEJKA J JR, MUCK A, ČEJKA J (1984) To the infrared spectroscopy of natural uranyl phosphates. *Phys Chem Miner* 11: 172–177
- DAI YS, HUGHES JM (1989) Crystal-structure refinements of vanadinite and pyromorphite. *Canad Mineral* 27: 189–192
- DAI YS, HUGHES JM, MOORE PB (1991) The crystal structures of mimetite and clinomimetite  $\text{Pb}_5(\text{AsO}_4)_3\text{Cl}$ . *Canad Mineral* 29: 369–376
- DELIENS M (1977) Associations de minéraux secondaires d’uranium à Shinkolobwe (région du Shaba, Zaïre). *Bull Soc Fr Minéral Cristallog* 100: 32–38
- DEMARTIN F, DIELLA V, DONZELLI S, GRAMACIOLLI CM, PILATI T (1991) The importance of accurate crystal structure determination of uranium minerals. I. Phosphuranylite  $\text{KCa}(\text{H}_3\text{O})_3(\text{UO}_2)_7(\text{PO}_4)_4\text{O}_4 \cdot 8\text{H}_2\text{O}$ . *Acta Crystallogr B47*: 439–466
- DIETRICH JÉ, ORLIC M, PERMINGEAT F (1969) L’agardite, une nouvelle espèce minérale, et le problème du chlorotile. *Bull Soc Fr Minéral Cristallog* 92: 420–434
- FINCH RJ, EWING RC (1992) The corrosion of uraninite under oxidizing conditions. *J Nucl Mater* 190: 133–156
- FINCH RJ, MURAKAMI T (1999) Systematics and paragenesis of uranium minerals. In: BURNS PC, EWING RC (eds) Uranium: Mineralogy, Geochemistry and the Environment. Mineralogical Society of America and Geochemical Society Reviews in Mineralogy and Geochemistry 38, Washington, pp 91–179
- FROST RL, WEIER ML (2004) Hot-stage Raman spectroscopic study of the thermal decomposition of saléeite. *J Raman Spectr* 35: 299–307

- FROST RL, ČEJKA J, WEIER M, MARTENS WM (2006a) A Raman spectroscopic study of the uranyl phosphate mineral parsonsite. *J Raman Spectr* 37: 879–891
- FROST RL, ČEJKA J, WEIER M, AYOKO GA (2006b) Raman spectroscopic study of the uranyl phosphate mineral dewindtite. *J Raman Spectr* 37: 1362–1367
- FROST RL, ČEJKA J, AYOKO GA (2008) Raman spectroscopic study of the uranyl phosphate minerals phosphuranylite and yingjiangite. *J Raman Spectr* 39: 495–502
- GINDEROW D (1988) Structure de l'uranophane alpha,  $\text{Ca}(\text{UO}_2)_2(\text{SiO}_3\text{OH})_2 \cdot 5 \text{H}_2\text{O}$ . *Acta Cryst C44*: 421–424
- GRENTHIE I, FUGER J, KONINGS RJM, LEMIRE RJ, MULLER AB, NGUYEN-TRUNG CREGU C, WANNER H (2004) Chemical thermodynamics of Uranium (reprint). OECD Nuclear Energy Agency, Issy-les-Moulineaux, France, pp 1–715
- HOGGART DD, NUFFIELD EW (1954) Studies of radioactive compounds: VII – phosphuranylite and dewindtite. *Amer Miner* 39: 444–447
- HUYNEN AM, PIRET-MEUNIER J, VAN MEERSSCHE M (1963) Structure de la kasolite. *Bull Cl Sci (Acad Roy Belg)* 49: 192–201
- JANSA J, NOVÁK F, PAULIŠ P, SCHARMOVÁ M (1998) Supergene minerals of the Sn-W Činovec deposit, Krušné hory Mts. (Czech Republic). *Bull mineral petrolog Odd Nár Muz (Praha)* 6: 83–101 (in Czech)
- JINGYI Z, ANWA W, WENSHU G (1992) New data on yingjiangite. *Acta Petrol Mineral* 11: 178–184 (in Chinese with English abstract)
- KLOMÍNSKÝ J (1969) The Krkonoše–Jizera granitoid massif. *Sbor Geol Věd* 15: 1–134
- KOHLMANN M, SOWA H, REITHMAYER K, SCHULZ H, KRUGER RR, ABRIEL W (1994) Structure of a  $\text{Y}_{(1-x)}(\text{Gd},\text{Dy},\text{Er})_x\text{PO}_4 \cdot 2\text{H}_2\text{O}$  microcrystal using synchrotron radiation. *Acta Cryst C50*: 1651–1652
- LANGMUIR D (1978) Uranium solution-mineral equilibria at low temperatures with applications to sedimentary ore deposits. *Geochim Cosmochim Acta* 42: 547–569
- LOCOCK AJ (2004) Crystal chemistry of uranyl phosphates, arsenates and oxysalts of chromium(V): implications for remediation. Unpublished PhD. thesis, University of Notre Dame, Notre Dame, pp 1–477
- LOCOCK AJ, BURNS PC (2003) Crystal structures and synthesis of the copper-dominant members of the autunite and meta-autunite groups: torbernite, zeunerite, metatorbernite and metazeunerite. *Canad Mineral* 41: 498–502
- LOCOCK AJ, BURNS PC, FLYNN TM (2005) The role of water in the structures of synthetic hallimondite,  $\text{Pb}_2[(\text{UO}_2)(\text{AsO}_4)_2](\text{H}_2\text{O})_n$  and synthetic parsonsite,  $\text{Pb}_2[(\text{UO}_2)(\text{PO}_4)_2](\text{H}_2\text{O})_n$ ,  $0 \leq n \leq 0.5$ . *Amer Miner* 90: 240–246
- MAKAROV ES, IVANOV VI (1960) The crystal structure of meta-autunite,  $\text{Ca}(\text{UO}_2)_2(\text{PO}_4)_2 \cdot 6\text{H}_2\text{O}$ . *Doklady Akademii Nauk USSR* 132: 601–603 (in Russian)
- MEREITER K, PREISINGER A (1986) Krystallstrukturdaten der Wismutminerale Atelestit, Mixit und Pucherit. *Anz Österr Akad Wiss* 123: 79–81
- MILLER SA, TAYLOR JC (1986) The crystal structure of saléeite  $\text{Mg}[\text{UO}_2\text{PO}_4]_2 \cdot 10\text{H}_2\text{O}$ . *Z Kristallogr* 177: 247–253
- MOENKE H (1966) Mineralspektren II. Akademie Verlag Berlin, pp 1–22
- OLMI F, SABELLI C, TROSTI-FERRONI R (1991) A contribution to the crystal chemistry of mixite group minerals from Sardinia (Italy). *Neu Jb Mineral, Mh* 11: 487–499
- ONDŘUŠ P, HYRŠL J (1989) New finds and revision of secondary minerals from Příbram district. *Acta Univ Carol, Geol*: 521–533
- ONDŘUŠ P, VESELOVSKÝ F, HLOUŠEK J, SKÁLA R, VAVŘÍN I, FRÝDA J, ČEJKA J, GABAŠOVÁ A (1997) Secondary minerals of the Jáchymov (Joachimsthal) ore district. *J Czech Geol Soc* 42: 3–76
- PAULIŠ P, ŠEVČŮ J, NOVOTNÝ J, RENDL J (1999) Saléeite and minerals of the phosphuranylite–yingjiangite series from the Kladská near Mariánské Lázně uranium deposit. *Bull Czech Geol Surv* 74: 47–49
- PAULIŠ P, KOPECKÝ S, NOVÁK F (2005) Uranophane from the deposit of uranium ores Medvědín near Špindlerův Mlýn. *Opera Corc* 42: 69–72 (in Czech)
- PDF-2 – POWDER DIFFRACTION FILE (ICDD- INTERNATIONAL CENTRE FOR DIFFRACTION DATA) ICDD (2003) „Powder Diffraction File“, International Centre for Diffraction Data, edited by Frank McClune, 12 Campus Boulevard, Newton Square, Pennsylvania 19073–3272
- PEACOR DR, DUNN PJ (1982) Petersite, a REE and phosphate analog of mixite. *Amer Miner* 67: 1039–1042
- PIRET P, DELIENS M (1980) Nouvelles données sur la saléeite holotype de Shinkolobwe. *Bull Minéral* 103: 630–632
- PIRET P, PIRET-MEUNIER J (1991) Composition chimique et structure cristalline de la phosphuranylite  $\text{Ca}(\text{UO}_2)_2[(\text{UO}_2)_3(\text{OH})_2(\text{PO}_4)_2]_2 \cdot 12\text{H}_2\text{O}$ . *Eur J Mineral* 3: 69–77
- PIRET P, PIRET-MEUNIER J, DELIENS M (1990) Composition chimique et structure cristalline de la dewindtite  $\text{Pb}_3[\text{H}(\text{UO}_2)_3\text{O}_2(\text{PO}_4)_2]_2 \cdot 12\text{H}_2\text{O}$ . *Eur J Mineral* 2: 399–405
- PLÁŠIL J (2007) A study of supergene mineralization at the Medvědín uranium deposit, Krkonoše Mts., Czech Republic. Unpublished BSci thesis, Faculty of Science, Charles University, Prague, pp 1–72 (in Czech)
- PLÁŠIL J, SEJKORA J, ONDŘUŠ P, VESELOVSKÝ F, BERAN P, GOLIÁŠ V. (2006a) Supergene minerals in the Horní Slavkov uranium ore district, Czech Republic. *J Czech Geol Soc* 51: 149–158
- PLÁŠIL J, SEJKORA J, ŠKODA R, GOLIÁŠ V (2006b) Supergene Y, REE minerals from the Medvědín deposit, The Krkonoše (Giant) Mts., Czech Republic. *Miner Pol (Special papers)* 28: 181–183
- PLÁŠIL J, SEJKORA J, GOLIÁŠ V (2008) Bismuth mineralization from the uranium deposit Medvědín near Špindlerův Mlýn. *Opera Corc* 45: 5–11 (in Czech with English abstract)

- PLUSKAL O (1993): Uranium mineral resources in the Czech Republic (The uranium world market and the Czech Republic, part II). Faculty of Science, Charles University, Prague, pp 1–99 (in Czech)
- POUCHOU JL, PICHOIR F (1985) "PAP" procedure for improved quantitative microanalysis. *Microbeam Anal* 20: 104–105
- ROSENZWEIG A, RYAN RR (1977) Kasolite,  $\text{Pb}(\text{UO}_2)(\text{SiO}_4)(\text{H}_2\text{O})$ . *Cryst Struct Comm* 6: 617–621
- ROSS M, EVANS HT, APPLEMAN DE (1964) Studies of the torbernite minerals (II): The crystal structure of meta-torbernite. *Amer Miner* 49: 1603–1621
- SEJKORA J (1992) Mineralogy of oxidic minerals containing bismuth. Unpublished MSci thesis, Faculty of Science, Charles University, Prague, pp 1–154 (in Czech)
- SEJKORA J (1993) Phosphuranylite occurrences in the Czech Republic. In: *Sbor V min cykl sem (Horní Bečva)*, Ústí nad Labem, pp 97–99 (in Czech)
- SEJKORA J, ŠREIN V (1996) Contribution to crystal chemistry of mixite from localities in the Bohemian Massif. *Zpr geol výzk v r* 1995: 153–155 (in Czech)
- SEJKORA J, VESELOVSKÝ F, ŠREIN V (1994) The supergene mineralization of uranium occurrence Rýžoviště near Harrachov (Krkonoše Mts., Czech Republic). *Acta Mus Nat Prague, ser B (Historia Nat)* 50: 55–91
- SEJKORA J, MAZUCH J, ABERT F, ŠREIN V, NOVOTNÁ M (1997a) Supergene mineralization of the Slavkovice uranium deposit in western Moravia. *Acta Mus Moraviae, Sci Nat* 81: 3–24 (in Czech)
- SEJKORA J, GABAŠOVÁ A, NOVOTNÁ M (1997b) Mixite from Smrkovec near Mariánské Lázně. *Bull mineral–petrolog Odd Nár Muz (Praha)* 4–5: 185–187 (in Czech)
- SEJKORA J, ČEJKA J, KOTRLÝ M, NOVOTNÁ M (1998) Saléeite from uranium exploration dumps at Rýžoviště near Harrachov. *Bull mineral–petrolog Odd Nár Muz (Praha)* 6: 217–221 (in Czech)
- SEJKORA J, ŘÍDKOŠIL T, ŠREIN V (1999) Zálesíte, a new mineral of the mixite group, from Zálesí, Rychlebské hory Mts., Czech Republic. *Neu Jb Mineral, Abh* 175: 150–124
- SEJKORA J, ČEJKA J, PAULIŠ P (2003) Dewindtite – a rare phosphate of lead and uranyl from uranium exploration site at Rýžoviště near Harrachov (Krkonoše Mts.). *Bull mineral–petrolog Odd Nár Muz (Praha)* 11: 177–183 (in Czech)
- SEJKORA J, NOVOTNÝ P, NOVÁK M, ŠREIN V, BERLEPSCH P (2005) Calciopetersite from Domašov nad Bystřicí, northern Moravia, Czech Republic, a new mineral species of the mixite group. *Can Mineral* 43: 1393–1400
- SEJKORA J, ONDRUŠ P, FIKAR M, VESELOVSKÝ F, MACH Z, GABAŠOVÁ A, ŠKODA R, BERAN P (2006) Supergene minerals at the Huber stock and Schnöd stock deposits, Krásno ore district, the Slavkovský les area, Czech Republic. *J Czech Geol Soc* 51: 57–101
- SEJKORA J, ČEJKA J, ŠREIN V (2007) Supergene uranium mineralization from Horní Halže near Mědenec (Krušné hory Mountains), Czech Republic. *J Geosci* 52: 119–210
- SOWDER AG, CLARK SB, FJELD RA (2000) Dehydration of synthetic autunite hydrates. *Radiochim Acta* 88: 533–538
- STERGIOU AC, RENTZEPERIS PJ, SKLAVOUNOS S (1993) Refinement of the crystal structure of metatorbernite. *Z Kristallogr* 205: 1–7
- STRUKOV NG (1958) Geological report on closing the deposit. MS Diamo Archive, Příbram, pp 15 (in Czech)
- ŠKÁCHA P, SEJKORA J (2001) Kasolite from the Jánšká vein, Březové Hory deposit, Příbram. *Bull mineral-petrolog Odd Nár Muz (Praha)* 9: 272–273 (in Czech)
- TAYLOR SR, McLENNAN SM (1985) The Continental Crust: its Composition and Evolution. Blackwell Scientific Publishers, Oxford, pp 1–321
- THOREAU J, VAES JF (1932) La saléeite, nouveau mineral uranifère. *Bull Soc belge Géol* 42: 96–99
- VESELÝ T (1982) Small uranium deposits in crystalline units of the Bohemian Massif. Part III.: The region of north-western and northern Bohemia. *Geol a hydrometallurg uranu* 6: 3–46 (in Czech)
- VOCHTEN R, VAN HAVERBEKE L, VAN SPRINGEL K (1991) Transformation of chernikovite into parsonsite and study of its solubility product. *Neu Jb Mineral, Mh* 1991: 551–558.
- WALENTE K (1965a) Die Uranglimmergruppe. *Chem Erde* 24: 254–275
- WALENTE K (1965b) Hallimondite, a new uranium mineral from the Michael Mine near Reichenbach (Black Forest, Germany). *Amer Miner* 50: 1143–1157
- WALENTE K, THEYE T (2004) Agarit-(Ce) von der Grube Clara im mittleren Schwarzwald, Aufschluss 55: 17–23
- WINCHESTER JA, PATOČKA F, KACLÍK V, MELZER M, NAWAKOWSKI C, CROWLEY QG, FLOYD PA (2003) Geochemical discrimination of metasedimentary sequences in the Krkonoše–Jizera terrane (West Sudetes, Bohemian Massif): paleotectonic and stratigraphic constraints. *Geol Carpath* 54: 267–280
- WISE WS (1978) Parnauite and goudeyite, two new copper arsenate minerals from the Majuba Hill Mine, Pershing County, Nevada. *Amer Miner* 63: 704–708
- WRONKIEWICZ DJ, BATES JK, GERDING TJ, VELECKIS E, TANI BS (1992) Uranium release and secondary phase formation during unsaturated testing of  $\text{UO}_2$  at 90 °C. *J Nucl Mater* 190: 107–127
- ZHANGRU C, YUZHU H, XIAOFA G (1990) A new mineral – yingjiangite. *Acta Mineral Sin* 10: 102–105 (in Chinese with English Abstract)

## Supergenní mineralizace uranového ložiska Medvědín, Krkonoše, Česká republika

Supergenní mineralizace hydrotermálního uranového žilného ložiska Medvědín (Krkonoše, Česká republika) byla nově studována a detailně popsána. Následující supergenní fáze byly studovány pomocí práškové rentgenové difrakce, elektronové mikroanalýzy, IČ spektroskopie a termické analýzy: agardit-(Y), autunit/metaautunit, dewindtit, churchit-(Y), kasolit, nová nepojmenovaná fáze  $Pb(Ce,REE)_3(PO_4)_3(OH)_2 \cdot nH_2O$ , parsonsit, phosphuranylit, plumbogummit, pseudomalachit, pyromorfit, saléйт, torbernit/metatorbernit, uranofán. Výsledky tohoto studia přispívají k rozšíření znalostí o krystalchemii těchto minerálních fází. Asociace minerálů, vzniklá alterací primární mineralizace, tvořená především fosfáty a silikáty uranylu, reprezentuje systém bohatý olovem a REE. Většina minerálních fází představuje směsné členy isomorfních minerálních sérií. Studovaná mineralizace představuje stabilní minerální asociaci v povrchových podmírkách, vzniklou dlouhodobou alterací primární mineralizace, v tomto případě uranového ložiska.